THE SUSY WORKING GROUP: Summary Report

Conveners:

S. Abdullin[1], M. Drees[2,3], H.–U. Martyn[4], G. Polesello[5]

Subgroup Coordinators:

S. Ambrosanio[6], H. Dreiner[7], R.M. Godbole[8]. J. Wells[6,9]

Contributing members*:

P. Chiappetta[10], D. Choudhury[11], A.K. Datta[11], A. Deandrea[6], O.J.P. Éboli[2], N. Ghodbane[12], S. Heinemeyer[13], V. Ilyin[14], T. Kon[15], S. Kraml[16], Y. Kurihara[17], M. Kuroda[18], L. Megner[19], B. Mele[20], G. Moreau[21], B. Mukhopadyaya[11], E. Nagy[22], S. Negroni[22], K. Odagiri[7], F.E. Paige[23], E. Perez[24], S. Petrarca[20], P. Richardson[7], A. Rimoldi[25], S. Roy[11], M.H. Seymour[7], M. Spira[26], J.M. Virey[10,27], F. Vissani[13], G. Weiglein[6]

[1] ITEP, Moscow, Russia.
[2] IFT, Univ. Estadual Paulista, Rua Pamplona 145, São Paulo, Brazil.
[3] Physik Department, TU München, James Franck Str., D–85748 Garching, Germany.
[4] I. Physikalisches Institut, RWTH Aachen, Germany.
[5] INFN, Sezione di Pavia, Via Bassi 6, Pavia, Italy.
[6] CERN Theory Group, CH-1211 Genève 23, Switzerland.
[7] Rutherford Appleton Laboratory, Chilton, Didcot, Oxon OX11 OQX, U.K.
[8] Centre for Theoretical Studies, Indian Institute of Science, Bangalore 560 012, India.
[9] Physics Department, University of California, Davis, CA 95616.
[10] Centre de Physique Théorique, UPR7061, CNRS-Luminy, F-13288 Marseille, France.
[11] Mehta Research Institute, Chhatnag Road, Jhusi, Allahabad 211 019, India.
[12] Inst. de Physique Nucléaire de Lyon, 43 Bd du 11 novembre 1918, 69622 Villeurbanne, France.
[13] DESY, Notkestrasse 85, D–22603 Hamburg, Germany.
[14] INP MSU, Moscow, Russia.
[15] Faculty of Engineering, Seikei University, Tokyo, Japan.
[16] Inst. f. Hochenergiephysik d. Öster. Akademie d. Wissenschaften, A-1050 Wien, Austria.
[17] KEK, Tsukuba, Japan.
[18] Institute of Physics, Meiji-Gakuin University, Tokyo, Japan.

*For non–contributing members, see *Pravda*, April 1, 2000.

[19] Physics Dept. Frescati, KTH, S-104 05 Stockholm, Sweden.
[20] INFN - Sezione di Roma I, and Dip. di Fisica, Univ. "La Sapienza", Rome, Italy.
[21] Service de Physique Théorique, CEA-Saclay, F91191, Gif-sur-Yvette, Cedex France.
[22] Centre de Physique des Particules, Université de la Méditerranée, F-13288 Marseille, France.
[23] Physics Department, Brookhaven National Laboratory, Upton, NY 11973.
[24] Service de Physique des Particules, DAPNIA, CEA-Saclay, F91191, Gif-sur-Yvette, France.
[25] CERN, EP–Division, CH-1211 Genève, Switzerland.
[26] II. Inst. für Theoretische Physik, Univ. Hamburg, D–22761 Hamburg, Germany.
[27] Université de Provence, Marseille, France.

Report of the SUSY working group for the Workshop
"Physics at TeV Colliders", Les Houches, France 8–18 June 1999.

CONTENTS

2c) $\tilde{\chi}_1^0$ *reconstruction in mSUGRA models with R−parity violation*

L. Megner and G. Polesello.

2d) *Supersymmetry with R−parity violation at the LHC: discovery potential from single top production*

F. Chiappetta, A. Deandrea, E. Nagy, S. Negroni, G. Polesello and J.M. Virey.

2e) *Probing* $\not R$ *couplings through indirect effects on Drell–Yan production at the LHC*

D. Choudhury and R.M. Godbole.

2f) *Neutrino masses, R−parity violating supersymmetry and collider signals*

A.K. Datta, B. Mukhopadhyaya and S. Roy.

3. Gauge–mediated supersymmetry breaking

3a) *Introduction to GMSB phenomenology at TeV colliders*,

S. Ambrosanio.

3b) *The light Higgs spectrum in GMSB models*

S. Ambrosanio, S. Heinemeyer and G. Weiglein.

3c) *Measuring the SUSY breaking scale at the LHC in the slepton NLSP scenario of GMSB models*

S. Ambrosanio, B. Mele, S. Petrarca, G. Polesello and A. Rimoldi.

4. Anomaly mediated SUSY breaking at the LHC

F.E. Paige and J.D. Wells.

SYNOPSIS

Supersymmetry remains the best motivated extension of the Standard Model, since it stabilizes the gauge hierarchy against quadratically divergent radiative corrections. However, this argument by itself does not yet tell us very much about the way supersymmetry is realized in Nature. In particular, it tells us nothing about the mechanism that breaks supersymmetry, except that sparticles masses should not greatly exceed 1 TeV (with the possible exception of first and second generation sfermions; this possibility will not be pursued here). One can be completely "agnostic" and simply parameterize SUSY breaking by soft terms. This approach has largely been taken by the first and second subgroup of this working group. Alternatively, one can explore the predictions of specific models, as has been done by subgroups three (on gauge mediated SUSY breaking) and four (on anomaly mediated SUSY breaking).

An additional complication arises because supersymmetric models allow new, gauge–invariant interactions that have no equivalent in the standard model; this is true even if one sticks to the minimal particle content. These interactions break $R-$parity. Some implications of this have been investigated in subgroup two.

Some aspects of SUSY phenomenology have already reached quite a high level of maturity. Radiative corrections have been computed for total cross sections and partial widths; their impact on kinematic distributions is now being explored. Finite width effects formally also belong to higher orders in perturbation theory. Finally, in some cases it is important to keep spin correlations through the entire sparticle production and decay process. Some investigations along these lines are described in contributions from subgroup one; they are (possibly with minor modifications) relevant for all SUSY models.

Another area of current interest is the determination of soft breaking parameters, in particular of sparticle masses. Here a realistic assessment of the capabilities of various experiments requires detailed Monte Carlo simulations. Several studies of this kind are described in contributions from subgroups one, two and four.

Manuel Drees (for the Working Group).

Acknowledgements: We thank the organizers of this workshop for giving us the opportunity to attend a true renaissance meeting, stimulating for body and mind. We are particularly indebted to Jean-Philippe Guillet et al., and the Lapp computer engineers, for providing state–of–the–art computing devices. We also wish to express our gratitude to the staff of the Les Houches center, whose efficient and friendly service greatly contributed to the pleasant memories we took away from the workshop.

SUSY particle production at hadron colliders

M. SPIRA*

Abstract

The determination of the full SUSY QCD corrections to the production of squarks, gluinos and gauginos at hadron colliders is reviewed. The NLO corrections stabilize the theoretical predictions of the various production cross sections significantly and lead to sizeable enhancements of the most relevant cross sections. We discuss the phenomenological consequences of the results on present and future experimental analyses.

1 Introduction

The search for Higgs bosons and supersymmetric particles is among the most important endeavors of present and future high energy physics. The novel colored particles, squarks and gluinos, and the weakly interacting gauginos can be searched for at the upgraded Tevatron, a $p\bar{p}$ collider with a c.m. energy of 2 TeV, and the LHC, a pp collider with a c.m. energy of 14 TeV. Until now the search at the Tevatron has set the most stringent bounds on the colored SUSY particle masses. At the 95% CL, gluinos have to be heavier than about 180 GeV, while squarks with masses below about 180 GeV have been excluded for gluino masses below ~ 300 GeV [1]. Stops, the scalar superpartners of the top quark, have been excluded in a significant part of the MSSM parameter space with mass less than about 80 GeV by the LEP and Tevatron experiments [1]. Finally charginos with masses below about 90 GeV have been excluded by the LEP experiments, while the present search at the Tevatron is sensitive to chargino masses of about 60–80 GeV with a strong dependence on the specific model [1]. Due to the negative search at LEP2 the lightest neutralino $\tilde{\chi}_1^0$ has to be heavier than about 30 GeV in the context of SUGRA models [1]. In the R-parity-conserving MSSM, supersymmetric particles can only be produced in pairs. All supersymmetric particles will decay to the lightest supersymmetric particle (LSP), which is most likely to be a neutralino, stable thanks to conserved R-parity. Thus the final signatures for the production of supersymmetric particles will mainly be jets, charged leptons and missing transverse energy, which is carried away by neutrinos and the invisible neutral LSP.

In Section 2 we shall summarize the details of the calculation of the NLO QCD corrections, as described in Refs. [2–4] for the case of $\tilde{q}\bar{\tilde{q}}$ production. The evaluation of the full SUSY QCD corrections splits into two pieces, the virtual corrections, generated by virtual particle exchanges, and the real corrections, which originate from gluon radiation and the corresponding crossed processes with three-particle final states.

In Section 3 we shall consider the production of squarks and gluinos except stops [2]. We assume the light-flavored squarks to be mass degenerate, which is a reasonable approximation for all squark flavors except stops, while the light quarks (u, d, s, c, b) will be treated as

*Heisenberg Fellow

massless particles. The production of stop pairs requires the inclusion of mass splitting and mixing effects [3] and will be investigated in Section 4. In Section 5 we will summarize the results for the production of charginos and neutralinos at NLO [4]. The calculation of the LO cross sections has been performed a long time ago [5]. Since in most of the cases the [unphysical] scale dependence of the LO quantities amounts up to about 50%, the determination of the NLO corrections is necessary in order to gain a reliable theoretical prediction, which can be used in present and future experimental analyses.

2 SUSY QCD corrections

2.1 Virtual corrections

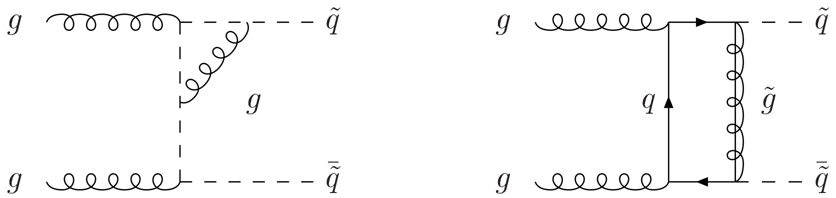

Figure 1: *Typical diagrams of the virtual corrections.*

The one-loop virtual corrections are built up by gluon, gluino, quark and squark exchange contributions [see Fig. 1]. They have to be contracted with the LO matrix elements. The calculation of the one-loop contributions has been performed in dimensional regularization, leading to the extraction of ultraviolet, infrared and collinear singularities as poles in $\epsilon = (4-n)/2$. For the chiral γ_5 coupling we have used the naive scheme, which is well justified in the present analysis at the one-loop level[†]. We have explicitly checked that after summing all virtual corrections no quadratic divergences are left over, in accordance with the general property of supersymmetric theories. The renormalization has been performed by identifying the squark and gluino masses with their pole masses, and defining the strong coupling in the $\overline{\text{MS}}$ scheme including five light flavors in the corresponding β function. The massive particles, i.e. squarks, gluinos and top quarks, have been decoupled by subtracting their contribution at vanishing momentum transfer [6]. In dimensional regularization, there is a mismatch between the gluonic degrees of freedom [d.o.f. $= n-2$] and those of the gluino [d.o.f. $= 2$], so that SUSY is explicitly broken. In order to restore SUSY in the physical observables in the massless limit, an additional finite counter-term is required for the renormalization of the novel $\tilde{q}\tilde{g}\bar{q}$ vertex [7].

[†]We have explicitly checked that the results obtained with a consistent γ_5 scheme are identical to the one with the naive scheme.

2.2 Real corrections

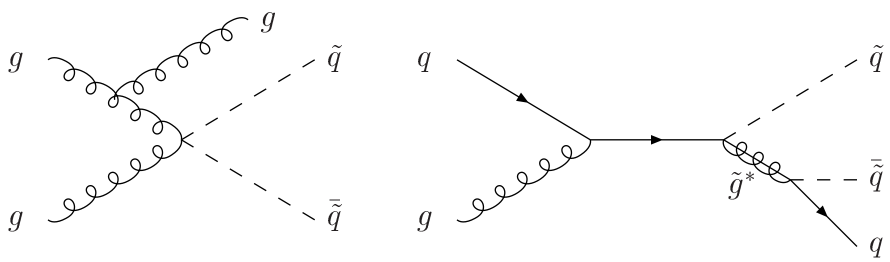

Figure 2: *Typical diagrams of the real corrections.*

The real corrections originate from the radiation of a gluon in all possible ways and from the crossed processes by interchanging the gluon of the final state against a light (anti)quark in the initial state. The phase-space integration of the final-state particles has been performed in $n = 4 - 2\epsilon$ dimensions, leading to the extraction of infrared and collinear singularities as poles in ϵ. After evaluating all angular integrals and adding the virtual and real corrections, the infrared singularities cancel. The left-over collinear singularities are universal and are absorbed in the renormalization of the parton densities at NLO. We defined the parton densities in the conventional $\overline{\mathrm{MS}}$ scheme including five light flavors, i.e. the squark, gluino and top quark contributions are not included in the mass factorization. Finally we end up with an ultraviolet, infrared and collinear finite partonic cross section.

However, there is an additional class of physical singularities, which have to be regularized. In the second diagram of Fig. 2 an intermediate $\tilde{q}\tilde{g}^*$ state is produced, before the [off-shell] gluino splits into a $q\bar{\tilde{q}}$ pair. If the gluino mass is larger than the common squark mass, and the partonic c.m. energy is larger than the sum of the squark and gluino masses, the intermediate gluino can be produced on its mass-shell. Thus the real corrections to $\tilde{q}\bar{\tilde{q}}$ production contain a contribution of $\tilde{q}\tilde{g}$ production. The residue of this part corresponds to $\tilde{q}\tilde{g}$ production with the subsequent gluino decay $\tilde{g} \to \bar{\tilde{q}}q$, which is already contained in the LO cross section of $\tilde{q}\tilde{g}$ pair production, including all final-state cascade decays. This term has to be subtracted in order to derive a well-defined production cross section. Analogous subtractions emerge in all reactions: if the gluino mass is larger than the squark mass, the contributions from $\tilde{g} \to \tilde{q}\bar{q}, \bar{\tilde{q}}q$ have to be subtracted, and in the reverse case the contributions of squark decays into gluinos have to subtracted.

3 Production of Squarks and Gluinos

Squarks and gluinos can be produced via $pp, p\bar{p} \to \tilde{q}\bar{\tilde{q}}, \tilde{q}\tilde{q}, \tilde{q}\tilde{g}, \tilde{g}\tilde{g}$ at hadron colliders. The hadronic squark and gluino production cross sections can be obtained from the partonic ones by convolution with the corresponding parton densities. We have performed the numerical analysis for the upgraded Tevatron and the LHC. For the natural renormalization/factorization scale choice $Q = m$, where m denotes the average mass of the final-state

SUSY particles, the SUSY QCD corrections are large and positive, increasing the total cross sections by 10–90% [2]. This is shown in Fig. 3, where the K factors, defined as the ratios of the NLO and LO cross sections, are presented as a function of the corresponding SUSY particle mass for the LHC. We have investigated the residual scale dependence in LO and

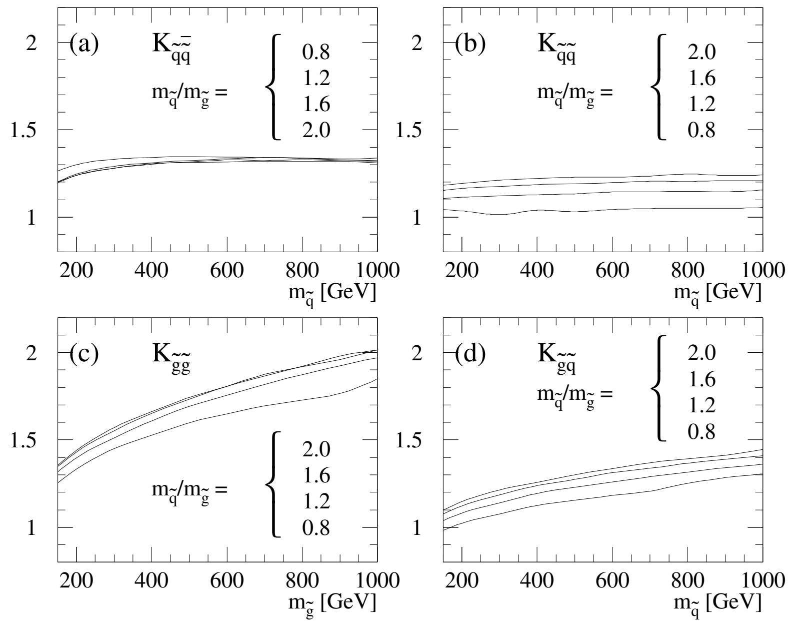

Figure 3: *K factors of the different squark and gluino production cross sections at the LHC* [$\sqrt{s} = 14$ *TeV*]*. Parton densities: GRV94 with* $Q = m$*. Top mass:* $m_t = 175$ *GeV.*

NLO, which is presented in Fig. 4. The inclusion of the NLO corrections reduces the LO scale dependence by a factor 3–4 and reaches a typical level of $\sim 15\%$, which serves as an estimate of the remaining theoretical uncertainty. Moreover, the dependence on different sets of parton densities is rather weak and leads to an additional uncertainty of $\sim 15\%$. In order to quantify the effect of the NLO corrections on the search for squarks and gluinos at hadron colliders, we have extracted the SUSY particle masses corresponding to several fixed values of the production cross sections. These masses are increased by 10–30 GeV at the Tevatron and 10–50 GeV at the LHC, thus enhancing the present and future bounds on the squark and gluino masses significantly. Finally we have evaluated the QCD-corrected transverse-momentum and rapidity distributions for all different processes. As can be inferred from Fig. 5, the modification of the normalized distributions in NLO compared to LO is less than about 15% for the transverse-momentum distributions and much less for the rapidity distributions. Thus it is a sufficient approximation to rescale the LO distributions uniformly by the K factors of the total cross sections.

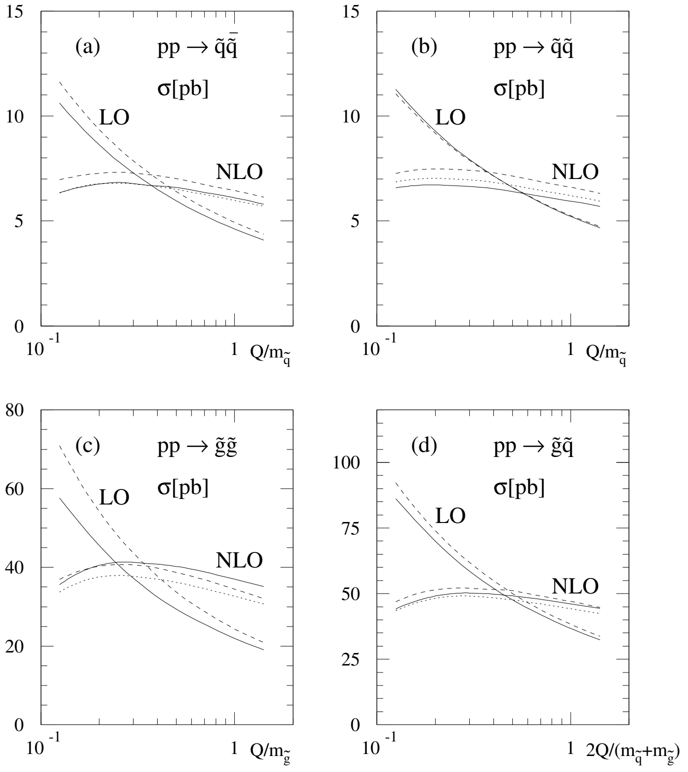

Figure 4: *Scale dependence of the total squark and gluino production cross sections at the LHC in LO and NLO. Parton densities: GRV94 (solid), CTEQ3 (dashed) and MRS(A') (dotted); mass parameters:* $m_{\tilde{q}} = 600$ *GeV,* $m_{\tilde{g}} = 500$ *GeV and* $m_t = 175$ *GeV.*

4 Stop Pair Production

At LO only pairs of $\tilde{t}_1$ or pairs of $\tilde{t}_2$ can be produced at hadron colliders. Mixed $\tilde{t}_1\tilde{t}_2$ pair production is only possible at NLO and beyond. However, we have estimated that mixed stop pair production is completely suppressed by several orders of magnitude and can thus safely be neglected [3]. The evaluation of the QCD corrections proceeds along the same lines as in the case of squarks and gluinos. The strong coupling and the parton densities have been defined in the $\overline{\rm MS}$ scheme with 5 light flavors contributing to their scale dependences, while the stop masses are renormalized on-shell. The QCD corrections increase the cross sections by up to about 40% [see Fig. 6] and thus lead to an increase of the extracted stop masses from the measurement of the total cross section. Moreover, as in the squark/gluino case the scale dependence is strongly reduced [see Fig. 7] and yields an estimate of about 15% of the remaining theoretical uncertainty at NLO. At NLO the virtual corrections depend on the stop mixing angle, the squark, gluino and second stop masses. However, it turns out that these dependences are very weak and can safely be neglected as can be inferred from Fig. 8.

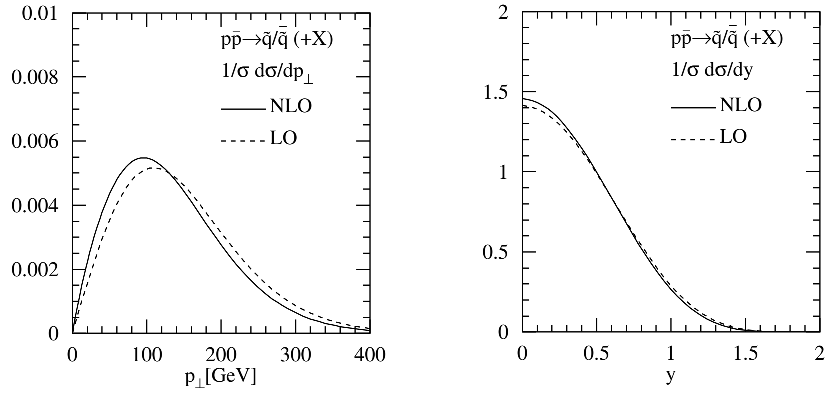

Figure 5: *Normalized transverse-momentum and rapidity distributions of $p\bar{p} \to \tilde{q}\bar{\tilde{q}} + X$ at the upgraded Tevatron [$\sqrt{s} = 2$ TeV] in LO (dotted) and NLO (solid). Parton densities: CTEQ4L (LO) and CTEQ4M (NLO) with $Q = m$; mass parameters: $m_{\tilde{q}} = 250$ GeV, $m_{\tilde{g}} = 300$ GeV and $m_t = 175$ GeV.*

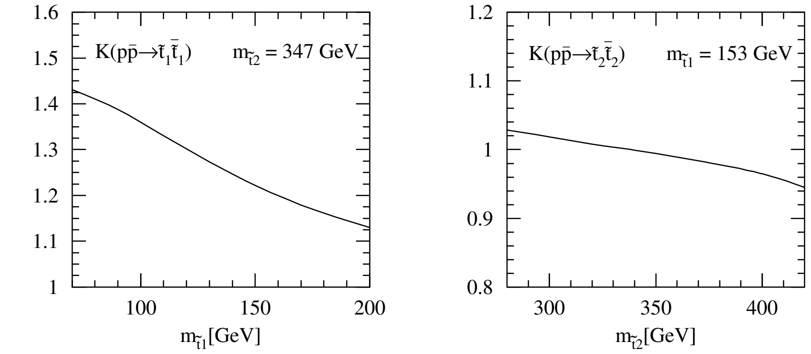

Figure 6: *K factor of the light stop production cross sections at the upgraded Tevatron [$\sqrt{s} = 2$ TeV]. Parton densities: CTEQ4L (LO) and CTEQ4M (NLO) with $Q = m_{\tilde{t}_1}$. Top mass: $m_t = 175$ GeV.*

5 Chargino and Neutralino Production

The production cross sections of charginos and neutralinos depend on several MSSM parameters, i.e. M_1, M_2, μ and $\tan\beta$ at LO [5]. The cross sections are sizeable for chargino/neutralino masses below about 100 GeV at the upgraded Tevatron and less than about 200 GeV at the LHC. Due to the strong dependence on the MSSM parameters the extracted bounds on the chargino and neutralino masses depend on the specific region in the MSSM parameter space [1]. The outline of the determination of the QCD corrections is analogous to the previous cases of squarks, gluinos and stops. The resonance contributions due to $gq \to \tilde{\chi}_i\tilde{q}$ with $\tilde{q} \to q\tilde{\chi}_j$ have to be subtracted in order to avoid double counting with the associated production of gauginos and strongly interacting squarks and gluinos. The parton densities have been defined with 5 light flavors contributing to their scale evolution in the $\overline{\rm MS}$ scheme, while the t-channel squark masses have been renormalized on-shell. The QCD

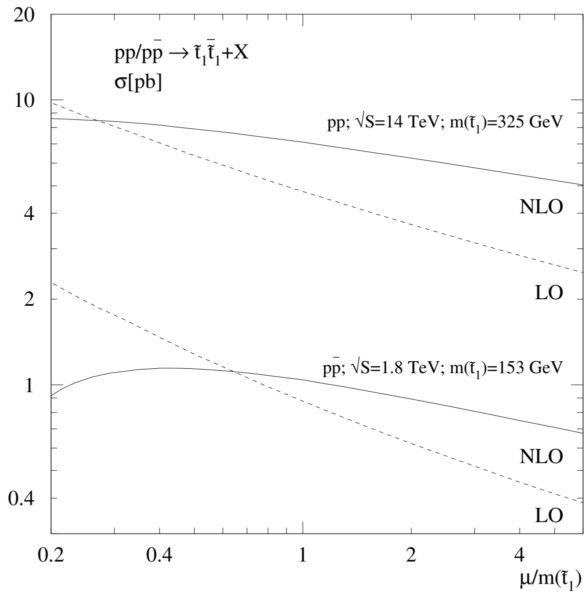

Figure 7: *Scale dependence of the total light stop production cross sections at the Tevatron and LHC in LO and NLO. Parton densities: CTEQ4L (LO) and CTEQ4M (NLO); Top mass:* $m_t = 175$ *GeV.*

corrections enhance the production cross sections of charginos and neutralinos by about 10–40% [see Fig. 9]. The LO scale dependence is reduced to about 10% at NLO [see Fig. 9], which signalizes a significant stabilization of the thoretical prediction for the production cross sections [4]. The dependence of the chargino/neutralino production cross sections on the specific set of parton densities ranges at about 15%.

6 Conclusions

In this work we have reviewed the status of SUSY particle production at hadron colliders at NLO. Most QCD corrections to the production processes are known, thus yielding a nearly complete theoretical status. There are especially large QCD corrections to the production of gluinos, which significantly increase the extracted bounds on the gluino mass from the negative search for these particles at the Tevatron. In all processes, which are known at NLO, the theoretical uncertainties are reduced to about 15%, which should be sufficient for the upgraded Tevatron and the LHC[‡].

Acknowledgements

[‡]The computer code PROSPINO [8] for the production of squarks, gluinos and stops at hadron colliders is available at `http://www.desy.de/~spira`. The NLO production of gauginos and sleptons will be included soon.

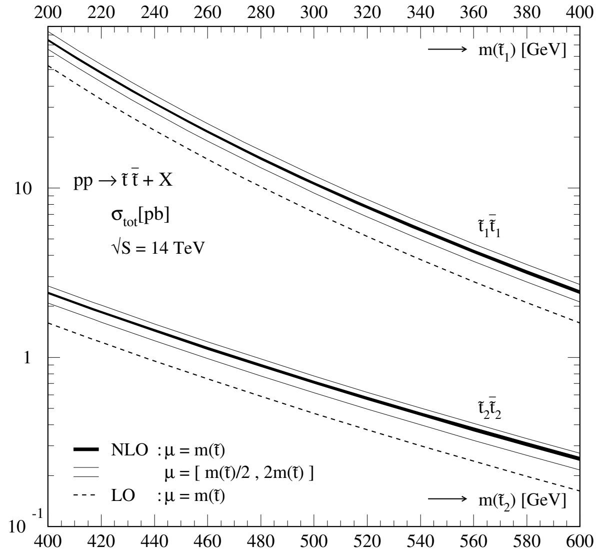

Figure 8: *Production cross sections of the light and heavy stop states at the LHC at LO [dashed] and NLO [solid]. The thickness of the NLO curves represents the dependence of the cross sections on the stop mixing angle and the squark and gluino masses. The shaded NLO bands indicate the theoretical uncertainties due to the scale dependence within* $m_{\tilde{t}}/2 < \mu < 2m_{\tilde{t}}$. *Parton densities: CTEQ4L (LO) and CTEQ4M (NLO); Top mass:* $m_t = 175$ *GeV.*

I would like to thank W. Beenakker, R. Höpker, M. Krämer, M. Klasen, T. Plehn and P.M. Zerwas for their collaboration and the organizers of the Les Houches workshop for the invitation, the pleasant atmosphere and financial support.

References

[1] M. Carena, R.L. Culbertson, S. Eno, H.J. Frisch and S. Mrenna, Rev. Mod. Phys. **71** (1999) 937.

[2] W. Beenakker, R. Höpker, M. Spira and P.M. Zerwas, Phys. Rev. Lett. **74** (1995) 2905, Z. Phys. **C69** (1995) 163, and Nucl. Phys. **B492** (1995) 51.

[3] W. Beenakker, M. Krämer, T. Plehn, M. Spira and P.M. Zerwas, Nucl. Phys. **B515** (1998) 3.

[4] T. Plehn, Ph.D. Thesis, University Hamburg 1998, hep-ph/9803319; W. Beenakker, M. Klasen, M. Krämer, T. Plehn, M. Spira and P.M. Zerwas, Phys. Rev. Lett. **83** (1999) 3780.

[5] G.L. Kane and J.P. Leveillé, Phys. Lett. **B112** (1982) 227; P.R. Harrison and C.H. Llewellyn Smith, Nucl. Phys. **B213** (1983) 223 [Err. Nucl. Phys. **B223** (1983) 542];

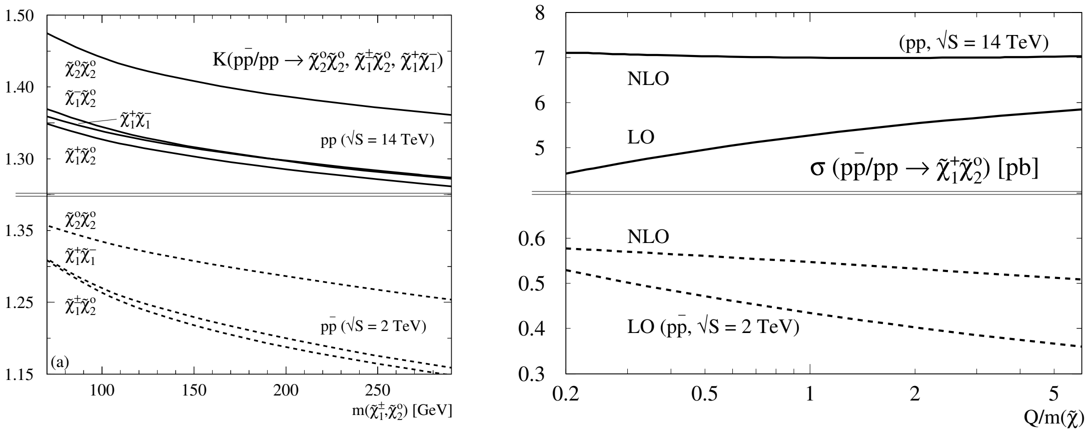

Figure 9: *K factor and scale dependence of the* $\tilde{\chi}_1^+\tilde{\chi}_2^0$ *production cross section at the Tevatron and LHC. Parton densities: CTEQ4L (LO) and CTEQ4M (NLO) with* $Q = m_{\tilde{t}_1}$. *Top mass:* $m_t = 175$ *GeV; SUGRA parameters:* $M_0 = 100$ *GeV,* $A_0 = 300$ *GeV,* $\tan\beta = 4$, $\mu > 0$.

E. Reya and D.P. Roy, Phys. Rev. **D32** (1985) 645; S. Dawson, E. Eichten and C. Quigg, Phys. Rev. **D31** (1985) 1581; H. Baer and X. Tata, Phys. Lett. **B160** (1985) 159.

[6] J. Collins, F. Wilczek and A. Zee, Phys. Rev. **D18** (1978) 242; W.J. Marciano, Phys. Rev. **D29** (1984) 580; P. Nason, S. Dawson and R.K. Ellis, Nucl. Phys. **B303** (1988) 607.

[7] S.P. Martin and M.T. Vaughn, Phys. Lett. **B318** (1993) 331; I. Jack and D.R.T. Jones, preprint LTH–400, hep-ph/9707278, in 'Perspectives in Supersymmetry', ed. G. Kane, Singapore 1997.

[8] W. Beenakker, R. Höpker and M. Spira, hep-ph/9611232.

Comparison of exact matrix element calculations with ISAJET and PYTHIA in case of degenerate spectrum in the MSSM

S. ABDULLIN, V. ILYIN AND T. KON

Abstract

We calculate the transverse momentum distribution of additional partons from $pp \to \tilde{g}\tilde{g} + X$ with $m_{\tilde{g}} = 1.2$ TeV at $\sqrt{s}$=14 TeV. The calculations are carried out with exact $2 \to 3$ matrix element generators CompHEP and GRACE, and widely used physics generators ISAJET and PYTHIA. In the latter cases only $2 \to 2$ subprocesses are included and additional partons originate mainly from initial and final states radiation. The results obtained by CompHEP and GRACE are in perfect agreement in the whole region of p_T (10 – 2000 GeV) of interest. The comparison with p_T distributions produced by ISAJET and PYTHIA does not show significant difference. ISAJET tends to overshoot for p_T values in the region of 200-900 GeV, while PYTHIA's distribution has quite a good agreement with exact ME calculations.

One of the main purposes of the LHC collider is to search for physics beyond the Standard Model (SM), in particular to look for superpartners of ordinary particles expected in SUperSYmmetric extensions of the SM (SUSY). SUSY, if it exists, is expected to reveal itself at the LHC firstly via an excess of $(multilepton+)$ $multijet$ + E_T^{miss} final states compared to Standard Model (SM) expectations [1, 2]. The bulk of these studies was carried out in the framework of the Minimal SuperSymmetric Model (MSSM), or the Supergravity-inspired subset of MSSM, minimal SUGRA (mSUGRA) with universal gaugino mass and corresponding mass hierarchy.

Unfortunately even in the framework of the MSSM one can expect scenarios with non-universal gaugino mass leading to some "pathological" SUSY cases which are difficult to observe due to a "degenerate" mass spectrum [3]. For instance, it is quite obvious that there are no visible objects in the SUSY event if $m_{\tilde{\chi}_1^0} \approx m_{\tilde{g}} \approx m_{\tilde{q}} = M_{SUSY}$. In this case one can rely mainly on observation of jet activity which is additional to sparticle pair production. The idea is that additional high p_T recoil partons can provide a clear $E_T^{miss} + jet(s)$ signature to observe the excess of SUSY events over SM expectations.

Our preliminary estimates of the MSSM signal generated with ISAJET [4] show that the limit of visibility (at the 5 σ level) in the MSSM is about 1.2 – 1.3 TeV with integrated luminosity of 100 fb^{-1} for $m_{\tilde{\chi}_1^0} \approx m_{\tilde{g}} \ll m_{\tilde{q}}$, thus much smaller than the squark-gluino mass reach ($\geq$ 2.5 TeV) in mSUGRA with the same integrated luminosity [2].

It is well known that data bases in ISAJET and PYTHIA [5] contain matrix elements only for $2 \to 2$ subprocesses. So, additional partons can be produced only *via* initial and final state radiation (ISR/FSR parton showering). If one discusses production of hard partons, this mechanism is an approximation with *a priori* unknown precision. From a general point of view this approximation should underestimate the result obtained within the perturbative QCD theory through evaluation of the complete set of relevant Feynman diagrams. Thus, one might assume that there will be a substantial number of events with high p_T of the heavy

SUSY system recoiling against observable jet(s), larger than predicted by the parton showering mechanism in ISAJET and PYTHIA. We use the packages CompHEP [6] and GRACE [7] to evaluate $2 \to 3$ matrix elements in leading order and calculate the distributions. Finally we compare these results with ones obtained with ISAJET and PYTHIA.

Calculational details

To make a coherent calculation we choose a set of parameters as follows:

- gluino mass $m_{\tilde{g}} = 1.2$ TeV;
- common squark mass $m_{\tilde{q}} = 100$ TeV (10 TeV for PYTHIA) to neglect squark contributions;
- CTEQ4M set of structure functions;
- $Q^2 = 4m_{\tilde{g}}^2$ (in PYTHIA $Q^2 = (m_{\perp 1}^2 + m_{\perp 2}^2)/2$);
- NLO running strong coupling with normalization $\alpha_S(M_Z) = 0.118$, so $\alpha_S(2400\ \mathrm{GeV}) = 0.0817$.

We use ISAJET 7.44 and PYTHIA 6.125 with multiple interactions switched off. We treat the jet in ISAJET/PYTHIA not as the single hardest final state parton, but use the final state parton list (excluding the two gluinos) as input to an iterative cone jet finder algorithm ($R_{cone} = 0.5$) to find a group of partons forming parton-level jets.

In CompHEP and GRACE we calculate exact tree level matrix elements for the subprocesses :

$$gg \to \tilde{g}\tilde{g} + g; \quad gq(Q) \to \tilde{g}\tilde{g} + q(Q); \quad qQ \to \tilde{g}\tilde{g} + g;$$

which were convoluted with the CTEQ4m parton distributions to get LHC cross sections and distributions. The q (Q) terms stand for quarks (antiquarks) of the first five flavours: u, d, c, s and b.

We ask the final (additional) parton, gluon or quark, to radiate within the typical ATLAS and CMS rapidity, $|\eta_j| < 4.5$, and to be hard enough, $E_T^j > 10$ GeV. No cuts are applied on the gluino pair.

Results and Conclusions

The cross section of the process $pp \to \tilde{g}\tilde{g} + jet$ within cuts on the jet turns out to be rather high, about 120 fb, with the following contributions from different channels :

$$\sigma_{gg} = 78.9\ \mathrm{fb}; \quad \sigma_{gq(Q)} = 21.9\ \mathrm{fb}; \quad \sigma_{qQ} = 20.0\ \mathrm{fb}.$$

We found that the shapes of the p_T distributions are quite different in these three cases, see Fig.1. Indeed, one can expect that the qQ channel produces less events than the gg

contribution, due to the dominance of the gluon component in the proton for small x. However, one can see that the $gq(Q)$ curve is higher than the gluon-gluon one for $p_T > 400$ GeV, being much smaller even than qQ at the soft end. Note that the set of topologies of Feynman diagrams is the same in all three channels. So, the observed difference connects surely with different interplay of contributions of vector and spinor virtual particles.

In Fig.2 the p_T distribution for $pp \to \tilde{g}\tilde{g} + jet$ is given as a sum of the three channels discussed above. The CompHEP/GRACE result is represented by solid histograms, ISAJET by dashed histograms and PYTHIA by dot-dashed ones. One can see that the PYTHIA distribution underestimates the *exact ME* result smoothly. Of course this (almost constant) difference can be explained (corrected) by a different setting of some QCD switches. At the same time one can see a more pronounced deviation from the *exact ME* in the shape of the ISAJET curve. In particular at moderate p_T ($\sim 200 - 900$ GeV) ISAJET overestimates the *exact ME* result. One can also see that for very high transverse momenta (≥ 1200 GeV for ISAJET and 1400 GeV for PYTHIA) the *parton showering* approximation is too crude.

Coming back to the initial idea to look at additional jet activity with high p_T recoiling against the heavy SUSY system one can conclude that parton shower approximation works well enough up to very high values of transverse momenta. Therefore, unfortunately one can not find room for sizable improvements of *parton shower* predictions by using exact matrix elements in the process discussed.

Some interesting discrepancy is observed in the region of relatively small transverse momenta, $p_T < 150$ GeV, where ISAJET and PYTHIA produce much weaker (by a factor of 2-3) jet activity than CompHEP/GRACE. However, this region is sensitive to higher order corrections (in particular due to resummation of large logarithms of $p_T/m_{\tilde{g}}$), thus a more careful analysis is necessary to get reliable conclusions.

References

[1] H. Baer, C.-H. Chen, F. Paige and X. Tata, Phys. Rev. **D52** (1995) 2746; Phys. Rev. **D53** (1996) 6241; CMS collaboration (S. Abdullin *et al.*), CMS NOTE 1998/006, hep–ph/9806366.

[2] S. Abdullin and F. Charles, Nucl. Phys. **B547** (1999) 60.

[3] S. Bituykov and N. Krasnikov, hep–ph/9901398, hep-ph/9907257.

[4] F.E. Paige et al., *ISAJET 7.40: a Monte Carlo event generator for pp, $\bar{p}p$, and e^+e^- reactions*, BNL-HET-98-39, Oct 1998, hep–ph/9810440.

[5] T. Sjöstrand, Comp. Phys. Commun. **82** (1994) 74.

[6] E.E. Boos et al, hep-ph/9503280; A.E. Pukhov et al, *CompHEP user's manual, v.3.3*, Preprint INP MSU 98-41/542, 1998, hep-ph/9908288; A. Semenov, Comp. Phys. Commun. **115** (1998) 124.

[7] T. Tanaka, T. Kaneko and Y. Shimizu, Comp. Phys. Commun. **64** (1991) 149; T. Ishikawa et al, *GRACE manual*, KEK Report 92-19, 1993; H. Tanaka et al, Nucl. Instrum. Meth. **A389** (1997) 295.

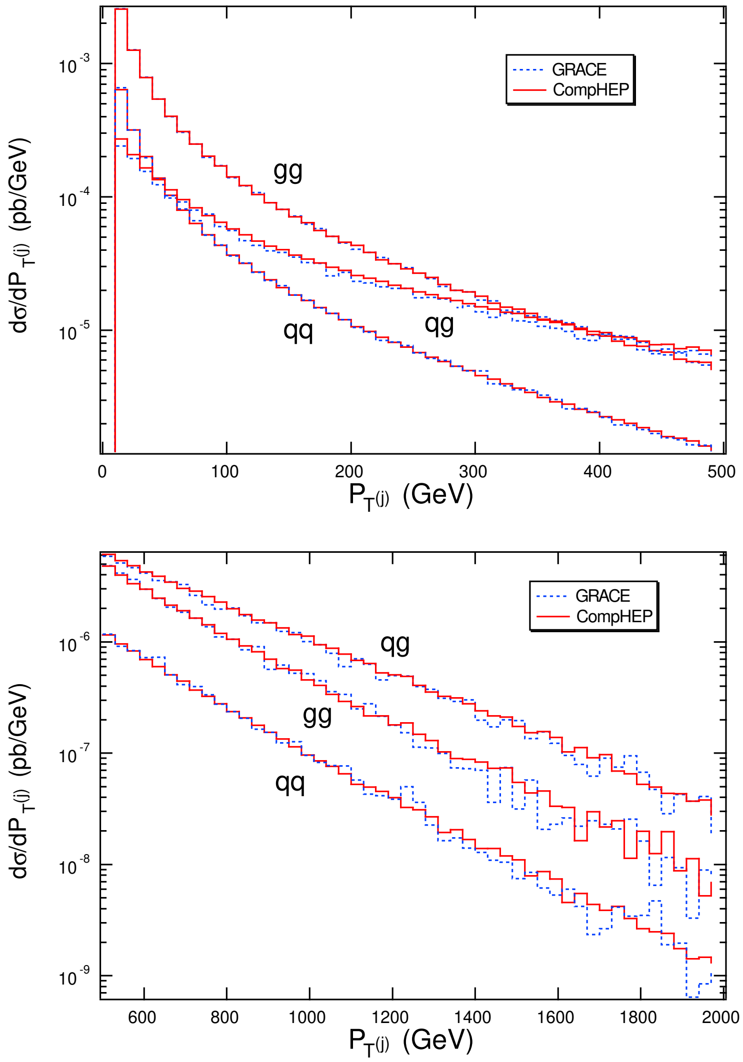

Figure 1: Contribution of different channels to the p_T distribution of the additional jet in $pp \to \tilde{g}\tilde{g} + X$, calculated with CompHEP and GRACE.

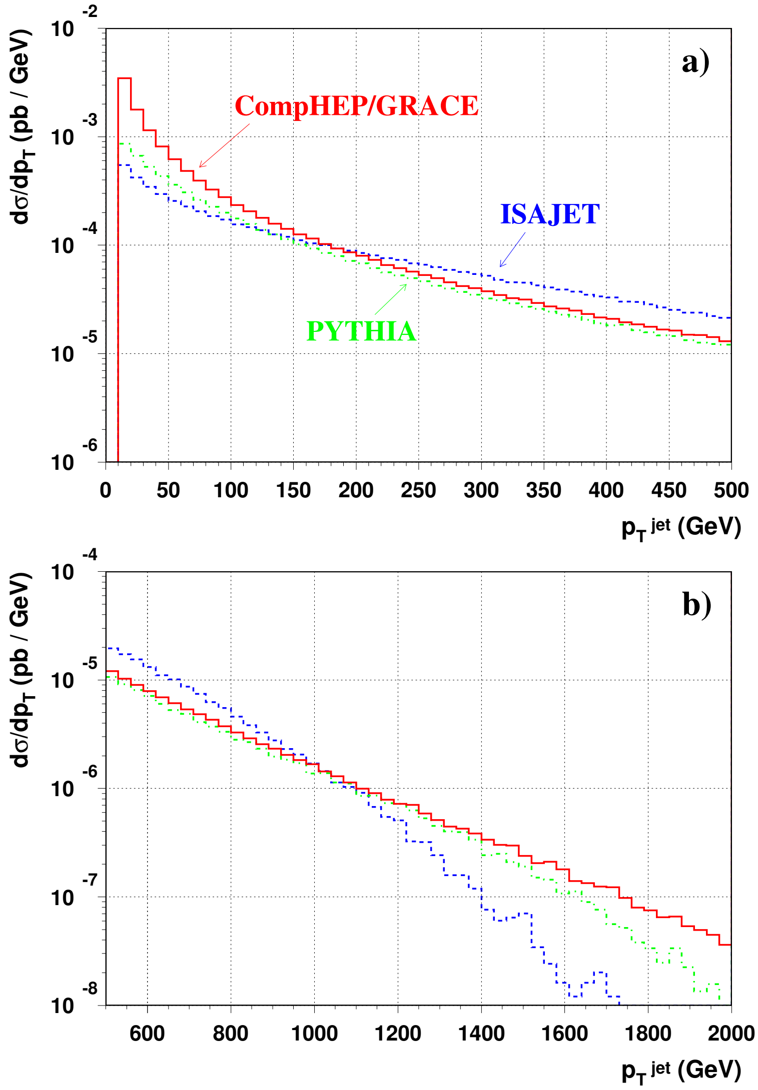

Figure 2: P_T distribution of the additional jet in $pp \to \tilde{g}\tilde{g} + X$, calculated with different packages.

The finite width effect on neutralino production

T. KON, Y. KURIHARA, M. KURODA AND K. ODAGIRI

It has been proposed in [1] that neutralino mass differences can be determined fairly accurately through the μ-pair invariant mass distribution $d\sigma/dM_{\mu\mu}$ of the process

$$pp \to \tilde{\chi}_1^+ \tilde{\chi}_2^0 X \to \tilde{\chi}_1^+ (\mu\tilde{\mu}) X \to \tilde{\chi}_1^+ \mu(\tilde{\chi}_1^0 \mu) X, \tag{1}$$

as the distribution exhibits a sharp decrease at its kinematic endpoint. When, however, the width of the neutralino is taken into account, the smearing of the cross section might make this observation obsolete and less appealing for the determination of the neutralino mass. Therefore, it is important to know to what extent the width of neutralino makes the mass determination less accurate.

We have investigated this problem by comparing the muon-pair invariant mass distribution in the following three cases.
(case 1) Zero width approximation for $\tilde{\chi}_2^0$. Only those diagrams which proceed via the chain decay (1) are taken into account.
(case 2) Same as (1) but finite width of $\tilde{\chi}_2^0$ is used. Only those diagrams that proceed via resonances as shown in (1) are considered.
(case 3) Finite width of $\tilde{\chi}_2^0$ as well as the entire set of diagrams (165 diagrams in unitary gauge) that creates the final state $\tilde{\chi}_1^+ \tilde{\chi}_1^0 \mu\mu$ are taken into account. The diagrams which are considered in case 3 but not in case 2 constitute the background to this process.

In the numerical evaluation of the muon pair distribution, we have used the following set of SUSY parameters,

$$\tan\beta = 12, \qquad M_2 = 200GeV, \qquad \mu = -500GeV, \tag{2}$$

which results in the following masses for charginos and neutralinos,

$$m_{\tilde{\chi}_i^0} = (97, 197, 507, 511), \tag{3}$$
$$m_{\tilde{\chi}_i^+} = (197, 514). \tag{4}$$

In particular, in the present set of parameters we are considering, $\tilde{\chi}_1^0$ is almost purely bino (the SUSY partner of the $U(1)$ gauge boson, B_μ), while $\tilde{\chi}_2^0$ is almost purely neutral wino (the SUSY partner of the neutral $SU(2)_L$ gauge-boson, W_3^μ). As for the slepton masses, we have used the common mass $m_{\tilde{\ell}} = 150$ GeV.

Assuming that other SUSY particles are heavy so that $\tilde{\chi}_2^0$ decays dominantly into $\ell\tilde{\ell}$, we have evaluated the width of $\tilde{\chi}_2^0$ as

$$\Gamma_{\tilde{\chi}_2^0} = 1.25GeV. \tag{5}$$

The process is described by the subprocess

$$q\bar{q}' \to \tilde{\chi}_1^+ \tilde{\chi}_2^0 \to \tilde{\chi}_1^+ (\mu\tilde{\mu}) \to \tilde{\chi}_1^+ \mu(\tilde{\chi}_1^0 \mu). \tag{6}$$

For the quark distribution functions, we have used QTEC-3D [2].

The numerical evaluation was performed by `HERWIG` [3] in case 1 and case 2, while the case 3 was calculated by `GRACE` [4].

Results are shown in Fig.1(a) and (b), where the distributions of the invariant mass $M_{\mu\mu}$ in the second neutralino decay are shown. In Fig.1(a), the dashed line represents the zero width approximation (case 1), the dotted line represents the distribution for the finite $\tilde{\chi}_2^0$ width but with only the resonance diagrams (case 2), while the solid line represents the distribution for the finite $\tilde{\chi}_2^0$ width and full set of diagrams which give the final states $\tilde{\chi}_1^+\tilde{\chi}_1^0\mu\mu$ (case 3). We show a detailed comparison between case 2 and case 3 around the end point region of $M_{\mu\mu}$ in Fig.1(b). As one sees from the figures, the edge of the distribution at the end point of the phase space remains, although it is broadened by the finite width effect. As a result, the exact position of the end point acquires an ambiguity of about 5 GeV, although the precision of mass determination, which may additionally make use of the shape of the distribution, can presumably be made much less than this. A full analysis will need to take into account the experimental resolutions and signal selection efficiency, and this is beyond the scope of our study. The total cross section of the signal process (1) is 0.015 pb.

Acknowledgements One of the authors, K.O., would like to thank Drs. J. Kanzaki and P. Richardson for their computing help.

References

[1] I. Hinchliffe, F.E. Paige, M.D. Shapiro, J. Soderqvist and W. Yao, Phys. Rev. **D55**, 5520 (1997).

[2] H. Plothow-Besch, Comput. Phys. Commun. **75**, 396 (1993).

[3] G. Corcella, I.G. Knowles, G. Marchesini, S. Moretti, K. Odagiri, P. Richardson, M.H. Seymour and B.R. Webber, hep–ph/9912396.

[4] T.Tanaka, T.Kaneko and Y.Shimizu, Comp. Phys. Commun. **64**, 149 (1991); T.Ishikawa et al, *GRACE manual*, KEK Report 92-19, 1993; H.Tanaka et al, Nucl. Instrum. Meth. **A389**, 295 (1997).

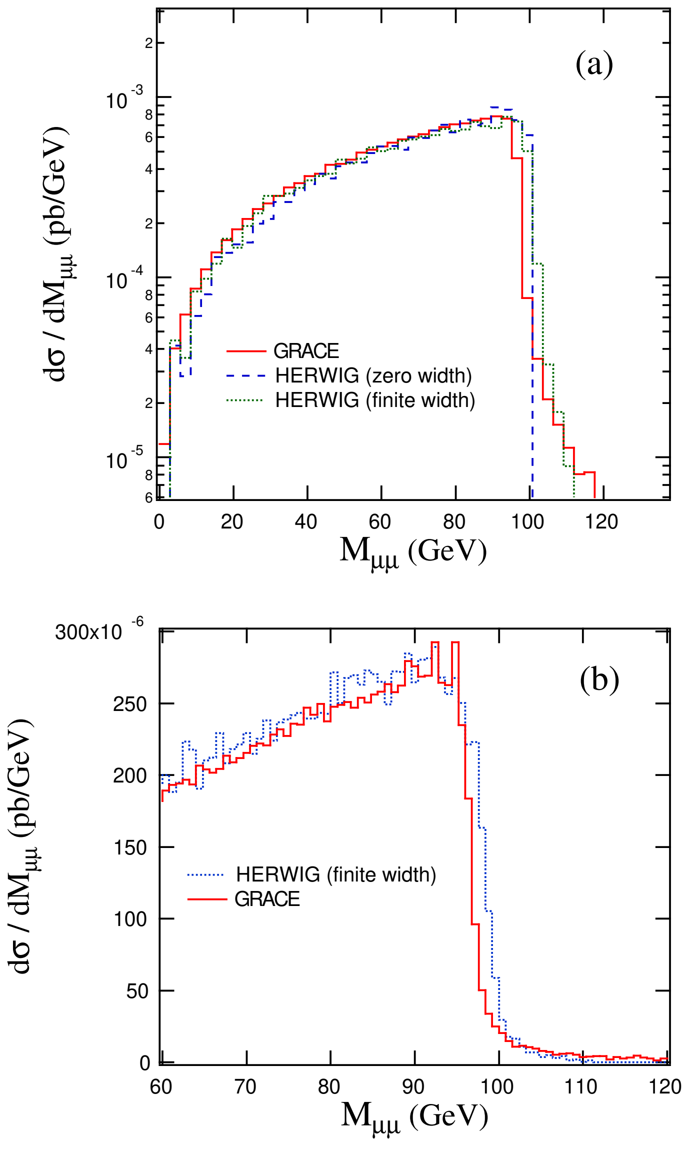

Figure 1: Distribution of the invariant mass $M_{\mu\mu}$ in the second neutralino decay from the $\tilde{\chi}_1^+\tilde{\chi}_2^0$ associated production. In (a) a comparison is made among the full calculation using `GRACE` (continuous line, case 3), the calculation with `HERWIG` assuming a narrow width and an isotropic decay (dashed line, case 1), and another calculation using `HERWIG` incorporating a finite $\tilde{\chi}_2^0$ width (dotted line, case 2). (b) corresponds to the detailed comparison between case 2 and case 3 around the end point region of $M_{\mu\mu}$.

Width effects in slepton production $e^+e^- \to \tilde{\mu}_R^+ \tilde{\mu}_R^-$

H.-U. MARTYN

Abstract

A case study will be presented to investigate width effects in the precise determination of slepton masses at the e^+e^- TESLA Linear Collider.

1 Introduction

If supersymmetry will be discovered in nature a precise measurement of the particle spectrum will be very important in order to determine the underlying theory. The potential of the proposed TESLA Linear Collider [1] with its high luminosity and polarization of both $e^\pm$ beams will allow to obtain particle masses with an accuracy of 10^{-3} or better [2]. At such a precision width effects of primary and secondary particles may become non-negligible.

The present case study is based on a particular R-parity conserving mSUGRA scenario, also investigated in the ECFA/DESY Study [3], with parameters $m_0 = 100$ GeV, $m_{1/2} = 200$ GeV, $A_0 = 0$ GeV, $\tan\beta = 3$ and $\mathrm{sgn}(\mu) > 0$. The particle spectrum is shown in fig. 1. Typical decay widths of the scalar leptons are expected to be $\Gamma \sim 0.3 - 0.5$ GeV, while the widths of the light gauginos, decaying into 3-body final states, are (experimentally) negligible.

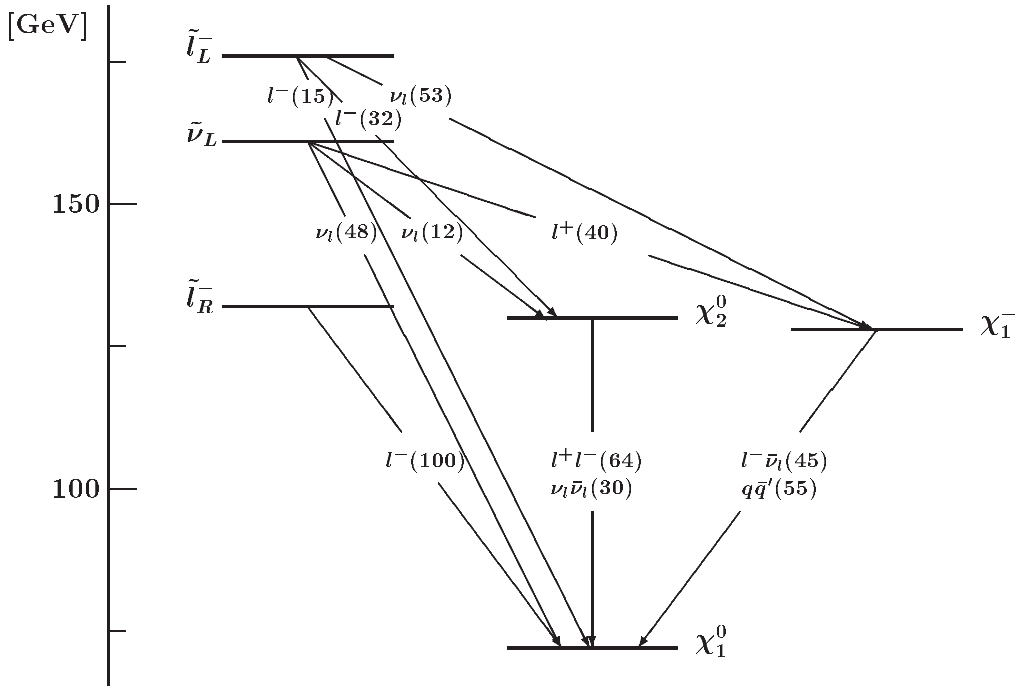

Figure 1: Mass spectrum and decay modes of sleptons and light gauginos

This note presents, as an example, a simulation of right scalar muon production

$$
\begin{aligned}
e^-_R e^+_L &\to \tilde{\mu}^-_R \tilde{\mu}^+_R \,, \\
&\to \mu^- \chi^0_1 \mu^+ \chi^0_1 \,.
\end{aligned} \tag{1}
$$

The analysis is based on the methods and techniques described in a comprehensive study of the same SUSY spectrum [4]. The detector concept, acceptances and resolutions are taken from the TESLA Conceptual Design Report [1]. Events are generated with the Monte Carlo program PYTHIA 6.115 [5], which includes the width of supersymmetric particles as well as QED radiation and beamstrahlung [6]. It is assumed that both beams are polarized, right-handed electrons to a degree of $\mathcal{P}_{e^-_R} = 0.80$ and left-handed positrons by $\mathcal{P}_{e^+_L} = 0.60$. A proper choice of polarizations increases the cross section by a factor of ~ 3 and reduces the background substantially, e.g. by more than an order of magnitude for Standard Model processes.

2 Mass determinations

Scalar muons $\tilde{\mu}_R$ are produced in pairs via s channel γ and Z exchange and decay into an ordinary muon and a stable neutralino χ^0_1 (LSP), which escapes detection. The experimental signatures are two acoplanar muons in the final state with large missing energy and nothing else in the detector. Simple selection criteria [1] (essentially cuts on acollinearity angle and missing energy) suppress background from W^+W^- pairs and cascade decays of higher mass SUSY particles and result in detection efficiencies around $\sim 70\%$.

Two methods to determine the mass of $\tilde{\mu}_R$ will be discussed: (i) a threshold scan of the pair production cross section, and (ii) a measurement of the energy spectrum of the decay muons, which simultaneously constrains the mass of the primary smuon and the secondary neutralino. The particle mass parameters given by the chosen SUSY model are $m_{\tilde{\mu}_R} = 132.0$ GeV, $\Gamma_{\tilde{\mu}_R} = 0.310$ GeV and $m_{\chi^0_1} = 71.9$ GeV.

2.1 Threshold scan

Cross section measurements close to production threshold are relatively simple. One essentially counts additional events with a specific signature, here two oppositely charged, almost monoenergetic muons, over a smooth background. The cross section for slepton pair production rises as $\sigma \propto \beta^3$, where $\beta = \sqrt{1 - 4\, m^2_{\tilde{\mu}_R}/s}$ is the velocity related to the $\tilde{\mu}_R$ mass. The excitation curve as a function of the cms energy, including effects due to QED initial state radiation and beamstrahlung, is shown in figure 2. The sensitivity to the width $\Gamma_{\tilde{\mu}_R}$ is most pronounced close to the kinematic production limit and diminishes with increasing energy. A larger width 'softens' the rise of the cross section with energy. Fits to various mass and/or width hypotheses are performed by simulating measurements with a total integrated luminosity of 100 fb^{-1} distributed over 10 equidistant points around $\sqrt{s} = 264 - 274$ GeV. The data may be collected within a few months of TESLA operation.

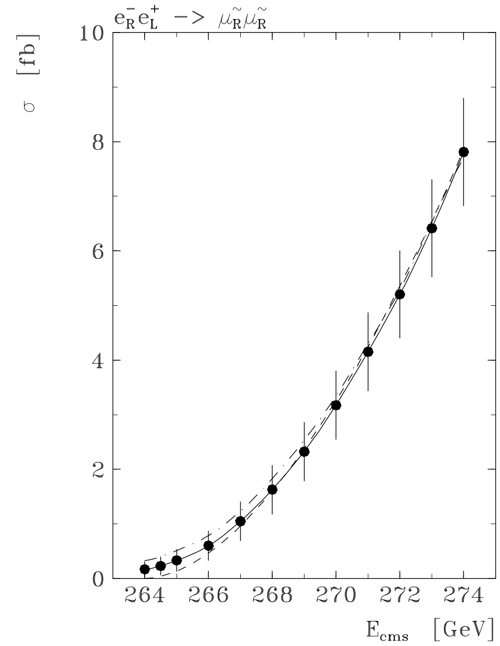

Figure 2: Observable cross section near threshold of the reaction $e^-_R e^+_L \to \tilde{\mu}_R \tilde{\mu}_R$ including QED radiation and Beamstrahlung. Curves assume a mass $m_{\tilde{\mu}_R} = 132.0$ GeV and width $\Gamma_{\tilde{\mu}_R}$ of 310 MeV (full curve), 0 MeV (dashed curve) and 620 MeV (dashed-dotted curve). Measurements correspond to $\mathcal{L} = 10$ fb^{-1} per point.

Taking the width from the model prediction $\Gamma_{\tilde{\mu}_R} = 310$ MeV, a fit to the threshold curve gives a statistical accuracy for the smuon mass of $\delta m_{\tilde{\mu}_R} = 90$ MeV. This error is considerably smaller than the expected width. A two-parameter fit yields $m_{\tilde{\mu}_R} = 132.002 \; ^{+0.170}_{-0.130}$ GeV and $\Gamma_{\tilde{\mu}_R} = 311 \; ^{+560}_{-225}$ MeV. However, both parameters are highly correlated with a correlation coefficient of 0.95. Finally, if one may fix the $\tilde{\mu}_R$ mass from another measurement, the width can be determined to $\delta\Gamma_{\tilde{\mu}_R} = \pm 190$ MeV. It should be noted that the scan procedure and choice of energy points is by no means optimized. Possibilities to reduce the correlations should be studied.

2.2 Energy spectrum of $\mu^\pm$

For energies far above threshold, the kinematics of the decay chain of reaction (1) allows to identify and to reconstruct the masses of the primary and secondary sparticles. The isotropic decays of the scalar muons lead to a flat energy spectrum of the observed final $\mu^\pm$ in the laboratory frame. The endpoints of the energy distribution are related to the masses of the $\tilde{\mu}_R$ and χ^0_1 via

$$\frac{m^2_{\tilde{\mu}} - m^2_{\chi^0}}{2\,(E_{\tilde{\mu}} + p_{\tilde{\mu}})} \;\leq\; E_\mu \;\leq\; \frac{m^2_{\tilde{\mu}} - m^2_{\chi^0}}{2\,(E_{\tilde{\mu}} - p_{\tilde{\mu}})}\;. \tag{2}$$

In practice the sharp edges of the energy spectrum will be smeared by effects due to detector resolution, selection criteria and in particular initial state radiation and beamstrahlung. The results of a simulation at $\sqrt{s} = 320$ GeV assuming an integrated luminosity of 160 fb^{-1} are shown in figure 3. One observes a clear signal from $\tilde{\mu}_R$ pair production above a small background of cascade decays $\chi_2^0 \to \mu^+\mu^-\chi_1^0$ from the reaction $e_R^- e_L^+ \to \chi_2^0\chi_1^0$. Contamination from chargino or W pair production is completely negligible.

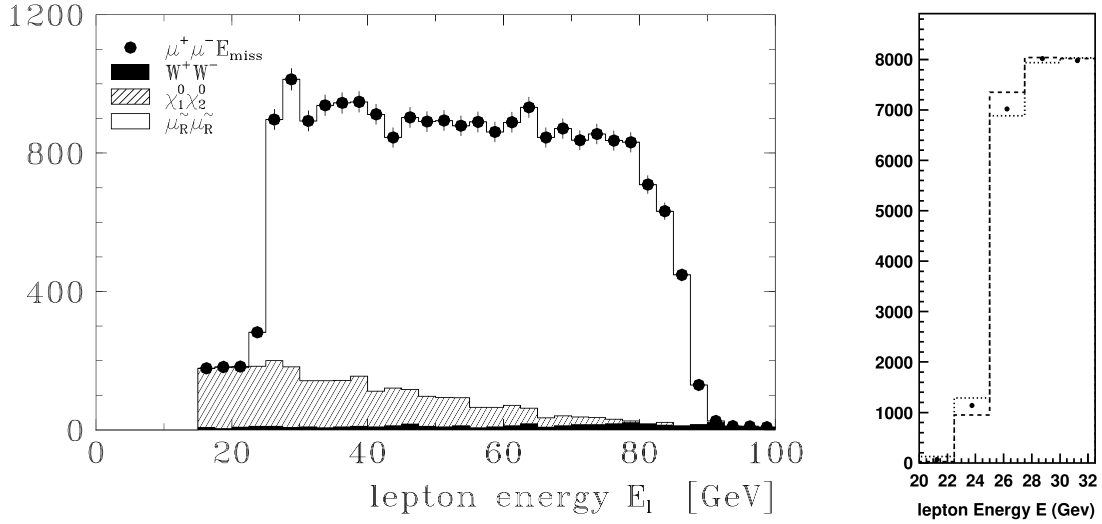

Figure 3: **Left:** Energy spectrum of di-muon events from the reaction $e_R^- e_L^+ \to \tilde{\mu}_R\tilde{\mu}_R$ and the background $e_R^- e_L^+ \to \chi_1^0\chi_2^0$ at $\sqrt{s} = 320$ GeV assuming $\mathcal{L} = 160$ fb^{-1}. **Right:** Lower endpoint region of the μ energy spectrum illustrating the effect of various widths $\Gamma_{\tilde{\mu}_R}$ of 310 MeV (dots), 0 MeV (dashed) and 620 MeV (dotted) using the tenfold luminosity.

A two-parameter fit to the μ energy spectrum yields masses of $m_{\tilde{\mu}_R} = 132.0 \pm 0.3$ GeV and $m_{\chi_1^0} = 71.9 \pm 0.2$ GeV. The statistical accuracy is of the same size as the expected width of the scalar muon. Choosing a different width $\Gamma_{\tilde{\mu}_R}$ in the simulation modifies essentially the μ energy spectrum at the low endpoint and has little impact at higher energies. This is illustrated in figure 3, right part, which compares the lower part of the spectrum with the predictions of width zero and twice the expected value. The sharp rise is getting smeared out with increasing width. With the anticipated luminosity of 160 fb^{-1} it may be feasible to distinguish these cases.

2.3 Production of other sparticles

It should be noted that estimates on the sensitivity of width effects in other slepton production channels can be obtained from the above results by scaling the cross section and taking the branching ratios into final states into account. Thus one expects e.g. a gain by a factor of $\sim$2 for selectron $\tilde{e}_R$ and sneutrino $\tilde{\nu}_e$ pair production. For the higher mass chargino $\chi_2^\pm$ and neutralinos $\chi_{3,4}^0$ mass resolutions of $\sim 0.25 - 0.50$ GeV may be obtained from threshold scans [4], where the cross sections rise as $\sigma \propto \beta$. The corresponding widths are expected to be $\sim 2-5$ GeV (two-body decays in a gauge boson and gaugino) and have certainly to be considered.

3 Conclusions

The high luminosity of TESLA allows to study the production and decays of the accessible SUSY particle spectrum. Polarization of both e^- and e^+ beams is very important to optimize the signal and suppress backgrounds. A simulation of slepton production $e^+e^- \to \tilde{\mu}_R^+\tilde{\mu}_R^-$ shows that for precision mass measurements with an accuracy of $\mathcal{O}(100$ MeV$)$ the widths of the primary particles have to be taken into account. Finally, it is worth noting that the anticipated mass resolutions from threshold scans or lepton energy spectra can only be obtained if beamstrahlung effects are well under control.

References

[1] 'Conceptual Design of a 500 GeV e^+e^- Linear Collider', eds. R. Brinkmann et al., DESY 1997-048 and ECFA 1997-182.

[2] E. Accomando et al., Phys. Rep. 299 (1998) 1.

[3] 2^{nd} ECFA/DESY Study on Physics and Detectors for a Linear e^+e^- Collider, http://www.desy.de/conferences/ecfa-desy-lc98.html

[4] H.-U. Martyn and G.A. Blair, hep-ph/99104161.

[5] T. Sjöstrand, Comp. Phys. Comm. 82 (1994) 74.

[6] T. Ohl, Comp. Phys. Comm. 101 (1996) 269.

Radiative Effects on Squark Pair Production at e^+e^- Colliders

M. DREES, O.J.P. ÉBOLI, R.M. GODBOLE AND S. KRAML

Abstract

We study the impact of various radiative effects on the kinematic reconstruction of squark pair events at future e^+e^- colliders. We focus on the simplest case where both squarks decay directly into a stable neutralino, but include both photon radiation off the initial state and gluon radiation during the production and/or decay of the squarks. These effects change the shapes of the distributions used to determine the squark mass; they can therefore also introduce additional systematic uncertainties.

Among the advantages of e^+e^- colliders over hadron colliders are the fairly well defined center–of–mass energy in hard (annihilation) events, and the comparative cleanliness of the environment. Taken together, these properties make the kinematic reconstruction of e^+e^- events much easier than that of comparable events at hadron colliders. In particular, experiments at e^+e^- colliders should be able to measure the masses of new particles (with unsuppressed electroweak couplings) with an error of 1% or less [1], either through threshold scans, or through fitting kinematic distributions of events well above threshold. The latter method is more versatile, since the same data set can well contain several kinds of "new physics" events, which can be separated from each other (and from backgrounds) using kinematical cuts. Moreover, kinematical reconstruction allows to determine not only the masses of the new particles produced in the primary interaction, but also those of their decay products.

However, in order to correctly interpret the information contained in various distributions one needs an accurate model of the final state. In particular, if one wants to achieve errors of 1% or less, various radiative effects have to be taken into account. These are of special importance if the new particles and/or their decay products have strong interactions, since a significant fraction of all signal events will then contain hard gluons. Here we study the impact of these radiative effects on the measurement of squark masses at e^+e^- colliders. Squarks are the currently most plausible new particles that have both strong and electroweak interactions.

In the last few years considerable progress has been made [2] in the accurate calculation of total cross sections for squark pair production and of squark branching ratios. In particular, one–loop corrections to these quantities from both ordinary QCD and SUSY QCD, as well as from Yukawa interactions, are now known. These have been used [3] to estimate the error with which the squark mass can be extracted from a measurement of the total squark pair production cross section times branching ratio into a given final state. However, in such a "dynamical" determination of the squark mass one has to assume values for all the other input parameters that affect the cross section times branching ratio. These include the gluino mass and, for third generation squarks, also the masses and mixing angles of squarks, charginos, neutralinos, and Higgs bosons [2].

In contrast, relatively little attention has been paid to the kinematical determination of squark masses at e^+e^- colliders. The pioneering work by Feng and Finnell [4] investigates the usefulness of various kinematical distributions, and concludes that experiments at a 500 GeV collider should be able to determine the mass of 200 GeV squarks with an error of $\leq 0.5\%$ using just 20 fb^{-1} of data, if all squarks decay directly into a massless quark and an invisible (stable or long–lived) neutralino $\tilde{\chi}_1^0$. However, their study did not include any radiative effects. Here we update their analysis by including initial state radiation of photons, as well as the emission of hard gluons during the production ($e^+e^- \to \tilde{q}\tilde{q}^* g$) and/or decay ($\tilde{q} \to q\tilde{\chi}_1^0 g$) of the squarks. We also take larger squark masses ($m_{\tilde{q}} \sim 300$ GeV) to account for recent experimental bounds from the Tevatron [5], and a correspondingly higher center–of–mass energy of 800 GeV.

For reasons of space we only briefly summarize the ingredients of our analysis; details will be given elsewhere. We treat the emission of photons off the initial state in the structure function formalism [6]. The differential cross section is then given by

$$d\sigma = \int dx_1 dx_2 f_{e|e}(x_1, \sqrt{s}) f_{e|e}(x_2, \sqrt{s}) d\hat{\sigma}(\hat{s} = x_1 x_2 s), \tag{1}$$

where $\hat{\sigma}$ is the cross section in the absence of ISR, and

$$f_{e|e}(x, \sqrt{s}) = \beta \left[(1-x)^{\beta-1} \left(1 + \frac{3}{4}\beta \right) - \frac{\beta}{2}(1+x) \right], \tag{2}$$

with $\beta = \frac{\alpha_{\rm em}}{\pi} \left(\log \frac{s}{m_e^2} - 1 \right)$, is the leading–log resummed effective $e^\pm$ distribution function. Note that we do not include beamstrahlung (which is expected to further smear out the peak in the e^+e^- luminosity at $\hat{s} = s$), since it depends on details of accelerator design. Moreover, we conservatively assume that all ISR photons escape detection, even though eq.(2) is strictly valid only if there are no experimental constraints on the phase space of the emitted photons. However, we will see that the main effect of ISR is an overall reduction of the cross section by $\sim 15\%$; kinematical distributions are little affected even if all ISR photons are invisible.

We treat the emission of gluons during $\tilde{q}\tilde{q}^*$ production as described in [7]. In particular, we introduce a minimal gluon energy $E_{g,\rm min}$ to regularize IR divergences. The final results will not depend on the value of this regulator after contribution from $\tilde{q}\tilde{q}^*$ and $\tilde{q}\tilde{q}^* g$ events have been added, if $E_{g,\rm min}$ is sufficiently small.* In the numerical results presented below we take $E_{g,\rm min} = 1$ GeV. For $\sqrt{s} = 800$ GeV and $m_{\tilde{q}} = 300$ GeV this implies that only 18% of all squark pairs are produced together with a "hard" gluon.

The squared matrix element for $\tilde{q} \to q\tilde{\chi}_1^0 g$ can be found in [8]. We again have to include virtual QCD corrections, in this case to $\tilde{q} \to q\tilde{\chi}_1^0$ decays, to cancel IR singularities. In this case we regularize these singularities by introducing a finite gluon mass m_g, which we also set to 1 GeV in our numerical examples. For our choice $m_{\tilde{q}} = 300$ GeV, $m_{\tilde{\chi}} = 50$ GeV this means that nearly 90% of all squark decays produce a "hard" gluon. Altogether more

*Of course, virtual QCD corrections to $\tilde{q}\tilde{q}^*$ production have to be added for this cancellation to work.

than 95% of all $e^+e^- \to \tilde{q}\tilde{q}^* \to q\bar{q}\tilde{\chi}_1^0\tilde{\chi}_1^0 X$ events therefore contain at least one "hard" gluon, as defined through our two IR regulators. Note that, unlike for $e^+e^- \to \tilde{q}\tilde{q}^*$, virtual QCD corrections to $\tilde{q} \to q\tilde{\chi}_1^0$ decays introduce UV divergences. These cancel only after including full SUSY–QCD corrections [8], which depend on the mass of the gluino. We take $m_{\tilde{g}} = 450$ GeV; the shapes of the kinematical distributions we study here are almost independent of this choice.

Due to the emission of hard gluons we have up to 5 visible partons in the final state†. In the numerical results presented below we group these into exactly 2 jets (except for events with < 2 partons in the acceptance region defined by $|\cos(\theta)| \leq 0.9$, which we discard), using the k_T clustering ("Durham") algorithm [9]. We have checked that one obtains very similar results if one merges partons with a fixed y_{cut} parameter, rather than a fixed number of final state jets, and only uses the two hardest jets for the kinematical analysis. In order to simulate experimental resolutions, we smear the energies (but not directions) of all partons before jet merging, with a Gaussian error given by $\delta(E) = 0.3/\sqrt{E} \oplus 0.01$ (E in GeV). Finally, we apply a set of cuts in order to suppress backgrounds. We require that the energy of each jet exceeds 15 GeV, that the missing p_T exceeds 56 GeV (taken from [4] after scaling up from $\sqrt{s} = 500$ GeV to 800 GeV), and that the acoplanarity angle between the two jets exceed 30°.

In Figs. 1a,b we show the resulting distribution in the jet energy (1a) and in the variable $m_{\tilde{q},\text{min}}$ (1b) defined below. In the absence of cuts, radiative effects and energy smearing, the jet energy distribution should be constant (flat) between two kinematical endpoints, and zero elsewhere. The cuts distort this simple shape, producing a small peak near the lower edge of the spectrum; this is shown by the solid curve in Fig. 1a. The histograms show "experimental" distributions, based on 3,500 events before cuts; for a single $q = 2/3$ $SU(2)-$singlet ($\tilde{u}_R$) squark, this would require an integrated luminosity of about 205 fb^{-1} (including ISR and QCD corrections, and assuming all squarks decay directly into $q\tilde{\chi}_1^0$); the total cross section is 17.0 (11.7) fb before (after) cuts.‡ The dotted histogram still does not include any radiative effects, but includes a finite energy resolution as described above; clearly this has little effect on the shape of the spectrum. As mentioned earlier, including ISR (dashed histogram) reduces the cross section, but again does not distort the shape of the spectrum very much; in particular, there is only little "leakage" beyond the nominal endpoints. In contrast, including gluon emission (solid histogram) does change the shape of the distribution. In particular, there are now quite a few entries below the lower nominal endpoint. In most of these events one of the quarks falls out of the acceptance region, so that one of the jets is entirely made up of gluons. QCD corrections also increase the total

†We allow gluon emission during the production and both decays simultaneously, i.e. we include events with 2 or 3 gluons. These contributions are formally of NNLO. However, since production and decays are independent processes, up to terms $\mathcal{O}(\Gamma_{\tilde{q}}/\sqrt{s})$, other (as yet unknown) NNLO contributions cannot cancel these known contributions.

‡The total cross section for $\tilde{u}_L$ pair production for the same mass is 26.8 fb. However, in most models one expects $SU(2)$ doublet squarks to predominantly decay into charginos and heavier neutralinos, rather than directly into the LSP.

cross section before (after) cuts by 24% (42%)[§]

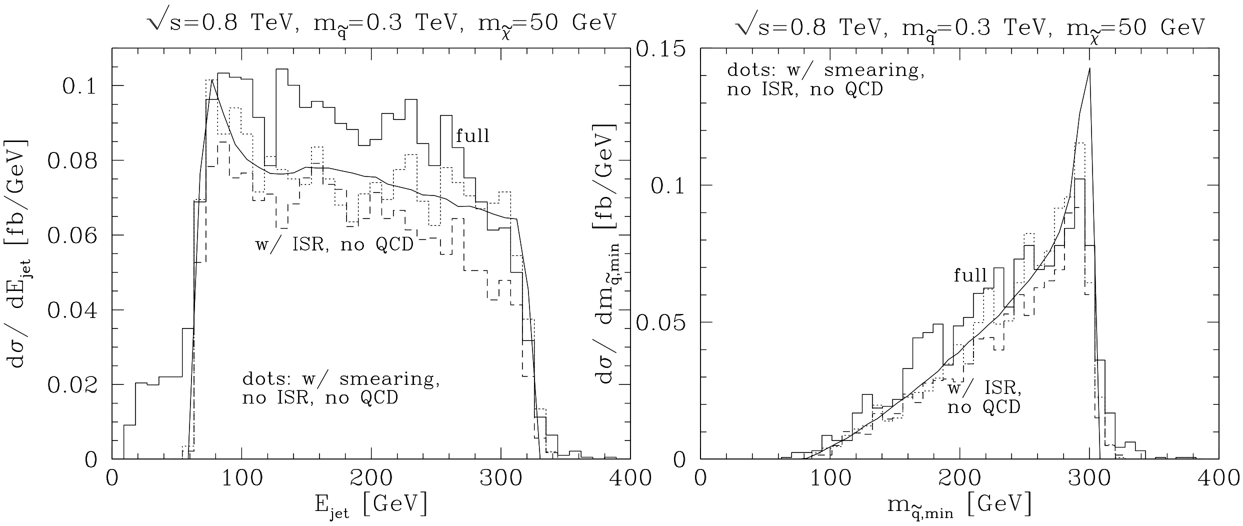

Figure 1: The jet energy (left) and $m_{\tilde{q},\min}$ (right) distributions after cuts. The solid curves show the "ideal" distributions in the absence of energy smearing and radiative effects. In the dotted, dashed and solid histograms, resolution smearing, ISR, and gluon radiation are "switched on" successively. See the text for further details.

The variable $m_{\tilde{q},\min}$ plotted in Fig. 1b has been introduced in [4]. It is the minimal possible squark mass, *if* one assumes a fixed value of $\sqrt{s}$ (no ISR), and *if* the final state consists of exactly two massless quarks and two neutralinos with equal (and known) mass.[¶] None of these assumptions hold in our case. In fact, in some cases the reconstruction described in [4] is impossible, i.e. some trigonometrical function acquires a value exceeding unity; we discard these events. We nevertheless find that radiative effects introduce only a modest amount of "leakage" beyond the nominal endpoint of the distribution, which is at $m_{\tilde{q}}$. Note, however, that these effects significantly broaden the distribution, i.e. many events have migrated to lower values of $m_{\tilde{q},\min}$ (compare the solid and dotted histograms). Since events in the peak contribute most to the determination of $m_{\tilde{q}}$ [4], this broadening is expected to increase the error on $m_{\tilde{q}}$.

Fig. 2 shows that a fit of the $m_{\tilde{q},\min}$ distribution nevertheless yields a smaller statistical error for $m_{\tilde{q}}$ than a fit of the E_{jet} distribution does. In this figure we compare a mock data set for $m_{\tilde{q}} = 300$ GeV, based on an integrated luminosity of just 50 fb^{-1} (852 events before cuts), with "template" distributions, which have been computed for 13 different values of $m_{\tilde{q}}$, leaving all other input parameters unchanged, and applying the cuts described above.

[§]Note that QCD corrections markedly increase the acceptance of the cuts. It is therefore also important to include their effect on the *kinematics* when trying to extract $m_{\tilde{q}}$ from measurements of the $\tilde{q}\tilde{q}^*$ production cross section.

[¶]The neutralino mass is expected to be known from analyses of data at lower energy, e.g. from chargino pair events.

This gives 13 different values of χ^2; the open (filled) squares have been computed from the $E_{\rm jet}$ ($m_{\tilde{q},\rm min}$) distributions. A parabola is then fitted to $\chi^2(m_{\tilde{q}})$. The minimum of this parabola gives the "measured" value $m_{\tilde{q},0}$ of $m_{\tilde{q}}$, while the (1σ) error is computed from $\chi^2(m_{\tilde{q},0} \pm \delta m_{\tilde{q}}) = \chi^2_{\rm min} + 1$. Note that the χ^2 values are only based on the *shapes* of the distributions, i.e. the "data" have been normalized to the template before computing χ^2 for a given assumed value of $m_{\tilde{q}}$. Fig. 2 therefore shows the results of purely kinematical determinations of $m_{\tilde{q}}$.

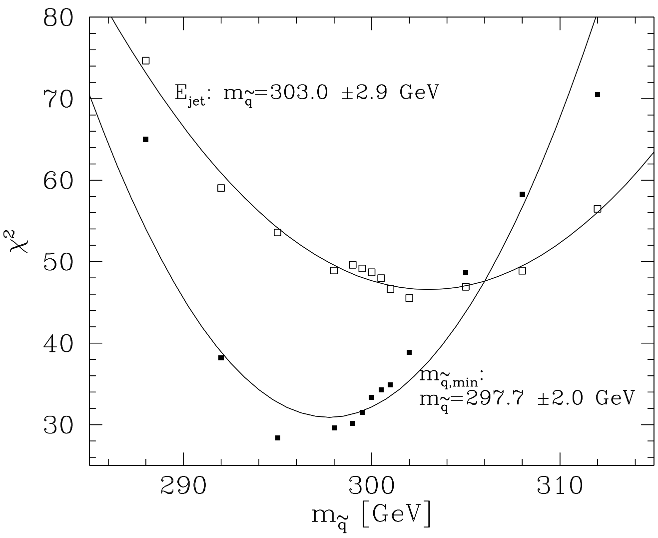

Figure 2: The χ^2 values computed by comparing a mock data set with 13 different template distributions. The "data" are for $m_{\tilde{q}} = 300$ GeV, while the templates are for values of $m_{\tilde{q}}$ between 288 and 312 GeV. The open (full) boxes are for the $E_{\rm jet}$ ($m_{\tilde{q},\rm min}$) distributions, and the curves are parabolic fits to the corresponding functions $\chi^2(m_{\tilde{q}})$. These parabolas determine the "measured" $m_{\tilde{q}}$, including its error.

We see that even after radiative effects have been included, a fit of the $m_{\tilde{q},\rm min}$ distribution determines the squark mass with a statistical error of well under 1% already with 50 fb^{-1} of data, which corresponds to only about 1 month of running time for the planned TESLA collider [10]. However, radiative effects also introduce possible new systematic errors, e.g. due to the choice of scale in α_s. (In our calculation we used $\sqrt{\hat{s}}$ for the corrections to $\tilde{q}\tilde{q}^*$ production, and $m_{\tilde{q}}$ in $\tilde{q}$ decays.) Moreover, we haven't included any hadronization effects yet. Note that the lighter scalar top eigenstate $\tilde{t}_1$, which is likely to be the lightest, and hence most easily accessible squark, might well hadronise before it decays [7]. In addition, the massless quarks and gluons in the final state will hadronise into jets with finite masses.

Finally, the error on the assumed LSP mass also propagates into the error on $m_{\tilde{q}}$ [4]. We plan to investigate these issues in a future publication.

Acknowledgements

This work was supported in part by Conselho Nacional de Desenvolvimento Científico e Tecnológico (CNPq), by Fundação de Amparo à Pesquisa do Estado de São Paulo (FAPESP), by Programa de Apoio a Núcleos de Excelência (PRONEX), by "Fonds zur Förderung der wissenschaftlichen Forschung" of Austria, project no. P13139–PHY, by the Department of Science and Technology (India), and by the US National Science Foundation under NSF grant INT-9602567.

References

[1] ECFA/DESY LC Physics Working Group (E. Accomando et al.). Phys. Rept. **299**, 1 (1998) [hep–ph/9705442]. A recent study in the framwork of minimal supergravity is H.–U. Martyn and G.A. Blair, hep–ph/9910416.

[2] See H. Eberl, S. Kraml, W. Majerotto, A. Bartl and W. Porod, hep–ph/9909378, and references therein.

[3] E.g. M. Berggren, R. Keranen, H. Nowak and A. Sopczak, hep–ph/9911345.

[4] J.L. Feng and D.E. Finnell, Phys. Rev. **D49**, 2369 (1994) [hep–ph/9310211].

[5] Particle Data Group, Eur. Phys. J. **C3**, 1 (1998).

[6] E.A. Kuraev and V.S. Fadin, Sov. J. Nucl. Phys. **41**, 466 (1985).

[7] M. Drees and O.J.P. Éboli, Eur. Phys. J. **C10**, 337 (1999) [hep–ph/9902391].

[8] K.–I. Hikasa and Y. Nakamura, Z. Phys. **C70**, 139 (1996), E: **C71**, 356 (1996).

[9] S. Catani, Yu.L. Dokshitzer, M. Olsson, G. Turnock, and B.R. Webber, Phys. Lett. **B269**, 432 (1991).

[10] R. Brinkmann, talk at LCWS99, Sitges, Spain, May 1999.

Spin correlations and phases for SUSY particle searches at e^+e^- colliders

N. GHODBANE

1 Introduction

Since one expects high luminosities for the next generation of linear colliders (e.g. $\sim 500 fb^{-1}$ for the TESLA project), one can use beam polarization to reduce the standard model backgrounds and use the polarization dependence of the cross sections to study specific SUSY parameters. Moreover, as it has been stressed by several authors [1], spin correlations play a major role in the kinematic distributions of final particles. For this reason, we upgraded the `SUSYGEN` Monte Carlo generator* [2].

Here, we firstly study the spin correlations effects in the gaugino and the stau searches. Then, in a second part, we show how the newly reconsidered CP violating phases arising from MSSM can affect the chargino searches.

2 Beam polarization and spin correlations

As it has been stressed by several papers [1] the study of the angular distribution of $e^\pm$ produced in $e^+e^- \to \tilde{\chi}_2^0\tilde{\chi}_1^0 \to \tilde{\chi}_1^0\tilde{\chi}_1^0 e^+e^-$ will give valuable information concerning the neutralino nature and then enable MSSM parameter extraction. Here we consider the two scenarios (**A**: $M_2 = 78$ GeV/c^2, $\mu = -250$ GeV/c^2, $\tan\beta = 2$) and (**B**: $M_2 = 210$ GeV/c^2, $\mu = -60$ GeV/c^2, $\tan\beta = 2$). In model **A**, $\tilde{\chi}_1^0$ is Bino like ($m_{\tilde{\chi}_1^0} = 42.5$ GeV/c^2, $\tilde{\chi}_1^0 = +0.98\tilde{B} + 0.17\tilde{W}^3 - 0.09\tilde{H}_1^0 + 0.04\tilde{H}_2^0$) whereas $\tilde{\chi}_2^0$ is Wino like ($m_{\tilde{\chi}_2^0} = 91.9$ GeV $/c^2$, $\tilde{\chi}_2^0 = +0.14\tilde{B} - 0.95\tilde{W}^3 - 0.28\tilde{H}_1^0 + 0.05\tilde{H}_2^0$). In model **B**, the two lightest neutralinos are Higgsino like ($m_{\tilde{\chi}_1^0} = 55.1$ GeV/c^2, $\tilde{\chi}_1^0 = +0.16\tilde{B} - 0.09\tilde{W}^3 - 0.78\tilde{H}_1^0 - 0.60\tilde{H}_2^0$) and ($m_{\tilde{\chi}_2^0} = 88.9$ GeV $/c^2$, $\tilde{\chi}_2^0 = +0.21\tilde{B} - 0.24\tilde{W}^3 + 0.62\tilde{H}_1^0 - 0.71\tilde{H}_2^0$). For each one of these two models, we considered the common sfermions mass at the GUT scale, m_0, being equal to 80 GeV/c^2 and 200 GeV/c^2.

The right side of figure 1 illustrates the effect of spin-correlations in angular distributions of e^-, decay product of $\tilde{\chi}_2^0$. One can notice that the angular distribution of the final leptons depends strongly on the sfermion mass parameter m_0. For small m_0 of inclusion of spin correlations gives an effect $\sim 20\%$ in the angular distributions. For higher selectron masses, the total cross section is smaller, but the spin correlation effects appear to be more important $\sim 30\%$. If the two neutralinos are Higgsino like, the effects are negligible ($\sim 0.7\%$) (see figure 2). Moreover these angular distributions depend strongly on the center of mass energy.

Recent studies [3] have shown that τ polarization effects yield valuable information for the MSSM parameters e.g for $\tan\beta$, the nature of the LSP and the mixing angle $\theta_{\tilde{\tau}}$.

*A description of the Monte Carlo generator can be found in the Higgs working group report.

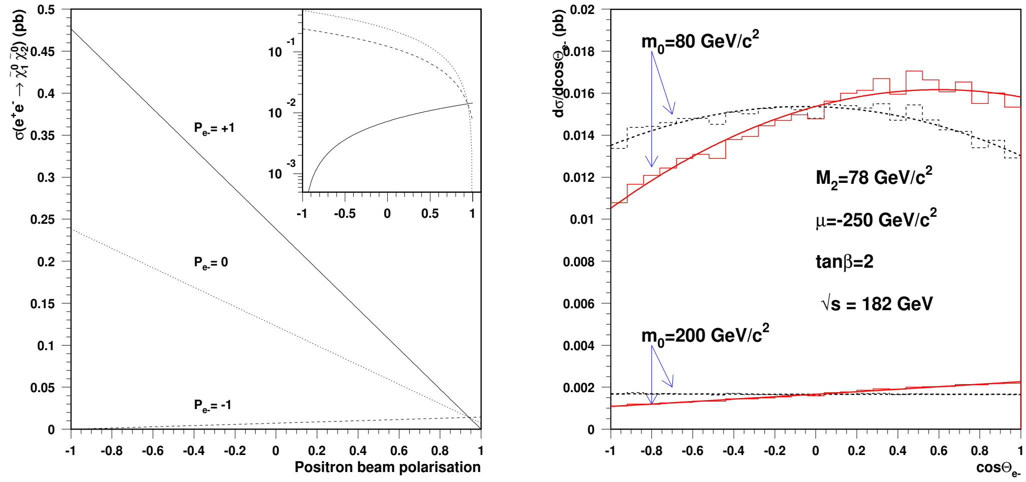

Figure 1: The figure on the left side shows the evolution of the cross section associated to the production of $\tilde{\chi}^0_1\tilde{\chi}^0_2$ for different beam polarizations. The figure on the right side shows the $d\sigma/d\cos\theta$ distribution for the final e^- decay product of the $\tilde{\chi}^0_2$ with (solid line) and without spin correlations (dashed line) for two assumptions on the m_0 parameter (scenario **A**).

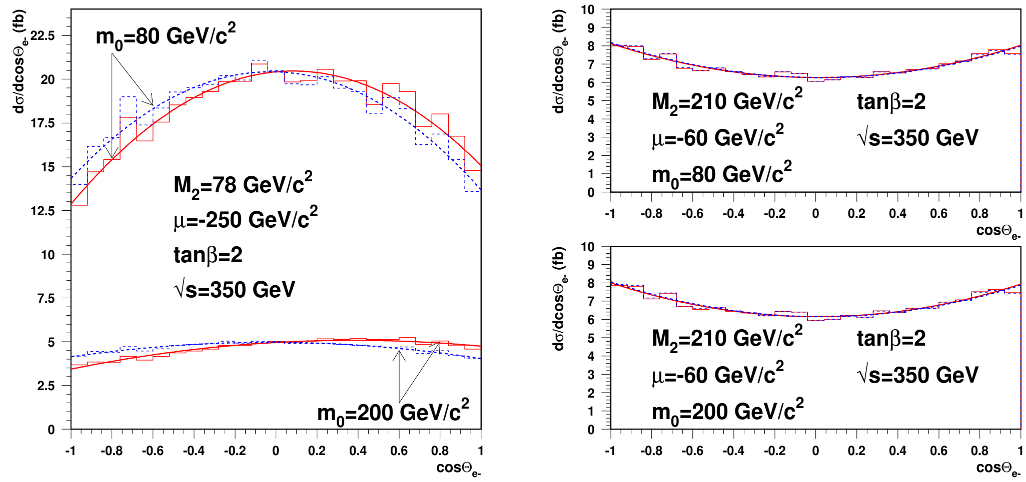

Figure 2: The figure on the left side shows the $d\sigma/d\cos\theta$ distribution for the final e^- decay product of the $\tilde{\chi}^0_2$ with (solid line) and without spin correlations (dashed line) for two assumptions on the m_0 parameter assuming the neutralino being bino like (scenario **A**). The Higgsino like case (scenario **B** and figure on the right) shows no strong dependence on the spin correlations.

Figure 3 shows the momentum distribution of pions produced by $e^+e^- \to \tilde{\tau}^+_1\tilde{\tau}^-_1 \to \tau^+\tilde{\chi}^0_1\tau^-\tilde{\chi}^0_1 \to \pi^+\nu_\tau\tilde{\chi}^0_1\pi^-\bar{\nu}_\tau\tilde{\chi}^0_1$. The distributions have been plotted assuming two scenarios for the stau mixing angle $\Theta_{\tilde{\tau}} = 0$ and π, and $\tilde{\chi}^0_1$ nature (Bino, Higgsino). One can see that the final particle distributions will give access to the tau polarization $\mathcal{P}_\tau$, to $\tan\beta$, and to $\tilde{\chi}^0_1$ nature and through them, to the MSSM parameters.

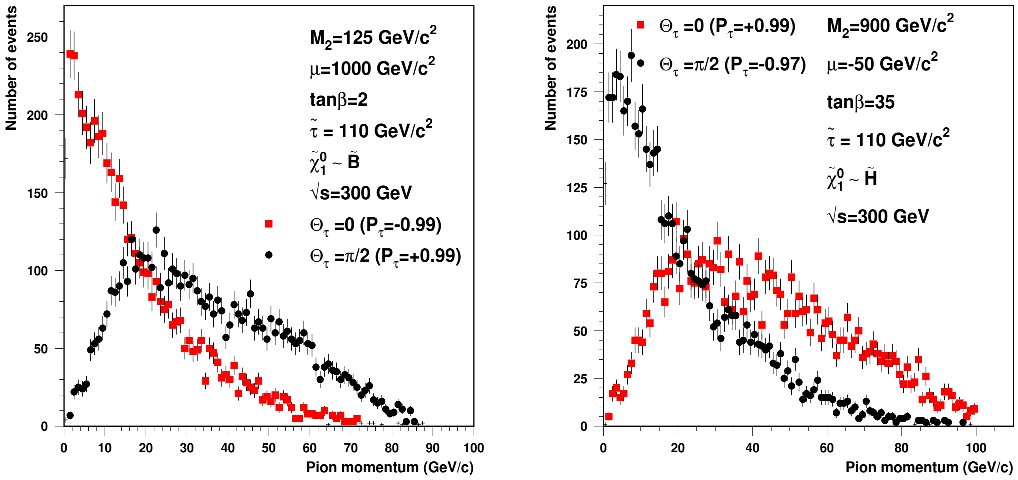

Figure 3: Momentum distributions of π, decay product of τ produced in the process $e^+e^- \rightarrow \tilde{\tau}_1^+\tilde{\tau}_1^- \rightarrow \tau^+\tilde{\chi}_1^0\tau^-\tilde{\chi}_1^0$. The distributions have been plotted for two hypotheses concerning the stau mixing angle $\theta_{\tilde{\tau}}$ ($\tilde{\tau}_L$ and $\tilde{\tau}_R$) and for two hypotheses concerning the neutralino $\tilde{\chi}_1^0$ nature.

3 Phases in supersymmetry searches

In the MSSM, there are new potential sources of CP non conservation [4]. Complex CP violating phases can arise from several parameters present in the MSSM Lagrangian: the Higgs mixing mass parameter μ, the gauginos masses M_i, the trilinear couplings A_i. Experimental constraints on these CP violating phases come from the electric dipole moment of the electron and the neutron [5].

Figure 4 (left side) shows the chargino pair production cross section variation in terms of ϕ_μ, the phase associated to the μ parameter, for several values of the sneutrino mass $m_{\tilde{\nu}_e}$ and for a value of $\tan\beta = 1.5$. One sees that there is a local minimum between the two extreme values ($\Phi_\mu = 0, \pi$), which are tested at LEP searches ($\mu > 0, \mu < 0$), but also that it is not so deep as to raise doubts on the exhaustiveness of "phaseless" searches. Further the electric dipole moment experimental upper limit ($E_e^{exp} < 4.3 \cdot 10^{-27} e \cdot cm$) [5] will constrain these phases (figure on the right side) and rule out many scenarios for which the smallest cross section for chargino pair production is obtained for a ϕ_μ parameter different from 0 and π.

At the linear collider, one cannot neglect this strong dependence of the cross section on phases.

References

[1] G. Moortgat-Pick *et al*, Phys. Rev. **D59**, 015016 (1999), hep–ph/9708481; S.Y. Choi *et al.*, Eur. Phys. J. **C7**, 123 (1999), hep–ph/9806279; V. Lafage *et al.*, hep-ph/9810504;

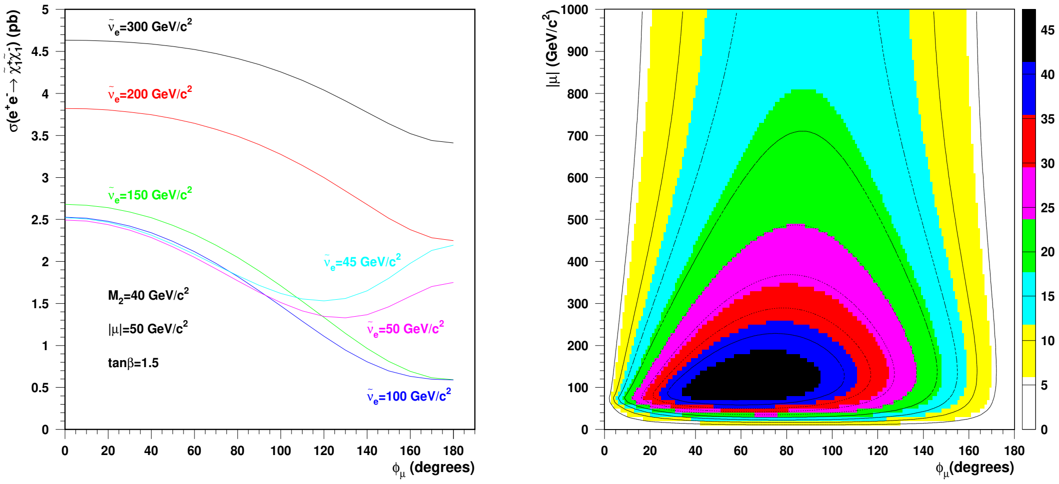

Figure 4: The figure on the left side shows the evolution of the cross section for $e^+e^- \to \tilde{\chi}_1^+\tilde{\chi}_1^-$ in terms of the ϕ_μ phase ($\mu = |\mu|e^{i\phi_\mu}$) for a center of mass energy of 189 GeV. The figure on the right side shows the evolution of the dipole electric moment divided by the experimental upper limit ($E_e^{exp} < 4.3 \cdot 10^{-27} e \cdot cm$) in terms of $\mu = |\mu|e^{i\phi_\mu}$ parameter.

see also the talk by D. Perret-Gallix at the International Workshop on Linear Colliders 99, Sitges.

[2] S. Katsanevas and P. Morawitz, Comp. Phys. Commun. **112**, 227 (1998); N. Ghodbane, S. Katsanevas, P. Morawitz and E. Perez, `SUSYGEN3` `http://lyoinfo.in2p3.fr/susygen/susygen3.html`.

[3] K. Fujii, M.M. Nojiri and T. Tsukamoto, hep–ph/9511338; A. Bartl *et al*, Z. Phys. **C73**, 469 (1997), hep–ph/9603410.

[4] T. Ibrahim and P. Nath, Phys. Rev. **D58**, 111301 (1998), hep–ph/9807501; T. Falk and K.A. Olive, Phys. Lett. **B439**, 71 (1998), hep–ph/9806236; M. Brhlik, G.J. Good and G.L. Kane, Phys. Rev. **D59**, 115004 (1999), hep–ph/9810457; S. Pokorski, J. Rosiek and C.A. Savoy, hep-ph/9906206.

[5] E. Commins *et al.*, Phys. Rev. **A50** (1994) 2960; K. Abdullah *et al.*, Phys. Rev. Lett. **65** (1990) 234.

The three-leptons signature from resonant sneutrino production at the LHC

G. MOREAU, E. PEREZ AND G. POLESELLO

Abstract

The resonant production of sneutrinos at the LHC via the R-parity violating couplings $\lambda'_{ijk} L_i Q_j D^c_k$ is studied through its three-leptons signature. A detailed particle level study of signal and background is performed using a fast simulation of the ATLAS detector. Through the full reconstruction of the cascade decay, a model-independent and precise measurement of the masses of the involved sparticles can be performed. Besides, this signature can be detected in a large part of the SUSY parameter space and for wide ranges of values of several λ'_{ijk} coupling constants.

1 Introduction

In extensions of the Minimal Supersymmetric Standard Model (MSSM) where the so-called R-parity symmetry is violated, the superpotential contains some additional trilinear couplings which offer the opportunity to singly produce supersymmetric (SUSY) particles as resonances. The analysis of resonant SUSY particle production allows an easier determination of the these R-parity violating ($\not R_{\rm p}$) couplings than the displaced vertex analysis for the Lightest Supersymmetric Particle (LSP) decay, which is difficult experimentally especially at hadronic colliders.

In this paper, we study the sensitivity provided by the ATLAS detector at the LHC on singly produced charginos via the λ'_{211} coupling, the main contribution coming from the resonant process $pp \to \tilde{\nu}_\mu \to \tilde{\chi}^\pm_1 \mu^\mp$. At hadron colliders, due to the continuous energy distribution of the colliding partons, the resonance can be probed over a wide mass range. We have chosen to concentrate on $\lambda'_{ijk} L_i Q_j D^c_k$ interactions since $\lambda''_{ijk} U^c_i D^c_j D^c_k$ couplings lead to multijet final states with large QCD background. Besides, we focus on λ'_{211} since it corresponds to first generation quarks for the colliding partons and it is not severely constrained by low energy experiments: $\lambda'_{211} < 0.09$ (for $\tilde{m} = 100$ GeV) [1]. We consider the cascade decay leading to the three-leptons signature, namely $\tilde{\chi}^\pm_1 \to \tilde{\chi}^0_1 l^\pm_p \nu_p$ (with $l_p = e, \mu$), $\tilde{\chi}^0_1 \to \mu u \bar{d},\ \bar{\mu} \bar{u} d$. The main motivation lies in the low Standard Model background for this three-leptons final state. The considered branching ratios are typically of order $B(\tilde{\chi}^\pm_1 \to \tilde{\chi}^0_1 l^\pm_p \nu_p) \approx 22\%$ (for $m_{\tilde{l}}, m_{\tilde{q}}, m_{\tilde{\chi}^0_2} > m_{\tilde{\chi}^\pm_1}$) and $B(\tilde{\chi}^0_1 \to \mu u d) \sim 40\% - \sim 70\%$.

2 Mass reconstruction

The clean final state, with only two hadronic jets, three leptons and a neutrino allows the reconstruction of the $\tilde{\nu}$ decay chain and the measurement of the $\tilde{\chi}^0_1$, $\tilde{\chi}^\pm_1$ and $\tilde{\nu}_\mu$ masses. We perform full analysis for the following point of the MSSM: $M_1 = 75$ GeV, $M_2 = 150$ GeV,

$\mu = -200$ GeV, $\tan\beta = 1.5$, $A_t = A_b = A_\tau = 0$, $m_{\tilde{f}} = 300$ GeV and for λ'_{211}=0.09. For this set of MSSM parameters, the mass spectrum is: $m_{\tilde{\chi}_1^0} = 79.9$ GeV, $m_{\tilde{\chi}_1^\pm} = 162.3$ GeV and the total cross-section for the three-leptons production is 3.1 pb, corresponding to ~ 100000 events for the standard integrated luminosity of 30 fb^{-1} expected within the first three years of LHC data taking.

The single chargino production has been calculated analytically and implemented in a version of the SUSYGEN MonteCarlo [2] modified to include the generation of pp processes. The generated signal events were processed through the program ATLFAST [3], a parameterized simulation of the ATLAS detector response.

First, we impose the following loose selection cuts in order to select the considered final state and to reduce the Standard Model (SM) background (see Section 3.1): (a) Exactly three isolated leptons with $p_T^1 > 20$ GeV, $p_T^{2,3} > 10$ GeV and $|\eta| < 2.5$, (b) At least two of the three leptons must be muons, (c) Exactly two jets with $p_T > 15$ GeV, (d) The invariant mass of any $\mu^+\mu^-$ pair must lie outside ± 6.5 GeV of the Z mass.

The three leptons come in the following flavor-sign configurations (+ charge conjugates): (1) $\mu^- e^+ \mu^+$ (2) $\mu^- e^+ \mu^-$ (3) $\mu^- \mu^+ \mu^+$ (4) $\mu^- \mu^+ \mu^-$, where the first lepton comes from the $\tilde{\nu}_\mu$, the second one from the W and the third one from the $\tilde{\chi}_1^0$ decay. As a starting point for the analysis, we focus on configuration (1) where the muon produced in the $\tilde{\chi}_1^0$ decay is unambiguously identified as the one with the same sign as the electron. The distribution of the μ-jet-jet invariant mass exhibits a clear peak over a combinatorial background, shown on the left side of Figure 1. After combinatorial background subtraction (right of Figure 1) an approximately Gaussian peak is left, from which the $\tilde{\chi}_1^0$ mass can be measured with a statistical error of ~ 100 MeV. The combinatorial background is due to events where one jet from $\tilde{\chi}_1^0$ decay is lost and a jet from initial state radiation is used in the combination, and its importance is reduced for heavier sneutrinos or neutralinos. Once the position of the $\tilde{\chi}_1^0$ mass peak is known, the reconstructed $\tilde{\chi}_1^0$ statistics can be increased by also considering signatures (2), (3) and (4), and by choosing as the $\tilde{\chi}_1^0$ candidate the muon-jet-jet combination which gives invariant mass nearest to the peak measured previously using events sample (1). For further reconstruction, we define as $\tilde{\chi}_1^0$ candidates the μ-jet-jet combinations with an invariant mass within 12 GeV of the measured $\tilde{\chi}_1^0$ peak, yielding a total statistics of 6750 events for signatures (1) to (4) for an integrated luminosity of 30 fb^{-1} .

For $\tilde{\chi}_1^\pm$ reconstruction we consider only configurations (1) and (2), for which the charged lepton from W decay is unambiguously identified as the electron. The longitudinal momentum of the neutrino from the W decay is calculated from the missing transverse momentum of the event (p_T^ν) and by constraining the electron-neutrino invariant mass to the W mass. The resulting neutrino longitudinal momentum has a twofold ambiguity. We therefore build the invariant $W - \tilde{\chi}_1^0$ mass candidate using both solutions for the W boson momentum. The observed peak, represented on the left side of Figure 2, can be fitted with a Gaussian shape with a width of ~ 6 GeV. Only the solution yielding the $\tilde{\chi}_1^\pm$ mass nearer to the measured mass peak is retained, and the $\tilde{\chi}_1^\pm$ candidates are defined as the combinations with an invariant mass within 15 GeV of the peak, corresponding to a statistics of 2700 events.

Finally, the sneutrino mass is reconstructed by taking the invariant mass of the $\tilde{\chi}_1^\pm$ candidate and the leftover muon (Figure 2, right). The $\tilde{\nu}$ mass peak has a width of ~ 10 GeV and 2550 events are counted within 25 GeV of the measured peak.

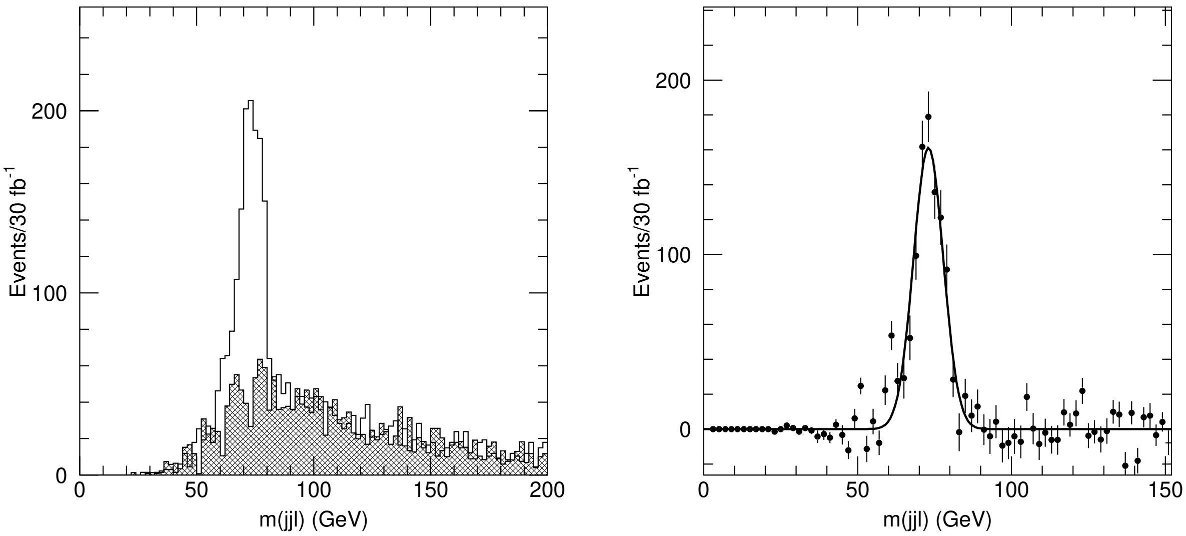

Figure 1: *μ-jet-jet invariant mass for events in configuration (1) (see text) before (left) and after (right) background subtraction.*

3 Analysis reach

3.1 Standard Model background

We consider the following SM processes for the evaluation of the background to the three-leptons signature: (1) $\bar{t}t$ production, followed by $t \to Wb$, where the two W and one of the b quarks decay leptonically, (2) WZ production, where both bosons decay leptonically, (3) Wt production, (4) Wbb production, (5) Zb production. These backgrounds were generated with the PYTHIA Monte Carlo [4], and the ONETOP parton level generator [5], and passed through the ATLFAST package [3].

We apply to the background events the loose selection cuts described in Section 2, and in addition we reject the three same-sign muons configurations which are never generated by our signal. The background to the sneutrino decay signal is calculated by considering the events with a μ-jet-jet invariant mass in an interval of ± 15 GeV around the $\tilde{\chi}_1^0$ peak measured for the signal. In order to optimize the signal to background ratio only events containing three muons (configurations (3) and (4)), which are less likely in the Standard Model, are considered. In each event two combinations, corresponding to the two same-sign muons, can be used for the $\tilde{\chi}_1^0$ reconstruction. Both configurations are used when counting the number of events in the peak. In most cases, however, the difference in mass between the two combinations is such that they do not appear in the same peak region.

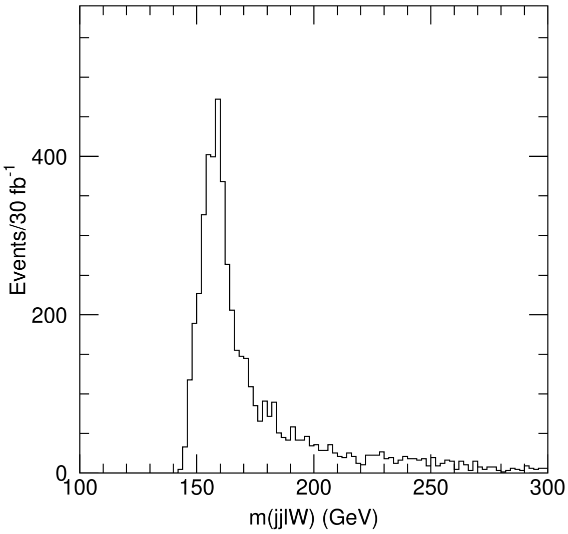

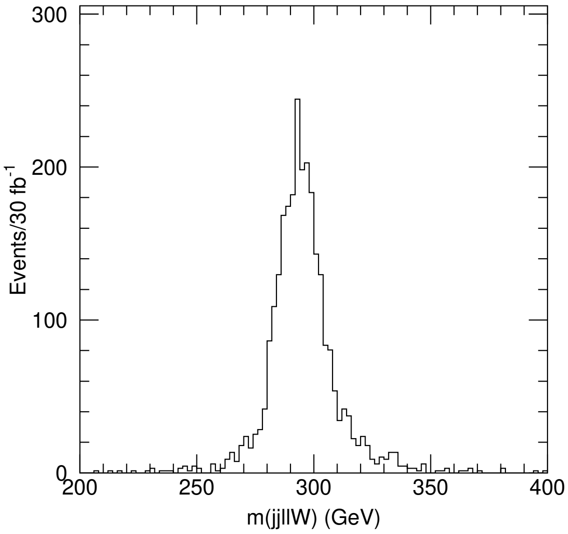

Figure 2: *Left: Invariant mass of the W with the $\tilde{\chi}_1^0$ candidate. Right: Invariant mass of the third lepton in the event with the $\tilde{\chi}_1^{\pm}$ candidate.*

3.2 Supersymmetric background

The pair production of SUSY particles through standard R_p-conserving processes represents another source of background. A study based on the HERWIG 6.0 MonteCarlo [6] has shown that all the SUSY events surviving the cuts described in Section 3.1 are mainly from $pp \to \tilde{\chi} + X$ reactions ($\tilde{\chi}$ being either a chargino or a neutralino and X any other SUSY particle), and that the SUSY background decreases as the $\tilde{\chi}^{\pm}$ and $\tilde{\chi}^0$ masses increase. This behavior is due to the combination of two effects: the $\tilde{\chi} + X$ production cross-section decreases with increasing $\tilde{\chi}$ mass, and the probability of losing two of the four jets from the decays of the two $\tilde{\chi}_1^0$ in the event becomes smaller as the $\tilde{\chi}^{\pm}$ and $\tilde{\chi}_1^0$ masses increase. The SUSY background is only significant for $\tilde{\chi}_1^{\pm}$ masses lower than 200 GeV.

Besides, it can be assumed that the $\tilde{\chi}_1^0$ mass will be derived from inclusive $\tilde{\chi}_1^0$ reconstruction in SUSY pair production as shown in [7] and [8]. Hence, even in the cases where a significant $\tilde{\chi}_1^0$ peak can not be observed above the SUSY background, we can proceed to the further steps in the kinematic reconstruction. The strong kinematic constraint obtained by requiring both the correct $\tilde{\chi}_1^0$ mass and a peak structure in the $\tilde{\chi}_1^0 - W$ invariant mass will then allow to separate the single sneutrino production from other SUSY processes.

Therefore, only the Standard Model background is considered in the evaluation of the analysis reach presented below.

3.3 Reach in the mSUGRA parameter space

In Figure 3, we show the regions of the $m_0 - m_{1/2}$ plane where the signal significance exceeds 5 σ ($\frac{S}{\sqrt{B}} > 5$ with $S = Signal$ and $B = SM\ Background$) after the set of cuts described in Section 3.1 has been applied, within the mSUGRA model. The full mass reconstruction analysis of Section 2 is possible only above the dashed line parallel to the m_0 axis. Below this line the decay $\tilde{\chi}_1^{\pm} \to \tilde{\chi}_1^0 W^{\pm}$ is kinematically closed, and the W mass constraint can not be applied to reconstruct the neutrino longitudinal momentum.

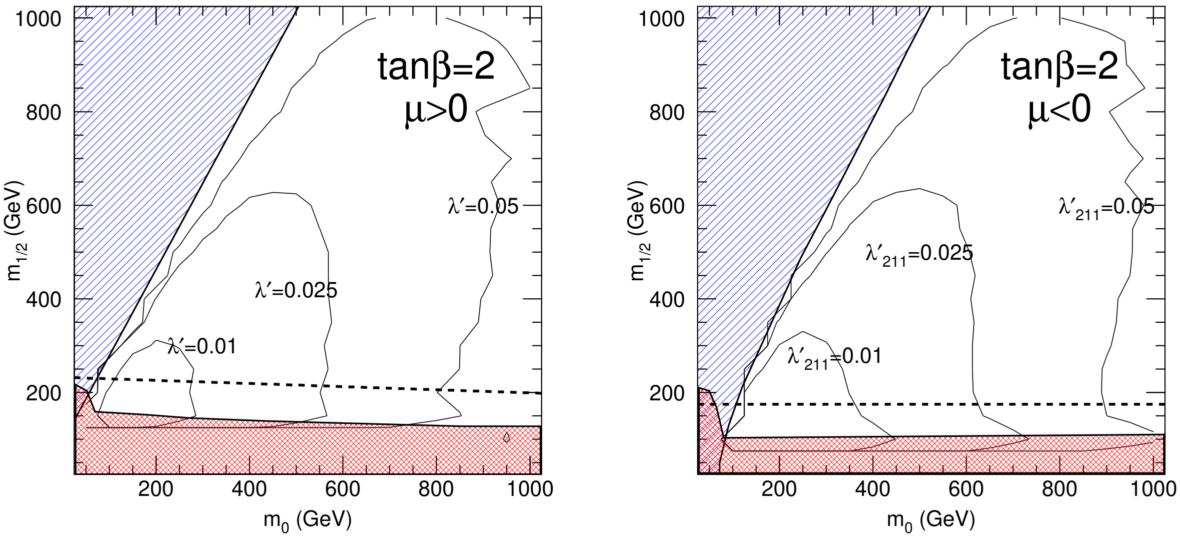

Figure 3: *5σ reach in the $m_0 - m_{1/2}$ plane for $A_0 = 0$, $\tan\beta = 2$, $\mu < 0$ (left) and $\mu > 0$ (right) and three different choices of the λ'_{211} coupling, with an integrated luminosity of 30 fb^{-1} at the LHC. A signal of at least ten events is required. The hatched region at the upper left corresponds to $m_{\tilde{\nu}} < m_{\tilde{\chi}_1^{\pm}}$. The cross-hatched region for low $m_{1/2}$ gives the kinematical limit for the discovery of $\tilde{\chi}_1^{\pm}$ or $\tilde{l}$ by LEP running at $\sqrt{s} = 196$ GeV [9]. The dotted line shows the region below which the $\tilde{\chi}_1^{\pm}$ decays to a virtual W.*

The basic feature in Figure 3 is a decrease of the sensitivity on λ'_{211} as m_0 increases. This is due to a decrease of the partonic luminosity as $m_{\tilde{\nu}}$ increases. The sensitivity on λ'_{211} is also observed to decrease as $m_{\tilde{\chi}_1^{\pm}}$ approaches $m_{\tilde{\nu}}$. There are two reasons. First, in this region the phase space factor of the decay $\tilde{\nu} \to \tilde{\chi}_1^{\pm}\mu^{\mp}$ following the resonant sneutrino production is suppressed, thus reducing the branching fraction. Secondly, as the $\tilde{\nu}_{\mu}$ and the $\tilde{\chi}_1^{\pm}$ become nearly degenerate the muon from the decay becomes on average softer, and its p_T can fall below the analysis requirements. In the region $m_{\tilde{\chi}_1^{\pm}} > m_{\tilde{\nu}}$, shown as a hatched region in the upper left of the plots, the resonant sneutrino production contribution vanishes and there is essentially no sensitivity to λ'_{211}. Finally, the the sensitivity vanishes for low values of $m_{1/2}$. This region, below the LEP 200 kinematic limit for $\tilde{\chi}_1^{\pm}$ detection, corresponds to low values of the $\tilde{\chi}_1^0$ mass. In this situation the two jets from the $\tilde{\chi}_1^0$ decay are soft, and one of them is often below the transverse momentum requirement, or they are reconstructed as a single jet.

For high $\tan\beta$, the three-lepton signature is still present, but it may be produced through the decay chain $\tilde{\chi}_1^{\pm} \to \tilde{\tau}_1 \nu_\tau$, followed by $\tilde{\tau}_1 \to \tau\tilde{\chi}_1^0$. The full kinematic reconstruction becomes very difficult, but the signal efficiency is essentially unaffected, as long as the mass difference between the lightest $\tilde{\tau}$ and the $\tilde{\chi}_1^0$ is larger than ~ 50 GeV. For a smaller mass difference the charged lepton coming from the τ decay is often rejected by the analysis cuts.

4 Conclusion

In conclusion we have shown that if minimal supersymmetry with R-parity violation is realized in Nature, the three-leptons signature from resonant sneutrino production will be a privileged channel for precisely measuring sparticle masses in a model-independent way as well as for testing a broad region of the mSUGRA parameter space.

This signature can lead to a high sensitivity to the λ'_{211} coupling and should also allow to probe an unexplored range of values for many other $\not{R}_\mathrm{p}$ couplings of the type λ'_{1jk} and λ'_{2jk}.

References

[1] H. Dreiner, published in *Perspectives on Supersymmetry* , ed. by G.L. Kane, World Scientific (1998), hep-ph/9707435.

[2] SUSYGEN 3.0/06, N. Ghodbane, S. Katsanevas, P. Morawitz and E. Perez, lyoinfo.in2p3.fr/susygen/susygen3.html; N. Ghodbane, hep-ph/9909499.

[3] E. Richter-Was, D. Froidevaux and L. Poggioli, 'ATLFAST 2.0: a fast simulation package for ATLAS', ATLAS Internal Note ATL-PHYS-98-131 (1998).

[4] T. Sjöstrand, Comp. Phys. Comm. **82**, 74 (1994).

[5] D.O. Carlson, S. Mrenna and C.P. Yuan, private communication; D.O. Carlson and C.P. Yuan, Phys. Lett. **B306**, 386 (1993).

[6] H. Dreiner, P. Richardson, and M.H. Seymour, OUTP-99-26P, RAL-TR-1999-080, hep-ph/9912407; G. Corcella et al., Cavendish HEP 99/17 (1999) hep-ph/9912396; G. Marchesini et al., Computer Phys. Commun. **67**, 465 (1992).

[7] The ATLAS Collaboration, 'ATLAS Detector and Physics Performance Technical Design Report', ATLAS TDR 15, CERN/LHCC/99-15 (1999).

[8] L. Megner and G. Polesello, these proceedings.

[9] The ALEPH collaboration, Internal Note ALEPH 99-078, CONF 99-050 (1999), contributed to HEP-EPS 99.

Resonant slepton production at the LHC

H. DREINER[*], P. RICHARDSON[†], AND M. H. SEYMOUR[‡]

Abstract

We consider the resonant production of charged sleptons at the LHC via R-parity violation ($\not{R}_{\rm p}$) followed by gauge decays to a charged lepton and a neutralino which then decays via $\not{R}_{\rm p}$. This gives a signature of two like-sign charged leptons. In the simulation we include the full hadronization via Monte Carlo programs. We find a background, after cuts, of 5.1 ± 2.5 events for an integrated luminosity of $10 fb^{-1}$. A preliminary study of the signal suggests that couplings of 2×10^{-3} for a smuon mass of 223GeV and smuon masses of up to 540GeV for couplings of 10^{-2} can be probed.

1 Introduction

In R-parity violating ($\not{R}_{\rm p}$) models the single resonant production of charged sleptons in hadron-hadron collisions is possible. The most promising channels for the discovery of these processes, at least with small $\not{R}_{\rm p}$ couplings, involve the gauge decays of these resonant sleptons. In particular if we consider the production of a charged slepton, this can then decay to give a neutralino and a charged lepton, *i.e.* the process

$$\mathrm{u} + \bar{\mathrm{d}} \longrightarrow \tilde{\ell}^+ \longrightarrow \ell^+ + \tilde{\chi}^0. \tag{1}$$

In addition to this s-channel process there are t-channel processes involving squark exchange. The neutralino decays via the crossed process to give a charged lepton, which due to the Majorana nature of the neutralino can have the same charge as the lepton from the slepton decay. We therefore have a like-sign dilepton signature which we expect to have a low Standard Model background.

2 Backgrounds

The dominant Standard Model backgrounds to this process come from

- Gauge boson pair production, *i.e.* production of ZZ or WZ followed by leptonic decays of the gauge bosons with some of the leptons not being detected.
- $\mathrm{t\bar{t}}$ production. Either the t or $\bar{\mathrm{t}}$ decays semi-leptonically, giving one lepton. The second top decays hadronically. A second lepton with the same charge can be produced in a

[*]E-mail address: dreiner@v2.rl.ac.uk
[†]E-mail address: p.richardson1@physics.ox.ac.uk
[‡]E-mail address: M.Seymour@rl.ac.uk

semi-leptonic decay of the bottom hadron formed in the hadronic decay of the second top, *i.e.*

$$\begin{aligned} \mathrm{t} &\rightarrow \mathrm{W^+b} \rightarrow \mathrm{e^+}\bar{\nu}_\mathrm{e}\mathrm{b}, \\ \bar{\mathrm{t}} &\rightarrow \mathrm{W^-}\bar{\mathrm{b}} \rightarrow \mathrm{q\bar{q}}\bar{\mathrm{b}}, \quad \bar{\mathrm{b}} \rightarrow \mathrm{e^+}\bar{\nu}_\mathrm{e}\bar{\mathrm{c}}. \end{aligned} \tag{2}$$

- $\mathrm{b\bar{b}}$ production. If either of these quarks hadronizes to form a $\mathrm{B^0_{d,s}}$ meson this can mix to give a $\mathrm{\bar{B}^0_{d,s}}$. This means that if both the bottom hadrons decay semi-leptonically the leptons will have the same charge as they are both coming from either b or $\bar{\mathrm{b}}$ decays.

- Single top production. A single top quark can be produced together with a $\bar{\mathrm{b}}$ quark by either an *s*- or *t*-channel W exchange. This can then give one charged lepton from the top decay, and a second lepton with the same charge from the decay of the meson formed after the b quark hadronizes.

- Non-physics backgrounds. There are two major sources: (i) from misidentifying the charge of a lepton, *e.g.* in Drell-Yan production, and (ii) from incorrectly identifying an isolated hadron as a lepton. This means that there is a major source of background from W production with an additional jet faking a lepton.

Early studies of like-sign dileptons at the LHC [1] only studied the backgrounds from heavy quark production. It was found that by imposing cuts on the transverse momentum and isolation of the leptons the heavy quark backgrounds could be significantly reduced. However more recent studies of the like-sign dilepton production at the LHC [2] and the Tevatron [3, 4] suggest that a major source of background to like-sign dilepton production is from gauge boson pair production and from fake leptons. Here we will consider the backgrounds from gauge boson pair production as well as heavy quark production. The study of the non-physics backgrounds (*e.g.* fake leptons) requires a full simulation of the detector and it is therefore beyond the scope of our study. In particular the background from fake leptons cannot be reliably calculated from Monte Carlo simulations and must be extracted from data [3]. We can use the differences between the $\not{R}_\mathrm{p}$ signature we are considering and the MSSM signatures considered in [2] to reduced the background from gauge boson pair production.

We impose the following cuts

- A cut on the transverse momentum of the like-sign leptons $p_T > 40$ GeV.

- An isolation cut on the like-sign leptons so that the transverse energy in a cone of radius $R = \sqrt{\Delta\phi^2 + \Delta\eta^2} = 0.4$ about the direction of each lepton is less than 5 GeV.

- A cut on the transverse mass, $M_T^2 = 2|p_{T_\ell}||p_{T_\nu}|(1-\cos\Delta\phi_{\ell\nu})$, where p_{T_ℓ} is the transverse momentum of the charged lepton, p_{T_ν} is the transverse momentum of the neutrino, assumed to be all the missing transverse momentum in the event, and $\Delta\phi_{\ell\nu}$ is the azimuthal angle between the lepton and the neutrino, *i.e.* the missing momentum in the event. We cut out the region where $60\mathrm{GeV} < \mathrm{M_T} < 85\mathrm{GeV}$.

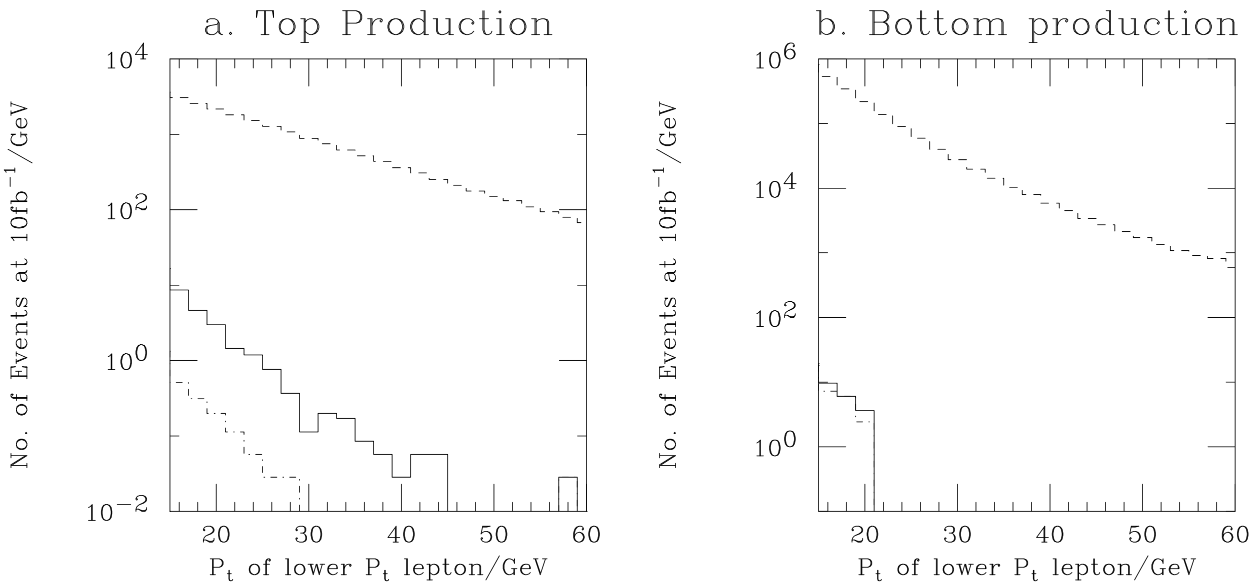

Figure 1: Effect of the isolation cuts on the $t\bar{t}$ and $b\bar{b}$ backgrounds. The dashed line gives the background before any cuts, the solid line shows the effect of the isolation cut described in the text. The dot-dash line gives the effect of all the cuts.

- A veto on the presence of a lepton in the event with the same flavor but opposite charge (OSSF) as either of the leptons in the like-sign pair if the lepton has $p_T > 10$ GeV and which passes the same isolation cut as the like-sign leptons.

- A cut on the missing transverse energy, $E^T_{miss} < 20$ GeV .

While these cuts were chosen to reduce the background we have not attempted to optimize them. The first two cuts are designed to reduce the background from heavy quark production. As can be seen in Fig. 1, these cuts reduce this background by several orders of magnitude. The remaining cuts are designed to reduce the background from gauge boson pair, in particular WZ, production which is the major source of background after the imposition of the isolation and p_T cuts. The transverse mass cut is designed to remove events with leptonic W decays as can be seen in Fig. 2a. The veto on the presence of OSSF leptons is designed to remove events where one lepton from the dilepton pair comes from the leptonic decay of a Z boson. The missing transverse energy cut again removes events with leptonic W decays, this is mainly to reduce the background from WZ production, as seen in Fig. 2b. The effect of these cuts on the heavy quark and gauge boson pair backgrounds are shown in Figs. 1 and 3, respectively.

The backgrounds from the various processes are summarized in Table 1. The simulations of the $b\bar{b}$, $t\bar{t}$ and single top production were performed using HERWIG6.1 [5]. The simulations of gauge boson pair production used PYTHIA6.1 [6]. The major contribution to the background comes from WZ production; the major contribution to the error comes from $b\bar{b}$. For the $b\bar{b}$ simulation we have required a parton-level cut of 40 GeV on the transverse

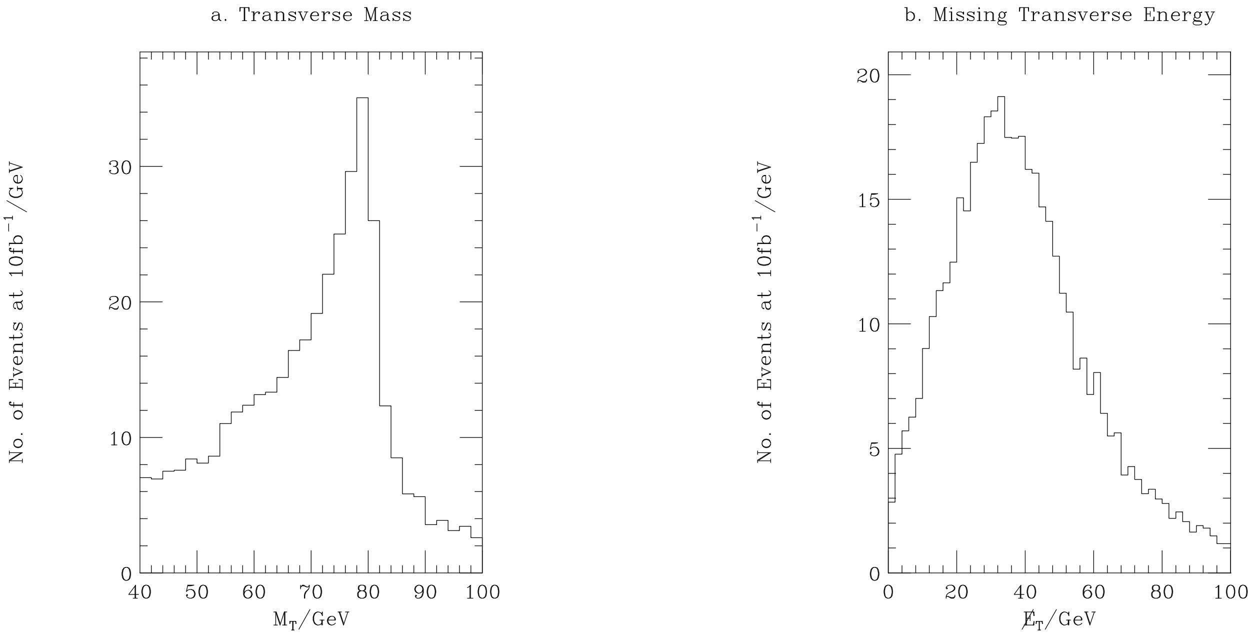

Figure 2: Transverse mass and missing transverse energy in WZ events

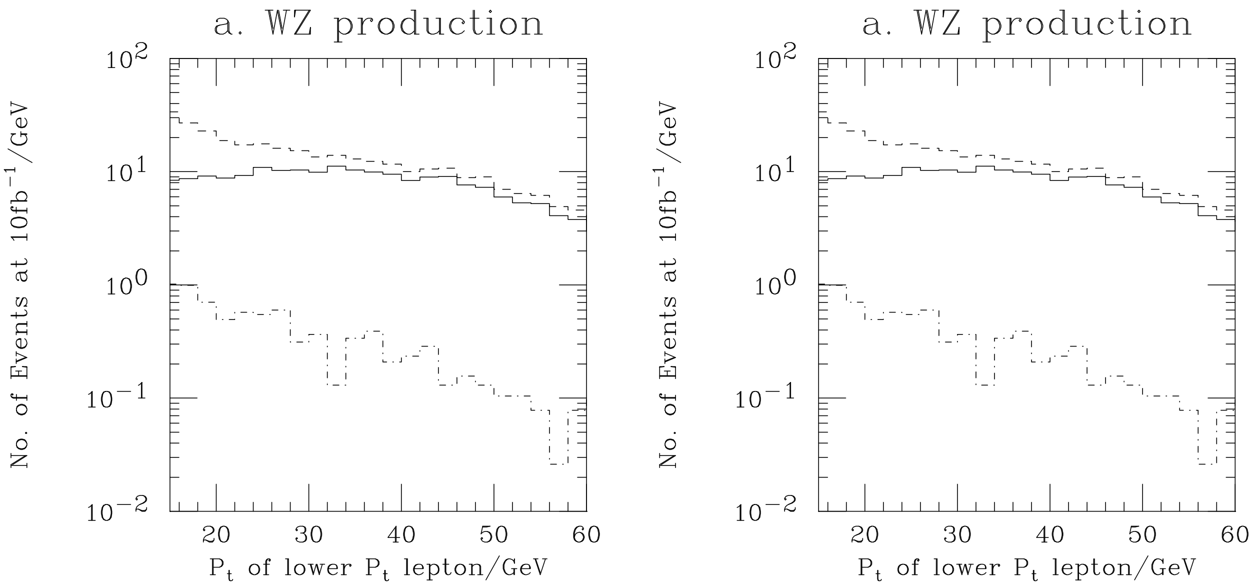

Figure 3: Effect of the isolation cuts on the WZ and ZZ backgrounds. The dashed line gives the background before any cuts, the solid line shows the effect of the isolation cut described in the text. The dot-dash line gives the effect of all the cuts.

Background Process	Number of Events		
	After p_T cut	After isolation and p_T cuts	After all cuts
WW	2.8 ± 0.6	0.0 ± 0.1	0.0 ± 0.1
WZ	226 ± 3	189 ± 3	4.1 ± 0.5
ZZ	50.4 ± 0.9	40.6 ± 0.8	0.9 ± 0.1
$\mathrm{t\bar{t}}$	$(4.8 \pm 0.3) \times 10^3$	0.34 ± 0.14	0.06 ± 0.06
$\mathrm{b\bar{b}}$	$(5.69 \pm 0.8) \times 10^4$	0.0 ± 2.4	0.0 ± 2.4
Single Top	11.5 ± 0.3	0.0 ± 0.008	0.0 ± 0.008
Total	$(6.2 \pm 0.8) \times 10^4$	230 ± 4	5.1 ± 2.5

Table 1: Backgrounds to like-sign dilepton production at the LHC. The numbers of events are based on an integrated luminosity of 10 fb^{-1}. We used the cross sections from the Monte Carlo simulation for $\mathrm{b\bar{b}}$ and single top production, the next-to-leading order cross section for gauge boson pair production from [7] and the next-to-leading order with next-to-leading-log resummation cross section from [8] for $\mathrm{t\bar{t}}$ production. We estimate an error on the cross section from the effect of varying the scale between half and twice the hard scale, apart from gauge boson pair production where we do not have this information for the next-to-leading order cross section. The error on the number of events is then the error in the cross section and the statistical error from the simulation added in quadrature.

momentum of the bottom quarks. This should not affect the results provided we impose a cut of at least 40 GeV on the p_T of the leptons. We also forced the B meson produced to decay semi-leptonically. In events where there was one $\mathrm{B^0_{d,s}}$ meson this meson was forced to mix, if there was more than one $\mathrm{B^0_{d,s}}$ then one of the mesons was forced to mix and the others forced to not mix. Even with these cuts it is impossible to simulate the full luminosity with the resources available, due to the large cross section for $b\bar{b}$ production. This gives the large error on the estimate of this background.

3 Signal

We used HERWIG6.1 [5] to simulate the signal. This version includes the resonant slepton production, including the t-channel diagrams, and the R-parity violating decay of the neutralino including a matrix element for the decay [9]. We will only consider first generation quarks as the cross sections for processes with higher generation quarks are suppressed by the parton distributions. There are upper bounds on the $\not{R}_\mathrm{p}$ couplings from low energy experiments. The bound on λ'_{111} from neutrino-less double beta decay [10, 11] is very strict so we consider muon production via the coupling λ'_{211}, which has a much weaker bound,

$$\lambda'_{211} < 0.059 \times \left(\frac{M_{\tilde{d}_R}}{100\mathrm{GeV}} \right), \tag{3}$$

from the ratio $R_\pi = \Gamma(\pi \to e\nu)/\Gamma(\pi \to \mu\nu)$ [10, 12].

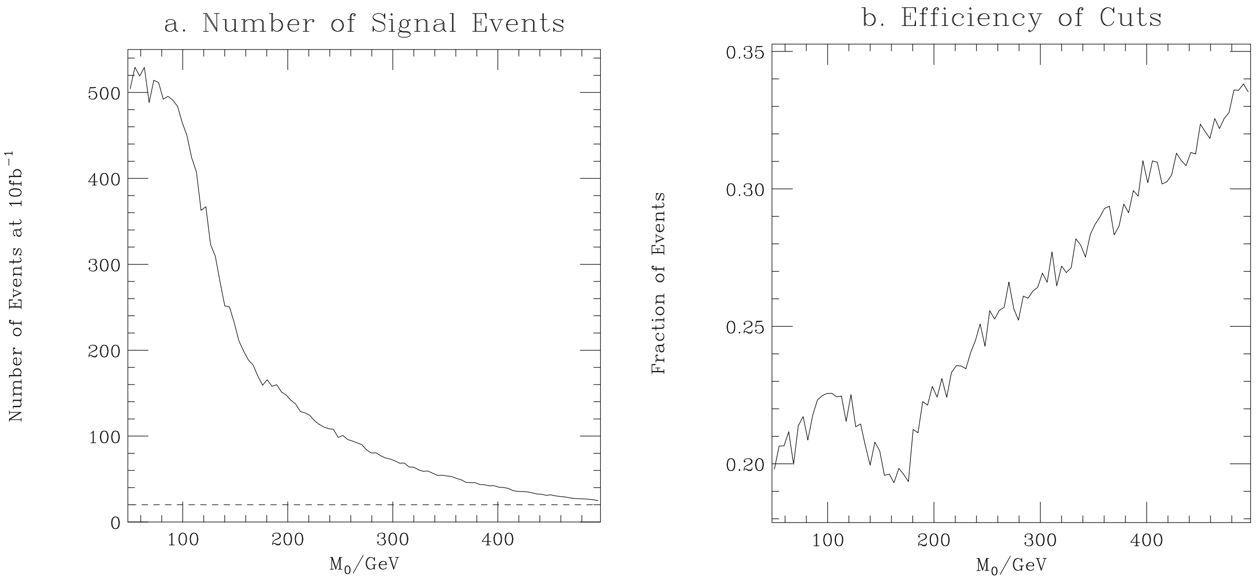

Figure 4: Number of signal events passing the cuts and the efficiency for $M_{1/2} = 300$GeV, $A_0 = 300$GeV, $\tan\beta = 2$, sgn$\mu = +$, with the $\not{R}_p$ coupling $\lambda'_{211} = 0.01$. The dashed line gives the number of events needed for a 5σ discovery.

We have performed a scan in M_0 using HERWIG with the following SUGRA parameters, $M_{1/2} = 300$GeV, $A_0 = 300$GeV, $\tan\beta = 2$, sgn$\mu = +$, and with the $\not{R}_p$ coupling $\lambda'_{211} = 0.01$. The number of events which pass the cuts given in Section 2 are shown in Fig. 4a, while the efficiency of the cuts, *i.e.* the fraction of the signal events which have a like-sign dilepton pair passing the cuts, is shown in Fig. 4b. The dip in the efficiency between 140GeV $<$ $\mathrm{M}_0 < 180$GeV is due to the resonant production of the second lightest neutralino becoming accessible. Just above threshold the efficiency for this channel is low due to the low p_T of the lepton produced in the slepton decay.

If we conservatively take a background of 7.6 events, *i.e.* 1σ above the central value of our calculation, a 5σ fluctuation of the background would correspond to 20 events, using Poisson statistics. This is given as a dashed line in Fig. 4a. As can be seen for a large range of values of M_0 resonant slepton production can be discovered at the LHC, for $\lambda'_{211} = 0.01$. The production cross section depends quadratically on the $\not{R}_p$ Yukawa coupling and hence it should be possible to probe much smaller couplings for small values of M_0.

As can be seen in Fig. 5, at this SUGRA point the sdown mass varies between 622GeV at $M_0 = 50$GeV and 784GeV at $M_0 = 500$GeV. The corresponding limit on the coupling λ'_{211} varies between 0.37 and 0.46. We can probe couplings of $\lambda'_{211} = 2 \times 10^{-3}$ for $M_0 = 50$GeV which corresponds to a smuon mass of 223GeV, and at couplings of $\lambda'_{211} = 10^{-2}$ we can probe values of M_0 up to 500GeV, *i.e.* a smuon mass of 540GeV. This is more than an order of magnitude smaller than the current upper bounds on the $\not{R}_p$ coupling given above for these values of M_0. This is a greater range of couplings and smuon masses than can be probed at

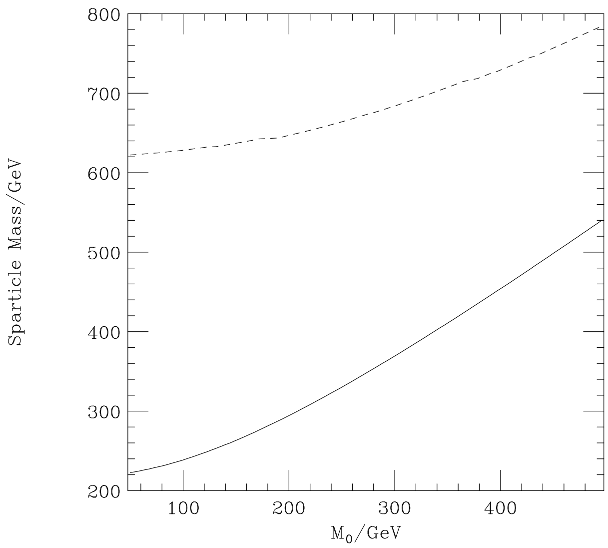

Figure 5: Masses of the left smuon, solid line, and the right sdown, dashed line, as a function of M_0 for $M_{1/2} = 300$GeV, $A_0 = 300$GeV, $\tan\beta = 2$, sgn$\mu = +$.

the Tevatron [13]. The backgrounds are higher at the LHC but this is compensated by the higher energy and luminosity leading to significantly more signal events.

4 Conclusions

We have considered the backgrounds to like-sign dilepton production at the LHC and find a background after cuts of 5.1 ± 2.5 events for an integrated luminosity of $10 fb^{-1}$. This means, taking a conservative estimate of the background of 7.6 events, that 20 events would correspond to a 5σ discovery. For a full analysis however, non-physics backgrounds must also be considered.

A preliminary study of the signal suggests that an efficiency for detecting the signal in excess of 20% can be achieved over a range of points in SUGRA parameter space. At the SUGRA point studied this means we can probe $\not{R}_p$ couplings of 2×10^{-3} for a smuon mass of 223GeV and up to smuon masses of 540GeV for couplings of 10^{-2}, and higher masses for larger couplings.

A more detailed scan of SUGRA parameter space for this signal remains to be performed.

References

[1] H. Dreiner, M. Guchait and D.P. Roy, Phys. Rev. **D49**, 3270 (1994); M. Guchait and D.P. Roy, Phys. Rev. **D52**, 133 (1995), hep–ph/9412329.

[2] H.A. Baer,C-H. Chen, F.E. Paige and X.R. Tata, Phys. Rev. **D53**, 6241 (1996), hep–ph/9512383; S. Abdullin and F. Charles, Nucl. Phys. **B547**, 60 (1999), hep–ph/9811402.

[3] K.T. Matchev and D.M. Pierce, Phys. Rev. **D60**, 075004 (1999), hep–ph/9904282; K.T. Matchev and D.M. Pierce, hep–ph/9907505; J. Nachtman, D. Saltzberg and M. Worcester, CDF collab., hep–ex/9902010.

[4] H.A. Baer, M. Drees, F.E. Paige, P. Quintana and X.R. Tata, hep–ph/9906233,

[5] G. Corcella et al., "HERWIG 6.1 release note", hep–ph/9912396; G. Marchesini et al., Comput. Phys. Commun. **67**, 465 (1992),

[6] T. Sjöstrand, Comput. Phys. Commun. **82**, 74 (1994).

[7] J.M. Campbell and R.K. Ellis, Phys. Rev. **D60**, 113006 (1999), hep–ph/9905386.

[8] R. Bonciani, S. Catani, M.L. Mangano and P. Nason, Nucl. Phys. **B529**, 424 (1998), hep–ph/9801375.

[9] H. Dreiner, P. Richardson and M.H. Seymour, hep–ph/9912407.

[10] B.C. Allanach, A. Dedes and H.K. Dreiner, hep–ph/9906209,

[11] M. Hirsch, H.V. Klapdor-Kleingrothaus and S.G. Kovalenko, Phys. Rev. Lett. **75**, 17 (1995); Phys. Rev. **D53**, 1329 (1996), hep–ph/9502385; K.S. Babu and R.N. Mohapatra, Phys. Rev. Lett. **75**, 2276 (1995), hep–ph/9506354.

[12] V. Barger, G.F. Giudice and T. Han, Phys. Rev. **D40**, 2987 (1989).

[13] H. Dreiner, P. Richardson and M.H. Seymour, hep–ph/9903419; B.C. Allanach et al., hep–ph/9906224.

$\tilde{\chi}_1^0$ reconstruction in mSUGRA models with $R-$parity breaking LQD term

L. MEGNER AND G. POLESELLO

Abstract

The reconstruction of the $\tilde{\chi}_1^0$ LSP through the decay to lepton-jet-jet is studied in the framework of the mSUGRA model. A detailed particle level analysis is performed on events generated with the HERWIG 6.0 Monte Carlo and passed through the ATLAS fast simulation program ATLFAST. The extraction of the $\tilde{\chi}_1^0$ mass peak and techniques for subtracting the combinatorial background are demonstrated on four example points in the mSUGRA parameter space.

1 Introduction

The $R-$parity violating ($\not{R}_{\rm p}$) extension of the MSSM contains the following additional terms in the superpotential, which are trilinear in the quark and lepton superfields,

$$W_{R-odd} = \sum_{i,j,k} \left(\frac{1}{2} \lambda_{ijk} L_i L_j E_k^c + \lambda'_{ijk} L_i Q_j D_k^c + \frac{1}{2} \lambda''_{ijk} U_i^c D_j^c D_k^c \right), \tag{1}$$

where i, j, k are flavor indices. The presence of R-violating terms will mainly manifest itself in two ways: by production of single sparticles, or by the fact that the LSP is not stable and decays to standard model particles. See [1] for a recent review on the subject.

The reconstruction of the $\tilde{\chi}_1^0$ from its decay products in SUSY particle pair production offers the possibility of detecting $R-$parity violation for values of the R-violating couplings too small to yield a significant cross-section for single sparticle production. The $\tilde{\chi}_1^0$ decay can be studied for all three coupling types, λ, λ' and λ'' [2] [3]. The hypothesis of a dominating λ' is the most favorable case for the kinematic reconstruction of SUSY cascade decays, if the decay of the $\tilde{\chi}_1^0$ into a charged lepton has a sizeable branching fraction. In this case, the charged lepton can be used as the initiator of the mass reconstruction, yielding a reduced combinatorial background with respect to three-jet case, and all three particles from the $\tilde{\chi}_1^0$ decay are reconstructed in the detector, allowing to fully reconstruct the $\tilde{\chi}_1^0$ mass peak. In a pioneering work [4] it was explicitly demonstrated that with appropriate selection criteria on jets and leptons a clear $\tilde{\chi}_1^0$ peak could be observed in the lepton-jet-jet invariant mass over an acceptable combinatorial background. That work was based on $\tilde{\chi}_1^0$ decaying with 100% branching fraction to eqq', with the momenta of the decay products distributed according to the phase space. The present study is based on a detailed implementation of the $R-$parity violating decays in the HERWIG 6.0 Monte Carlo including matrix elements for the $\tilde{\chi}_1^0$ decay [7]. We aim to to verify if the $\tilde{\chi}_1^0$ peak can be observed for a broad range of SUSY models, and to develop techniques for evaluating and subtracting the combinatorial background, as a starting point for performing precision measurements of the parameters of the underlying model.

2 The SUSY model

We work in the framework of the minimal Supergravity inspired model (mSUGRA) as implemented in the ISASUSY Monte Carlo [5]. The SUSY events were generated with version 6.0 of the HERWIG Monte Carlo [7], which implements all the $R-$parity conserving two-to-two SUSY processes. This version of HERWIG also includes the simulation of all $R-$parity violating sparticle decays [8]. The produced events were then passed through ATLFAST, a fast simulation of the ATLAS detector [9].

We assumed for this study a single dominant R-violating coupling λ'_{111}=0.01. The results obtained are independent of the precise value of the λ' coupling, as long as it induces a prompt $\tilde{\chi}_1^0$ decay. The results are valid for all the couplings of the type λ'_{ijk} with $i = 1, 2$. They should be taken with some care if j or k is equal to three, since in this case a b quark is among the $\tilde{\chi}_1^0$ decay products.

In models with a single dominant λ' term $\tilde{\chi}_1^0$ has two decay modes: $\tilde{\chi}_1^0 \to l^\pm qq'$ and $\tilde{\chi}_1^0 \to \nu q\bar{q}$. The relative branching ratio of the two modes is a function of the parameters of the model. The mode with a charged lepton is the better mode for reconstructing the $\tilde{\chi}_1^0$ mass, because there is no neutrino which escapes detection. We have verified [6] that the charged lepton mode has a significant branching fraction over all of the mSUGRA parameters space allowed by present experimental searches.

3 $\tilde{\chi}_1^0$ reconstruction in mSUGRA models

3.1 Introduction

The possibility to extract a $\tilde{\chi}_1^0$ mass peak is determined by:

- the number of produced $\tilde{\chi}_1^0$ for which the decay $\tilde{\chi}_1^0 \to l$-jet-jet with $l = e, \mu$ can be completely reconstructed in the detector;
- the combinatorial background, both from SUSY events and from Standard Model processes.

These factors depend on the SUSY model considered, in particular the $\tilde{\chi}_1^0$ mass, the squark and gluino masses, and the jet and lepton multiplicity in SUSY events. Our aim is to determine if the reconstruction can be performed for the full parameter space. For this reason we chose to perform a detailed study for a few representative points in parameter space, trying to span a range as broad as possible of the parameters listed above. A convenient choice are the models already studied in detail for R-conserving mSUGRA [2], which present very varied phenomenologies, and also give the possibility to cross-check the results of our analysis with previous detailed studies. We have therefore selected points 1, 4 and 5, and we have added a low mass point, which we call 7, in a region with low branching fraction ($\sim$ 27%) for the decay $\tilde{\chi}_1^0 \to l^\pm qq'$. The mSUGRA parameters of the studied points are given in Table 1.

Point	m_0	$m_{1/2}$	A_0	$\tan\beta$	sgn(μ)
1	400	400	0	2.0	+
4	800	200	0	10.0	+
5	200	300	300	2.1	+
7	200	200	0	2.0	+

Table 1: *Parameters of the example mSUGRA points studied.*

3.2 Selection criteria for jets

In order to extract a significant $\tilde{\chi}_1^0$ peak the selection criteria need to be optimized separately for each addressed model. At this level, the important parameter is not the purity of the obtained $\tilde{\chi}_1^0$ peak, but its significance, and the possibility of precisely measuring the peak position.

An initial event selection was first made in order to reject the Standard model background. The events were required to have:

- at least 6 jets with $\mathrm{p_t} > 15$ GeV
- at least one lepton with $\mathrm{p_t} > 20$ GeV in point 4 and point 7, and at least two leptons with $\mathrm{p_t} > 10$ GeV in point 1 and point 5.

The reason for requiring two leptons in point 1 and 5 is that a stronger $t\bar{t}$ background rejection is needed, since the SUSY cross-section for these points is lower. These are preliminary cuts and will be further optimized in the final analysis [6]. For the $\tilde{\chi}_1^0$ reconstruction the jets with the highest momentum were not considered, since there are likely to come from the start of the decay chain. The 3rd to the 8th jet in decreasing momentum scale were considered in point 1 and 5 and the 5th to the 8th jets in point 4 and 7. The $\tilde{\chi}_1^0$ was reconstructed starting from an identified electron, and the invariant mass was calculated for the electron-jet1-jet2 combinations such that ΔR(electron-j1)< 2, ΔR(electron-j2)< 2, ΔR(j1-j2)< 2 with $\Delta R = \sqrt{\Delta\eta^2 + \Delta\phi^2}$, where η is the pseudorapidity, and ϕ the angle in the plane perpendicular to the beam axis. In figure 1 the invariant mass distribution obtained in this way is shown in solid lines for the four points. A statistically significant peak, corresponding to the $\tilde{\chi}_1^0$ mass is seen in all four plots. The hatched histograms superimposed on the plots are the $t\bar{t}$ background. This important background can easily be evaluated and subtracted by performing the $\tilde{\chi}_1^0$ reconstruction procedure using the wrong flavor of the lepton as described in the 'wrong flavor' technique below. In the next section we concentrate on the more difficult combinatorics from SUSY events.

3.3 Subtraction of combinatorial background

In order to estimate the shape of the combinatorial background two different techniques were combined.

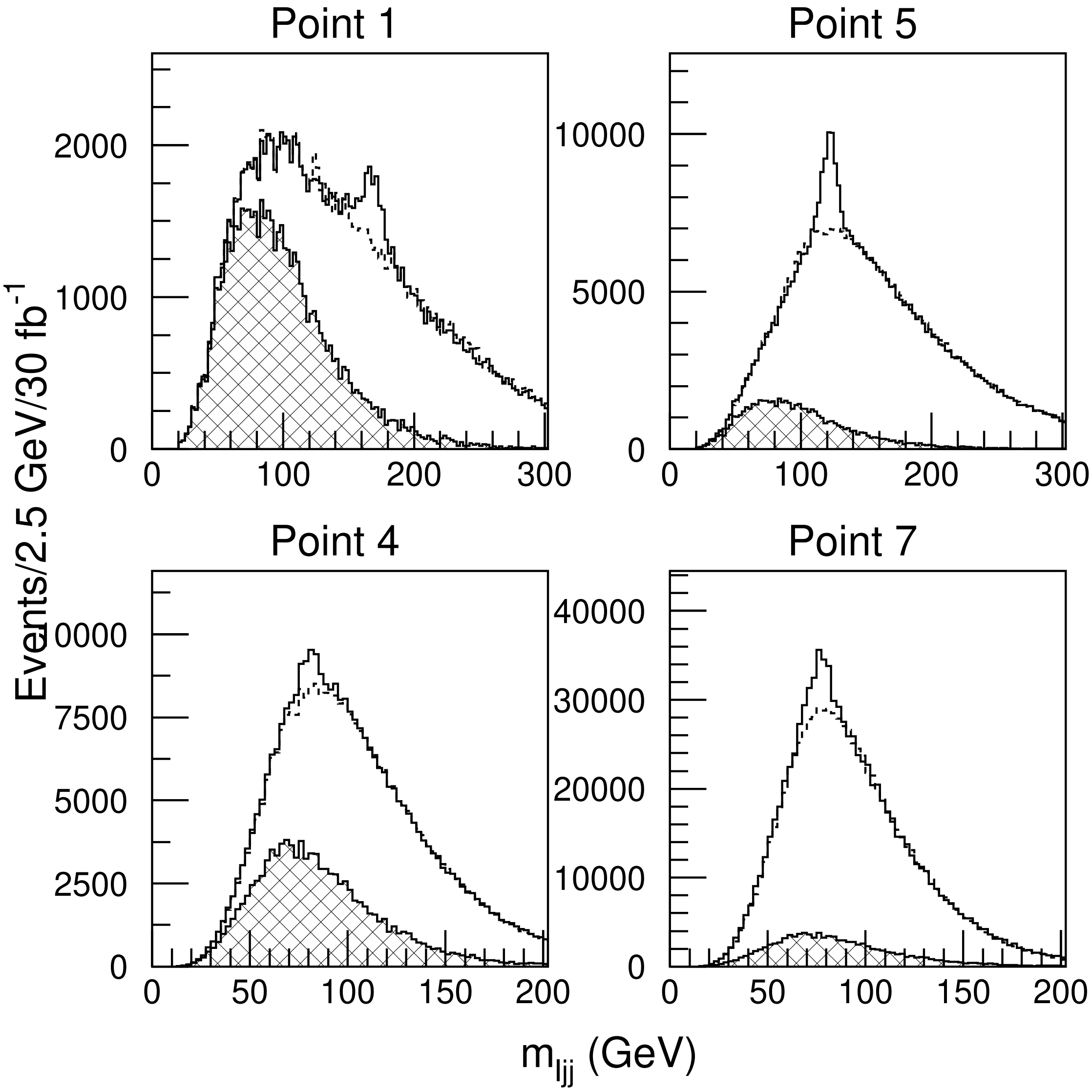

Figure 1: *Invariant mass of the accepted m_{ljj} combinations for the sum of the SUSY signal and the SM $t\bar{t}$ background for the four mSUGRA points studied (solid line). The background from $t\bar{t}$ production is shown as a hatched histogram. The dashed lines show the evaluation of the combinatorial background performed with the 'combined' method described in the text. The statistics shown correspond to an integrated luminosity of 30 fb^{-1}.*

In the 'wrong flavor' technique, the combinatorial background is evaluated using all of the lepton-jet-jet combinations satisfying the cuts for the $\tilde{\chi}_1^0$ candidate, but using the leptons with the wrong flavor, i.e. electrons if the $\tilde{\chi}_1^0$ decays into muons and vice versa.

In the 'mixed events' technique, the idea is to construct lepton-jet-jet combinations and make sure that not all objects in such a combination come from the same $\tilde{\chi}_1^0$, i.e. the combination does not contribute to the signal. In order to make sure that this is the case we use two different events (respectively 1 and 2). The directions (η,ϕ) of the three objects (lepton, jet, jet) and the momenta of two of the objects (lepton-jet or jet-jet) are taken from one of the candidate $\tilde{\chi}_1^0$ combinations in event 1. The momentum of the third object is taken from a combination in event 2.

These two approaches have complementary strengths and weaknesses. The 'wrong flavor' approach correctly subtracts all of the combinatorial background not involving one of the actual leptons from $\tilde{\chi}_1^0$ decay, whereas the 'mixed events' background approximately accounts for events where only two of the three particles come from a $\tilde{\chi}_1^0$ decay.

In order to combine the strengths of the two methods the background is estimated through a linear combination of the backgrounds calculated with the two previous methods. The relative weight of the two components is a function both of the characteristics of the SUSY model and of the applied cuts. In each case it is therefore necessary to optimize the parameters of the linear combination. A prescription which was found to give reasonable results is:

- Normalize the backgrounds estimated with the wrong lepton technique and with mixing events technique to the measured mass spectrum separately. This normalization is done in a region outside of the $\tilde{\chi}_1^0$ peak.
- Evaluate the relative weight of the two different background components by performing a least-square fit to the observed m_{ljj} mass distribution outside of the peak.

The relative weight factors obtained exhibit some sensitivity to the choice of the mass windows over which the least square fit is performed. The 'real' background shape is best reproduced when the lower limit of the mass window is as near as possible to the peak position. Thus the estimate of the peak purity is affected by a systematic uncertainty, whereas the peak position has been checked to be independent of the choice of the subtraction technique. The sum of the background calculated with this combined method and the $t\bar{t}$ background is shown for all the four points as dashed lines in figure 1. In all four cases the distribution for the combinatorial background is nicely reproduced.
We show in Figure 2 the results for Point 5 in order to illustrate the power of this method. In the upper plot the invariant mass distribution for all the accepted electron-jet-jet combinations in SUSY events (solid line) is shown. The combinatorial background evaluated with the 'combined' method is superimposed as a hatched histogram. The lower left plot shows the signal peak after background subtraction (full line); the actual signal from $\tilde{\chi}_1^0$ decay is superimposed (dashed line). Likewise, the full line in the lower right plot is the background distribution estimate obtained with the 'combined method', and the dashed line is the mass distribution for actual background combinatorics. Distributions showing the same excellent agreement are obtained for all four considered models.

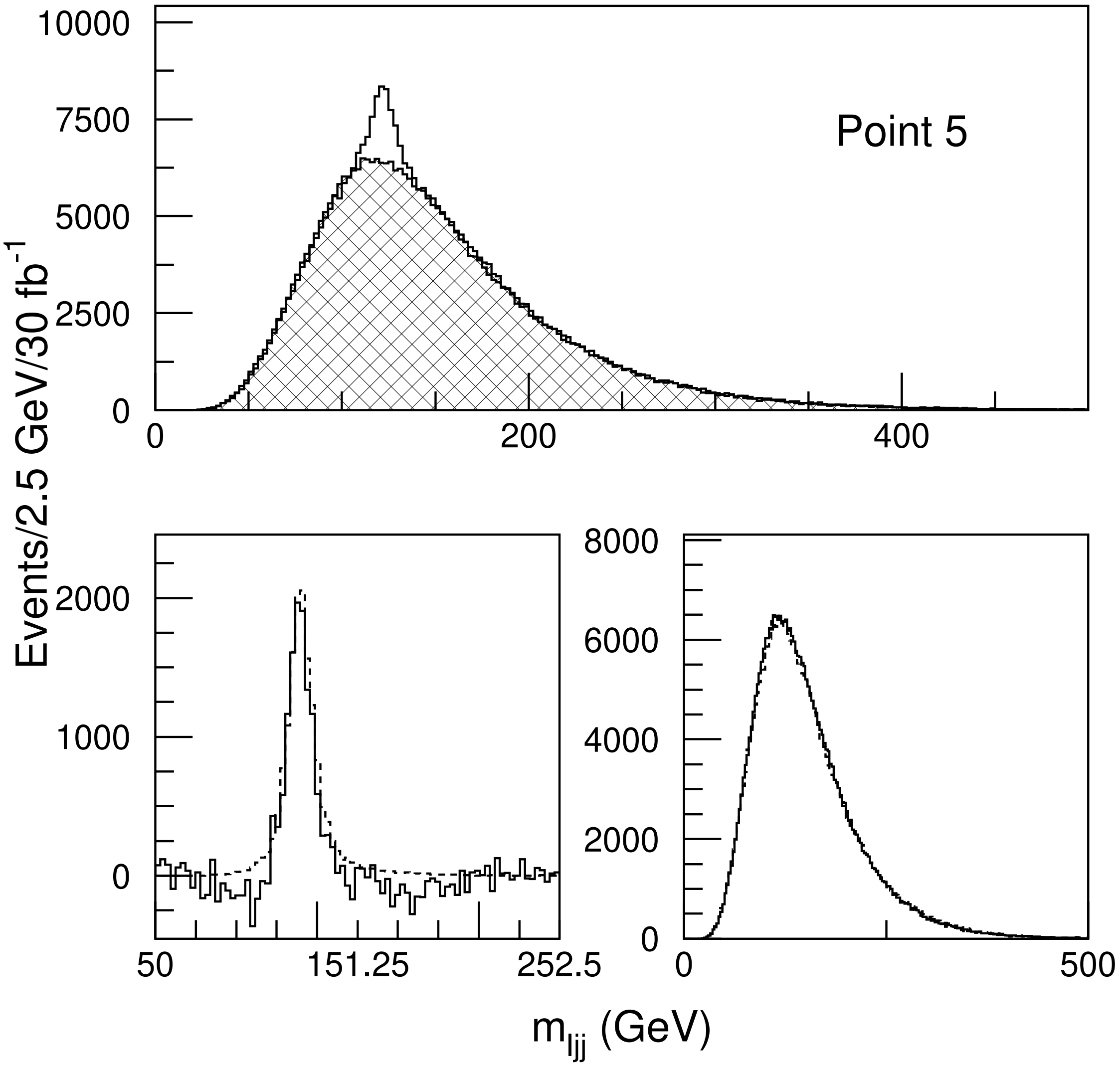

Figure 2: *Point 5: Invariant mass of the m_{ljj} combinations for SUSY events. In the upper plot the mass distribution for the combinatorial background evaluated with the 'combined' method (hatched) is shown superimposed on the observed signal+background distribution (solid line). In the lower plot the mass distributions for signal (left) and background (right) are shown separately. The actual signal/background distributions are shown as dashed lines. The solid lines are the corresponding distributions evaluated with the 'combined' method. The statistics shown corresponds to an integrated luminosity of 30 fb^{-1}.*

4 Conclusions

We have performed a reconstruction of $\tilde{\chi}_1^0$ for the decay $\tilde{\chi}_1^0 \to l^\pm qq'$ for different scenarios within the mSUGRA model with an $R-$parity violating λ' term. We have shown that it is possible to define simple cuts on the jet and lepton multiplicity and topology which allow to observe a statistically significant peak in the lepton-jet-jet invariant mass distribution, at the position of the $\tilde{\chi}_1^0$ mass. We have discussed a method to subtract the combinatorial background. Using this subtraction the $\tilde{\chi}_1^0$ mass and the number of reconstructed $\tilde{\chi}_1^0$s can be precisely measured. This technique works effectively for all four points considered in this analysis. The mass of the reconstructed $\tilde{\chi}_1^0$ can be used as a starting point for the reconstruction of particles further up in the decay chain.

References

[1] H. Dreiner, published in *Perspectives on Supersymmetry* , ed. by G.L. Kane, World Scientific (1998), hep–ph/9707435.

[2] The ATLAS Collaboration, 'ATLAS Detector and Physics Performance Technical Design Report', ATLAS TDR 15, CERN/LHCC/99-15 (1999).

[3] L. Drage and M.A. Parker, 'Measurement of the LSP mass in supersymmetric models with $R-$parity violation', Atlas internal note ATL-PHYS-2000-007.

[4] A. Connors, Ph.D. Thesis, University of Birmingham (UK) 1998; http://www.ep.bham.ac.ud/publications/thesis.

[5] H. Baer, F.E. Paige, S.D. Protopopescu, and X. Tata, hep–ph/9305342 (1993); hep-ph/9804321 (1998).

[6] L. Megner and G. Polesello, in preparation.

[7] G. Corcella et al., Cavendish HEP 99/17 (1999) hep-ph/9912396; G. Marchesini, B.R. Webber, G. Abbiendi, I.G. Knowles, M.H. Seymour and L. Stanco, Computer Phys. Commun. **67** (1992) 465.

[8] H. Dreiner, P. Richardson, and M.H. Seymour, these proceedings.

[9] E. Richter-Was, D. Froidevaux, L. Poggioli, 'ATLFAST 2.0: a fast simulation package for ATLAS', ATLAS Internal Note ATL-PHYS-98-131 (1998).

Supersymmetry with R parity violation at the LHC: discovery potential from single top production

P. CHIAPPETTA, A. DEANDREA, E. NAGY, S. NEGRONI, G. POLESELLO AND J.M. VIREY

Abstract

We study single top production through R-parity violating Yukawa type couplings at the LHC. We consider all $2 \to 2$ partonic processes at tree-level, including interference terms. The calculated $2 \to 2$ partonic cross sections are implemented in PYTHIA to generate complete particle final states. The generated events are processed through a fast particle level simulation of the ATLAS detector. We take into account all important SM backgrounds and study the signal-to-background ratio as a function of the initial partonic states, the exchanged sparticle mass and width, and of the value of the Yukawa couplings.

The feasibility of single top quark production via squark and slepton exchanges to probe several combinations of R parity violating couplings at hadron colliders has been studied [1]. According to those studies, the LHC is better at probing the B violating couplings λ'' whereas the Tevatron and the LHC have a similar sensitivity to λ' couplings. We perform a complete and detailed study including all signal channels using a Monte Carlo generator based on Pythia 6.1 [2], taking into account all the backgrounds and including the ATLAS detector response using ATLFAST 2.0 [3].

The R-parity violating parts of the Lagrangian that contribute to single top production are:

$$L_{\not R} = \lambda'_{ijk}\tilde{e}^i_L \bar{d}^k_R u^j_L - \lambda''_{ijk}(\tilde{d}^k_R \bar{u}^i_L d^j_L + \tilde{d}^j_R (\bar{d}^k_L)^c u^i_L) + h.c. \qquad (1)$$

The superscript c corresponds to charge conjugation. There are altogether 27 and 9 λ'_{ijk} and λ''_{ijk} Yukawa couplings, respectively. The most suppressed couplings are λ'_{111}, λ'_{133}, λ''_{112}, λ''_{113} (see [4] for detailed up to date reviews of the existing bounds). In order to fix the kinematical variables, the reaction we consider is

$$u_i(p_1) + d_j(p_2) \to t(p_3) + b(p_4) \quad , \qquad (2)$$

the p_k being the 4-momenta of the particles and the indices i and j refer to the generations of the u and d-type quarks.

For valence-valence (VV) or sea-sea (SS) subprocesses, the scalar slepton exchange in the $\hat{u}$-channel is taken into account but appears to be suppressed within our assumptions about the λ' couplings and sfermion masses. The down type squark exchange in the $\hat{s}$-channel squared amplitude is dominant.

Let us now consider the subprocesses involving valence-sea (VS) quarks. Concerning R parity violating terms, slepton exchange in the $\hat{s}$-channel and down type squark exchange in the $\hat{u}$-channel contribute. The dominant terms are the squared amplitude due to $\tilde{e}$ exchange, and for initial quarks of the same generation ($i = j$), the interference between W and $\tilde{d}$. The result is sensitive to the interference term only if the product of λ'' couplings is large (around 10^{-1}). For subprocesses involving quarks of different generations in the initial state the situation is more complex and all amplitudes have to be taken into account.

We have carried out a feasibility study to detect single top production through R-parity violation at the LHC by measuring the $l\nu bb$ final state using the following procedure.

First, we have implemented the partonic $2 \to 2$ cross sections in the PYTHIA event generator. Providing PYTHIA with the flavors and momenta of the initial partons using a given parton distribution function (p.d.f.)*, complete final states including initial and final state radiations and hadronization are generated.

The events were processed through ATLFAST to simulate the response of the ATLAS detector. In particular the energy of electrons, photons and muons was smeared according to the resolution of the relevant detector element in the pseudorapidity range $|\eta| < 2.5$. Finally, a simple fixed cone algorithm (of radius $R = 0.4$) was used to reconstruct the parton jets. The minimum transverse energy of a jet was set at 15 GeV. According to the expected b-tagging performance of the ATLAS detector [5] for low luminosity at the LHC we have assumed a 60% b-tag efficiency for a factor 100 of rejection against light jets.

The same procedure was applied to the SM background with the exception that we used besides PYTHIA also the ONETOP [6] event generator.

The integrated luminosity for one year at low luminosity at the LHC is taken to be 10 fb^{-1}. In Table 1 we display the total cross section values for different initial parton flavors in the case of exchanged squarks of mass of 600 GeV and of R-parity conserving width $\Gamma_R = 0.5$ GeV. We took for all $\lambda'' = 10^{-1}$, which yields a natural width of the squark which is smaller than the experimental resolution. Table 4 contains the same information for slepton exchange ($\lambda' = 10^{-1}$, for a slepton of mass of 250 GeV and a width of $\Gamma_R = 0.5$ GeV). Other processes are not quoted because the small value of the limits of their couplings prevents their detection.

Initial partons	cd	cs	ub	cb	
Exchanged particle	$\tilde{s}$	$\tilde{d}$	$\tilde{s}$	$\tilde{d}$	$\tilde{s}$
Couplings	$\lambda''_{212}\lambda''_{332}$	$\lambda''_{212}\lambda''_{331}$	$\lambda''_{132}\lambda''_{332}$	$\lambda''_{231}\lambda''_{331}$	$\lambda''_{232}\lambda''_{332}$
Cross section in pb	3.98	1.45	5.01	0.659	

Table 1: Total cross-section in pb for squark exchange in the $\hat{s}$-channel for a squark of mass of 600 GeV assuming $\Gamma_R = 0.5$ GeV.

In order to study the dependence of the signal on the mass and the width of the exchanged particle we have fixed the couplings to 10^{-1} and have chosen three different masses for the exchanged squarks: 300, 600 and 900 GeV, respectively. For each mass value we have chosen two different Γ_R: 0.5 and 20 GeV, respectively. For the first case $\Gamma_{\not{R}_p}$ dominates, whereas in the last one, when $\Gamma_{tot} \approx \Gamma_R$, the single top-production cross section decreases by a factor

*We have used the CTEQ3L p.d.f.

~ 10. We have considered here the ub parton initial state, since this has the highest cross section value.

In order to study the dependence on the parton initial state we have fixed the mass of the exchanged squark to 600 GeV and its width with $\Gamma_R = 0.5$ GeV and varied the initial state according to the first line of Table 1.

Finally, for the exchanged sleptons we have studied only one case, namely the $u\bar{d}$ initial state with a mass and width of the exchanged slepton of 250 GeV and 0.5 GeV, respectively. In each case we have generated about 10^5 signal events.

The irreducible backgrounds are single top production through a virtual W (noted W^*), or through W-gluon fusion. W-gluon fusion is the dominant process (for a detailed study see [7]). A Wbb final state can be obtained either in direct production or through Wt or $t\bar{t}$ production. Finally, the reducible background consists of W+nj events where two of the jets are misidentified as b-jets.

For the tb final state first we reconstruct the top quark. The top quark can be reconstructed from the W and from one of the b-quarks in the final state, requiring that their invariant mass satisfy $150 \leq M_{Wb} \leq 200$ GeV. The W can be in turn reconstructed from either of the two decay channels: $W \to u\bar{d}$, $W \to l\nu$. Here we have considered only the latter case which gives a better signature due to the presence of a high p_t lepton and missing energy. The former case suffers from multi-jets event backgrounds. As we have only one neutrino, its longitudinal momentum can be reconstructed by using the W and top mass constraints. The procedure used is the following :

- we select events with two b-jets of $p_t \geq 40$ GeV, with one lepton of $p_t \geq 25$ GeV, with $E_t^{miss} \geq 35$ GeV and with a jet multiplicity ≤ 3,
- we reconstruct the longitudinal component (p_z) of the neutrino by requiring $M_{l\nu} = M_W$. This leads to an equation with twofold ambiguity on p_z.
- More than 80% of the events have at least one solution for p_z. In case of two solutions, we calculate $M_{l\nu b}$ for each of the two b-jets and we keep the p_z that minimizes $|M_{top} - M_{l\nu b}|$.
- we keep only events where $150 \leq M_{l\nu b} \leq 200$ GeV.

Next, the reconstructed top quark is combined with the b quark not taking part in the top reconstruction. In order to reduce the $t\bar{t}$ background to a manageable level, we need to apply a strong jet veto on the third jet by requiring that its p_t should be ≤ 20 GeV.

The invariant mass distribution of the tb final state after the cuts described above is shown in Fig. 1. Once an indication for a signal is found, we count the number of signal (N_s) and background (N_b) events in an interval corresponding to 2 standard deviations around the signal peak for an integrated luminosity of 30 fb^{-1}. Then we rescale the signal peak by a factor α such that $N_s/\sqrt{N_b} = 5$. By definition the scale-factor α determines the limit of sensitivity for the lowest value of the λ'' (λ') coupling we can test with the LHC: $\lambda''_{ijk} \cdot \lambda''_{lmn} \leq 0.01 \cdot \sqrt{\alpha}$.

In Table 2 we show the limits obtained for the combinations of $\lambda''_{132}\lambda''_{332}$ for different masses and widths of the exchanged $\tilde{s}$-quark. Also shown are the current limits assuming a mass for $\tilde{m}_f = 100$ GeV, the number of signal and background events, as well as the experimentally observable widths of the peak (Γ_{exp}).

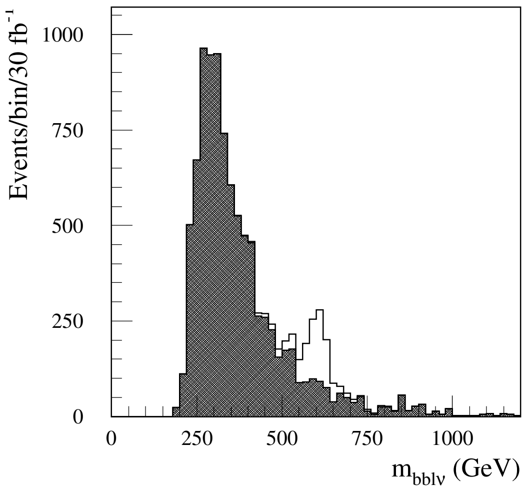

Fig. 1 - Invariant mass distribution of $l\nu bb$ for the signal and backgrounds (dashed histogram) after three years at LHC at low luminosity after having applied the cuts.

$m_{\tilde{s}}$ (GeV)	300		600		900	
Γ_R (GeV)	0.5	20	0.5	20	0.5	20
N_s	6300	250	703	69	161	22
N_b	4920	5640	558	1056	222	215
Γ_{exp} (GeV)	24.3	30.5	37.5	55.6	55.4	62.1
$\lambda'' \times \lambda''$	2.36×10^{-3}	1.21×10^{-2}	4.10×10^{-3}	1.51×10^{-2}	6.09×10^{-3}	2.09×10^{-2}

Table 2: Limits for the values of the $\lambda''_{132}\lambda''_{332}$ Yukawa couplings for an integrated luminosity of 30 fb^{-1}. For the other quantities see the text. The current limit is 6.25×10^{-1}.

In Table 3 we compile the sensitivity limit of the bilinear combination of the different Yukawa couplings one can obtain after 3 years of LHC run with low luminosity, if the exchanged squark has a mass of 600 GeV.

Initial partons	cd	cs	ub	cb	
Exchanged particle	$\tilde{s}$	$\tilde{d}$	$\tilde{s}$	$\tilde{d}$	$\tilde{s}$
Couplings	$\lambda''_{212}\lambda''_{332}$	$\lambda''_{212}\lambda''_{331}$	$\lambda''_{132}\lambda''_{332}$	$\lambda''_{231}\lambda''_{331}$	$\lambda''_{232}\lambda''_{332}$
N_s	660	236	703	96	
N_b	558				
Γ_{exp} (GeV)	38.5	31.3	37.5	40.1	
Limits on $\lambda'' \times \lambda''$	4.26×10^{-3}	7.08×10^{-3}	4.1×10^{-3}	1.11×10^{-2}	

Table 3: Limits on the Yukawa couplings for an exchanged squark of mass 600 GeV assuming $\Gamma_R = 0.5$ GeV, for an integrated luminosity of 30 fb^{-1}. Current limit is 6.25×10^{-1}.

For the exchanged sleptons (cf Table 4) we have calculated the sensitivity limit of the bilinear combination of the different Yukawa couplings only for the most favorable case, i.e. for the $u\bar{d}$ partonic initial state. We obtain 4.63×10^{-3} for the limits on $\lambda'_{11k}\lambda'_{k33}$ (in comparison with the limit of 2.8×10^{-3} obtained by Oakes *et al.*).

Initial partons	$u\bar{d}$	$u\bar{s}$	$c\bar{d}$	$c\bar{s}$	$u\bar{b}$	$c\bar{b}$
Couplings	$\lambda'_{11k}\lambda'_{k33}$	$\lambda'_{12k}\lambda'_{k33}$	$\lambda'_{21k}\lambda'_{k33}$	$\lambda'_{22k}\lambda'_{k33}$	$\lambda'_{13k}\lambda'_{k33}$	$\lambda'_{23k}\lambda'_{k33}$
Cross section in pb	7.05	4.45	2.31	1.07	2.64	0.525

Table 4: Total cross-section in pb for slepton exchange in the $\hat{s}$-channel for a slepton of mass of 250 GeV assuming $\Gamma_R = 0.5$ GeV.

For those cases where the exchanged squark (slepton) can be discovered at the LHC we have made an estimate on the precision with which one can determine its mass. For this purpose, we have subtracted the background under the mass peak and fitted a Gaussian curve on the remaining signal. For the assumed value of the coupling constant, the error on the mass determination is dominated by the 1% systematic uncertainty on the jet energy scale in ATLAS [5].

References

[1] H. Dreiner and G.G. Ross, Nucl. Phys. **B365** (191991) 597; A. Datta, J.M. Yang, B.L. Young and X. Zhang, Phys. Rev. **D56** (191997) 3107; R.J. Oakes, K. Whisnant, J.M. Yang, B.L. Young and X. Zhang, Phys. Rev. **D57** (191998) 534; P. Chiappetta, A. Deandrea, E. Nagy, S. Negroni, G. Polesello and J.M. Virey, hep-ph/9910483.

[2] T. Sjöstrand, Comput. Commun. 82 (1994) 74.

[3] E. Richter-Wąs, D. Froidevaux, L. Poggioli, ATLAS Internal Note Phys-No-79, 1996.

[4] G. Bhattacharyya, Nucl. Phys. Proc. Suppl. **52A** (1997) 83; H. Dreiner, hep-ph/9707435, in Perspectives on Supersymmetry, ed. G. Kane, World Scientific; Report of the R-parity group of GDR SUSY, hep-ph/9810232, available at http://www.in2p3.fr/susy/ and references therein; B.C. Allanach, A. Dedes and H.K. Dreiner, Phys. Rev. **D60** (191999) 07501; B. Allanach et al., in Physics at Run II: Workshop on Supersymmetry/Higgs, Batavia, IL, 19-21 Nov, 1998, hep-ph/9906224.

[5] The ATLAS Collaboration, Detector and Physics Performance Technical Design Report, CERN/LHCC/99-14, ATLAS TDR 14, 25 may 1999.

[6] Onetop, C.P. Yuan, D. Carlson, S. Mrenna, Barringer, B. Pineiro and R. Brock, http://www.pa.msu.edu/˜brock/atlas-1top/EW-top-programs.html

[7] T. Stelzer, Z. Sullivan and S. Willenbrock, Phys. Rev. **D58** (191998) 094021.

Probing $\not{R}_p$ couplings through indirect effects on Drell-Yan production at the LHC

D. CHOUDHURY and R.M. GODBOLE

Abstract

In this note we analyze the sensitivity to $\not{R}_p$ couplings at the LHC through the measurement of dilepton pairs, taking λ'_{211} as example. We show that by exploiting the differences in the kinematic distributions of the $\not{R}_p$ contributions from that of the SM case, we can do significantly better than the bounds obtained from low energy experiments. Further the possible LHC bound on the couplings does not scale as the mass of the squark. Similar analysis can also be done to assess the reach of the LHC to effects due to leptoquarks/compositeness etc.

Within the Standard Model, electroweak gauge invariance ensures both lepton number and baryon number conservation (at least in the perturbative context). However, this is not so within the Minimal Supersymmetric Standard Model (MSSM). In most standard treatments, such interactions are avoided by the imposition of a discrete symmetry called R-parity, which implies a conserved multiplicative quantum number, $R \equiv (-1)^{3B+L+S}$, where B is baryon number, L is lepton number, and S is spin [1]. All ordinary particles are R-parity even, while all superpartners are R-parity odd. If R-parity is conserved, superpartners must be produced in pairs and the lightest superpartner, or LSP, is absolutely stable. Unfortunately, R-parity invariance of the SUSY Lagrangian is an *ad hoc* assumption and not derived from any known fundamental principle. Hence, it is of interest to consider R-parity–violating extensions of the MSSM, especially since the experimental signatures of low energy supersymmetry would then be radically different. Curiously, $\not{R}_p$ interactions can improve the agreement between theory and precision electroweak measurements, and also offer explanations [2] for experimental anomalies such as the high-Q^2 excess reported at HERA [3].

The most general $\not{R}_p$ terms in the superpotential consistent with Lorentz invariance, gauge symmetry, and supersymmetry are*

$$W_{\not{R}} = \lambda_{ijk} L_i L_j E^c_k + \lambda'_{ijk} L_i Q_j D^c_k + \lambda''_{ijk} U^c_i D^c_j D^c_k, \tag{1}$$

where L_i and Q_i are the $SU(2)$ doublet lepton and quark fields and E^c_i, U^c_i, D^c_i are the singlet superfields. The UDD couplings violate baryon number while each of the other two sets violate lepton number. As our aim is to explore dilepton final states in pp collisions, we shall explicitly forbid the UDD interactions [5] as an economical way to avoid unacceptably rapid proton decay.

The remarkable agreement between low-energy experimental data and SM expectations imply quite severe bounds on the strength of many $\not{R}_p$ operators [6]. Thus, within the

*We do not consider here the bilinear terms that mix lepton and Higgs superfields [4].

context of colliders it is natural to consider the production of supersymmetric particles to be governed mainly by gauge interactions with $\not{R}_p$ being important only in the subsequent decay [7]. However, such analyses are neither very sensitive to the actual size of the $\not{R}_p$ coupling nor are they particularly useful for the case of heavy superpartners (when the pair-production cross sections are smaller). A complementary approach [8, 9] is afforded by processes like Drell-Yan production where the exchange of a heavy squark is governed by the relevant $\not{R}_p$ coupling. In this note, we refine the analysis of Ref. [8] in the context of the LHC, thereby extending its reach.

Expanding the superfield components in (1), we obtain the interaction Lagrangian that connects quarks to leptons:

$$\mathcal{L}_{LQD} = \lambda'_{ijk} \left\{ \tilde{\nu}_{i\mathrm{L}} \bar{d}_{k\mathrm{R}} d_{j\mathrm{L}} - \tilde{e}_{i\mathrm{L}} \bar{d}_{k\mathrm{R}} u_{j\mathrm{L}} + \tilde{d}_{j\mathrm{L}} \bar{d}_{k\mathrm{R}} \nu_{i\mathrm{L}} - \tilde{u}_{j\mathrm{L}} \bar{d}_{k\mathrm{R}} e_{i\mathrm{L}} + \tilde{d}^c_{k\mathrm{R}} \nu_{i\mathrm{L}} d_{j\mathrm{L}} - \tilde{d}^c_{k\mathrm{R}} e_{i\mathrm{L}} u_{j\mathrm{L}} \right\} + \mathrm{h.c.} \tag{2}$$

With only one λ'_{ijk} being nonzero, the simplest processes (with an observable final state) to which $\mathcal{L}_{LQD}$ would contribute are

- $u_j \bar{u}_j \to e_i^- e_i^+ \; (\tilde{d}_{k\mathrm{R}})$
- $d_k \bar{d}_k \to e_i^- e_i^+ \; (\tilde{u}_{j\mathrm{L}})$
- $u_j \bar{d}_j \to e_i^+ \nu_i \; (\tilde{d}_{k\mathrm{R}})$
- $q_j \bar{q}'_j \to q_j \bar{q}'_j \; (\tilde{\nu}_{i\mathrm{L}}, e_{i\mathrm{L}})$

with the particle in parentheses being exchanged in the t-channel. If we allow more than one $\not{R}_p$ coupling to be non-zero, more exotic final states would be possible. However, as simultaneous existence of more than one such coupling is disfavored from the data on flavor-changing neutral current processes [10], we shall not consider this possibility. Furthermore, the limits on LQD couplings of muons with the first-generation quarks found in nucleon targets are weaker than those for electrons. Hence, in this note, we shall restrict ourselves to perhaps the most optimistic case, namely the study of a $\mu^+\mu^-$ final state in the presence of a non-zero λ'_{211}. The corresponding details for the other cases will be presented elsewhere.

The signature we focus on is a $\mu^+\mu^-$ *without* any missing transverse momentum. To ensure detectability, we demand that

$$p_T(\mu^\pm) \geq 50\mathrm{GeV} \qquad \text{and} \qquad \left|\eta(\mu^\pm)\right| < 3 \; . \tag{3}$$

The lowest order SM process leading to such a final state is the Drell–Yan mechanism *i.e.* $q\bar{q} \to (\gamma^*, Z^*) \to \mu^+\mu^-$. A non-zero λ'_{211} induces an additional t–channel diagram and the expressions for the total cross sections can be found in Ref. [8]. QCD corrections to the Drell–Yan process have been calculated [11] to the next-to-leading order and are a function of the c.m. energy ($\sqrt{s}$) of the collider, the structure functions used and the subprocess scale M. The dependence on M is marginal though and one may approximate it by a scale–independent K-factor 1.12 (for the CTEQ4M [12] structure functions that we use). The same factor approximates the K-factor for the dimuon mass distributions also for the range of dimuon masses and rapidities that we use. In the absence of a calculation of the higher-order corrections to the $\not{R}_p$ contribution, we assume that K-factor for the full theory is the same as that within the SM.

To maximize the sensitivity, we need to consider the differential distributions especially since the event topology of the $\not{R}_p$ "signal" is quite different from that of the SM "background". A convenient set of independent kinematical variables is given by the dimuon invariant mass M, the rapidity of the $\mu^+\mu^-$ pair $\eta_{\rm pair}$ and the difference of the individual rapidities $\Delta\eta$.

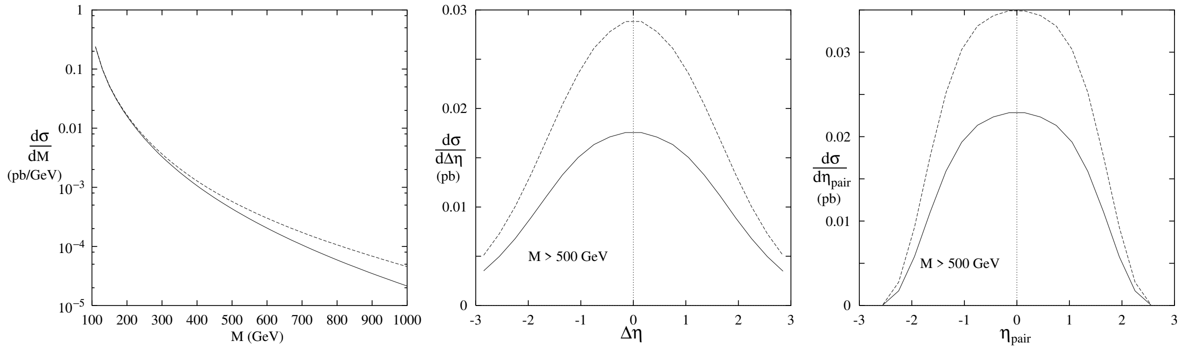

Figure 1: *The phase space distributions for the Drell-Yan process at the LHC. The kinematical cuts are as in 3. For the rapidity distributions, an additional cut ($M > 500\,GeV$) has been imposed. In each case, the lower curve corresponds to the SM and the upper curve to $\lambda'_{211} = 0.5$, $m_{\rm sq} = 800\,GeV$.*

It is obvious that the contribution due to a heavy squark exchange would be non-negligible only for $M \gtrsim m_{\rm sq}$. Thus the relative deviations are pronounced only for large values of M (see Fig.1). It has been demonstrated [13] that the parton luminosities can be measured with high accuracy at the LHC. Hence a change in the absolute value of the cross-section can indeed be used to look at the sensitivity of the signal to $\not{R}_p$ couplings. As a matter of fact such an analysis [14] of the differential distribution in the dimuon mass of the dimuon pair cross-section has been used by the D0 collaboration to put limits on the Quark-Electron Compositeness scale, using the Tevatron data. Recall that the analysis here does include the effect of the higher order corrections on the SM contribution to the $\mu^+\mu^-$ pairs.

Note that $\Delta\eta (= \eta_+ - \eta_-)$, the difference of the lepton rapidities is directly related to the scattering angle in the subprocess center-of-mass frame. Hence one expects to see the difference between an s–channel and a t–channel process in this distribution. This is borne out strikingly in the second of Fig. 1. The symmetry about $\Delta\eta = 0$ is dictated by the fact that the initial state is symmetric. And finally, one considers $\eta_{\rm pair}$ which is a measure of the Lorentz boost of the center-of-mass frame, or in other words, the mismatch of the quark and antiquark energies.

To quantify our comparison of the differential distributions in the two cases (SM vs. $\not{R}_p$), we devise a χ^2 test. We divide the M–$\eta_{\rm pair}$–$\Delta\eta$ hypervolume into equal sized bins and compare the number of signal ($N_n^{\mathrm{SM}+\not R}$) and background (N_n^{SM}) events in each bin for a given integrated luminosity. We then define a χ^2 test of discrimination

$$\chi^2 = \sum_n \frac{(N_n^{\mathrm{SM}+\not R} - N_n^{\mathrm{SM}})^2}{N_n^{\mathrm{SM}} + (\epsilon N_n^{\mathrm{SM}})^2} \tag{4}$$

where ϵ is a measure of the systematic errors, arising mainly from the uncertainties in luminosity measurement and quark densities. To be specific, we use a uniform grid of $(20\mathrm{GeV}, 0.15, 0.15)$ and choose two representative values for ϵ, namely 5% and 15%.

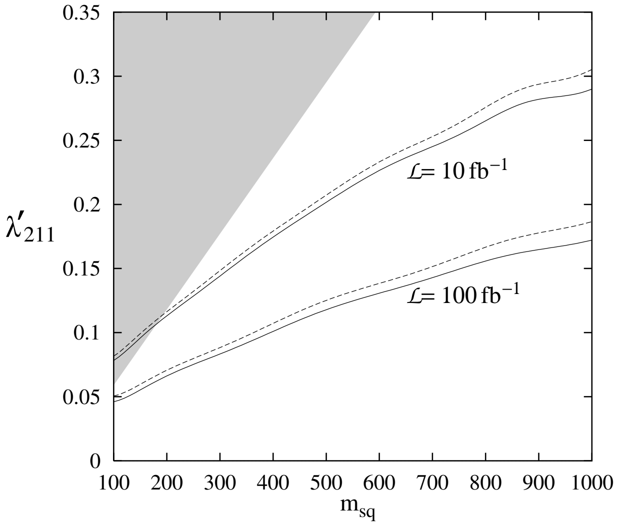

Figure 2: *The 95% C.L. exclusion curves that may be obtained at the LHC for two different values of integrated luminosity. In each case, the lower curve corresponds to a systematic uncertainty (see eq.4)* $\epsilon = 0.05$ *while the upper corresponds to* $\epsilon = 0.15$. *The shaded region indicates the region excluded by low energy measurements.*

In Fig. 2, we present the exclusion plots in the $(m_{\mathrm{sq}}, \lambda'_{211})$ plane that can be achieved at the LHC for a given luminosity. The interpretation is simple. The area above the respective curves can be ruled out at 95% C.L. As expected, for $\epsilon = 0.15$ we do slightly worse than for the case of $\epsilon = 0.05$. And similarly, we do better with larger luminosity. What is most interesting, however, is that we do significantly better than the bounds obtained [6] from low-energy experiments, *viz.*

$$\lambda'_{211} < 0.059\,(100\mathrm{GeV}/m_{\tilde{d}_R}) \,.$$

The LHC bound clearly does not scale as the mass of the squark. This is easily understood from a perusal of the first of Figs. 1. For smaller squark masses, the $\not R_{\mathrm{p}}$ contribution is also peaked at smaller values of M. However, the SM contribution is also much bigger at such M. Consequently, the relative deviations are smaller and so are the contributions to the

χ^2. For larger squark masses, the $\not{R}_p$ contributions concentrate at larger M and hence the relative deviations are larger too. This is also the reason why our analysis shows much more sensitivity to the $\not{R}_p$ couplings than the analysis of Ref. [9].

It is clear that a similar analysis can also be performed to study the sensitivity of LHC experiments to effects of Leptoquarks/compositeness etc. which would give rise to four-fermion currents with unusual chiral structure.

References

[1] P. Fayet, Phys. Lett. **B69** (19489) 77; G. Farrar and P. Fayet, Phys. Lett. **B76** (19575) 78.

[2] D. Choudhury and S. Raychaudhuri, Phys. Lett. **B401** (1954) 97; G. Altarelli, *et al.* , Nucl. Phys. **B506** (193) 97; H. Dreiner and P. Morawitz, Nucl. Phys. **B503** (1955) 97; J. Kalinowski, *et al.* , Z. Phys. **74** (19595) 97; T. Kon and T. Kobayashi, Phys. Lett. **B409** (19265) 97; G. Altarelli, G.F. Giudice and M. L. Mangano, Nucl. Phys. **B506** (1929) 97; J. Ellis, S. Lola and K. Sridhar, Phys. Lett. **B408** (19252) 97; M. Carena, D. Choudhury, S. Raychaudhuri and C.E.M. Wagner, Phys. Lett. **B414** (1992) 97.

[3] C. Adloff, *et al.* (H1 Collaboration), Z. Phys. **74** (19191) 97; J. Breitweg, *et al.* (ZEUS Collaboration), Z. Phys. **74** (19207) 97.

[4] See, *e.g.* , L. J. Hall and M. Suzuki, Nucl. Phys. **B231** (19419) 84.

[5] L. Ibañez and G. G. Ross, Phys. Lett. **B260** (19291) 91, Nucl. Phys. **B368** (193) 92; S. Lola and G.G. Ross, Phys. Lett. **B314** (19336) 93; P. Binétruy, E. Dudas, S. Lavignac and C.A. Savoy, Phys. Lett. **B422** (19171) 98; J. Ellis, S. Lola and G.G. Ross, Nucl. Phys. **B526** (19115) 98.

[6] V. Barger, G.F. Giudice and T. Han, *Phys. Rev.* **D40** (1989) 2987; G. Bhattacharyya and D. Choudhury, Mod. Phys. Lett. **A10**, 1699 (1995); G. Bhattacharyya, Nucl. Phys. B (Proc. Suppl.) **52A,** 38 (1997); H. Dreiner, hep-ph/9707435 v2; R. Barbieri et al, hep-ph/9810232.

[7] V. Barger, M.S. Berger, P. Ohmann and R.J. Phillips, Phys. Rev. **50** (194299) 94; H. Baer, C. Kao and X. Tata, Phys. Rev. **51** (192180) 95.

[8] G. Bhattacharyya, D. Choudhury and K. Sridhar, Phys. Lett. **B349** (19118) 95.

[9] J. Hewett and T. Rizzo, Phys. Rev. **56** (195709) 97.

[10] Stringent limits on products of R-parity–violating couplings are given by K. Agashe and M. Graesser, Phys. Rev. **54** (194445) 95; D. Choudhury and P. Roy, Phys. Lett. **B378** (19153) 96; F. Vissani and A. Yu. Smirnov, Phys. Lett. **B380** (19317) 96; R.M. Godbole, S. Pakvasa, S.D. Rindani and X. Tata, hep-ph/9912315.

[11] T. Matsuura, S.C. van der Marck and W.L. van Neerven, *Phys. Lett.* **B211** (1988) 171; *Nucl. Phys.* **B319** (1989) 570; R. Hamberg, W.L. Van Neerven and T. Matsuura, *Nucl. Phys.* **B359** (1991) 343.

[12] H.L. Lai, *et al.* (CTEQ Collaboration), Phys. Rev. **55** (191280) 97.

[13] M. Dittmar, Phys. Rev. **55** (19161) 97.

[14] B. Abbott *et al.* (D0 Collaboration), Phys. Rev. Lett. **82** (194769) 99.

Neutrino masses, R-parity violating supersymmetry and collider signals

A.K. DATTA, B. MUKHOPADHYAYA, S. ROY AND F. VISSANI

In a scenario with R-parity violating supersymmetry one can have masses for the neutrinos. The seed of this lies in the superpotential, where, upon admission of lepton number violation, one can write the following terms over and above those of the minimal SUSY standard model (MSSM):

$$W_{\not R} = \lambda_{ijk} L_i L_j E_k^c + \lambda'_{ijk} L_i Q_j D_k^c + \lambda''_{ijk} U_i^c D_j^c D_k^c + \epsilon_i L_i H_2 \tag{1}$$

If one considers the framework where R-parity is violated through a term of the type $\epsilon_i L_i H_2$, then one neutrino acquires a mass at the tree level through mixing with neutralinos. We have argued that this may give rise to the mass splitting corresponding to the $\nu_\mu \to \nu_\tau$ oscillation, which provides an explanation of the atmospheric muon neutrino deficit recorded by the superkamiokande (SK) experiment [1]. The other two neutrinos remain massless at the tree level. However, the λ-and λ'-type terms can at the same time induce mass terms for all the three generations at the one-loop level, which can be responsible for a smaller mass splitting between the the first two neutrino generation, thereby explaining the solar neutrino problem.

The relevant parameters in this scenario, in addition to those contained in the MSSM, are the ϵ_i's mentioned above and vacuum expectation values (vev) for the scalar neutrinos, which are unavoidable consequences of the former. These can be lumped into one 'basis-independent' parameter, namely, the vev of the sneutrino corresponding to the state which acquires the tree-level mass. The SK results restrict this vev to be of the order of 100 keV. It is also possible to constrain the parameter space of the soft bilinear SUSY breaking terms of this theory from large angle mixing and neutrino mass-squared difference as demanded by the atmospheric ν_μ data. In addition, non-trivial restrictions on the hierarchy of the ϵ-parameters of different flavors or between the ϵ's and μ follow if we demand that flavor-changing neutral currents be suppressed [2]. Moreover, if one wants to solve the solar neutrino problem in this scenario, either through MSW solution or vacuum oscillation, then the λ and λ' couplings also get restricted to values $\leq 10^{-5}$ for the MSW solution, and to much smaller values for the 'just-so' solution.

Apart from the neutrino-neutralino mixing mentioned above, such a scenario induces mixing in the chargino-charged lepton sector as well. These mixings result in some couplings like $\tilde\chi_1^0 \tau W$, $\tilde\chi_1^0 \nu Z$ etc., which are characteristic of bilinear R-parity violation.

If the lightest neutralino ($\tilde\chi_1^0$) is heavier than the Z, then we have the following additional decay channels of $\tilde\chi_1^0$ [3]:

$$\tilde\chi_1^0 \to \nu_l Z, \qquad l = e, \mu, \tau \tag{2}$$

$$\tilde\chi_1^0 \to l W, \qquad l = e, \mu, \tau \tag{3}$$

This kind of decay will not be possible with only the trilinear R-violating interactions. Also, if the λ and λ' terms have to be responsible for loop-induced solutions to the solar neutrino problem, then they are restricted to such values that three-body decays of the lightest neutralino triggered by them are dominated by the two-body decays as and when they are allowed. In such a case, demanding maximal mixing between the second and third generations (as required by the SK data), one would expect to get equal numbers of muons and taus in decays in the channel $\tilde{\chi}_1^0 \to lW$ [4]. This can be a remarkable feature in collider searches of the lightest neutralino. Another important observation is that, thanks to the small R-violating couplings necessitated by the small tree-level neutrino mass, the decay length of the lightest neutralino can be as large as 1 - 10 mm or so. This implies a decay gap that can be observed in collider experiments.

Among other signals that have been investigated [5], the signal in the form of *equal* number of *like sign* μ and τ events accompanied by *like sign on-shell* W's may be seen at the upgraded Tevatron, LHC or future generation e^+e^- colliders when a pair of lightest neutralinos ($\tilde{\chi}_1^0$) is produced directly or via cascades. Each neutralino may decay directly to μ or τ (with BR $\sim 40\%$) [4] along with *on-shell* W's. We emphasize that this is a consequence of neutralino-neutrino mixing triggered exclusively by the bilinear R-parity violating terms in the superpotential. A very interesting possibility, essentially due to the Majorana nature of neutralinos, is that of having like-sign dilepton events accompanied by two W's of identical charge [6]. Of course, for such a signal to be distinct, one requires the associated W's to be *on-shell*. In other words, such a signal is typical of a situation where χ_1^0 is heavier than the W. Otherwise, 3-body decays of the lightest neutralino take place, and these can have contributions from trilinear R-violating couplings as well.

The interesting feature is that there is almost no Standard Model background for such a signal. Taming the MSSM background, too, is unlikely to pose any serious difficulty, so long as the W's can be identified [6]. One may further exploit the large decay gap ($\sim$ few mm) [4] in the lightest neutralino decay for strengthening the signal.

References

[1] SuperKamiokande Collaboration, Y. Fukuda *et al.*, Phys. Rev. Lett. **81**, 1562 (1998); Phys. Lett. **B433**, 9 (1998); Phys. Lett. **B436**, 33 (1998).

[2] A.K. Datta, B. Mukhopadhyaya and S. Roy, hep-ph/9905549.

[3] S. Roy and B. Mukhopadhyaya, Phys. Rev. **D55**, 7020 (1997).

[4] B. Mukhopadhyaya, S. Roy and F. Vissani, Phys. Lett. **B443**, 191 (1998).

[5] S.Y. Choi, E.J. Chun, S.K. Kang and J.S. Lee, hep-ph/9903465.

[6] A.K. Datta, B. Mukhopadhyaya and F. Vissani, work in progress.

Anomaly mediated SUSY breaking at the LHC

F.E. PAIGE AND J. WELLS

Abstract

Anomaly Mediated SUSY Breaking models are reviewed. Possible signatures at the LHC for one case of the minimal realistic model are examined.

1 Introduction

The signatures for SUSY at the LHC depend very much on the SUSY masses, which presumably result from spontaneous SUSY breaking. It is not possible to break SUSY spontaneously using just the MSSM fields; instead one must do so in a hidden sector and then communicate the breaking through some interaction. In supergravity models, the communication is through gravity. In gauge mediated models it is through gauge interactions; the gravitino is then very light and can play an important role. Simple examples of both have been discussed previously. A third possibility is that the hidden sector does not have the right structure to provide masses through either mechanism; then the leading contributions come from a combination of gravity and anomalies. This is known as Anomaly Mediated SUSY Breaking (AMSB), and it predicts a different pattern of masses and signatures.

2 Anomaly-Mediated Supersymmetry Breaking

In the supersymmetric standard model there exist AMSB contributions to the soft mass parameters that arise via the superconformal anomaly [1, 2]. The effect can be understood by recognizing several important features of supersymmetric theories. First, supersymmetry breaking can be represented by a chiral superfield $\Phi = 1 + m_{3/2}\theta^2$ which also acts as a compensator for super-Weyl transformations. Treating Φ as a spurion, one can transform a theory into a super-conformally invariant theory. Even if a theory is superconformal at the outset (i.e., no dimensionful couplings), the spurion Φ is employed since the quantum field theory requires a regulator that implies scale dependence (Pauli-Villars mass, renormalization scale in dimensional reduction, etc.). To preserve scale invariance the renormalization scale parameter μ in a quantum theory then becomes $\mu/\sqrt{\Phi^\dagger\Phi}$. It is the dependence of the regulator on Φ that induces supersymmetry breaking contributions to the scalars and gauginos.

The anomaly induced masses can be derived straightforwardly for the scalar masses. The Kähler kinetic terms depend on wave function renormalization as in the following superfield operator,

$$\int d^2\theta d^2\bar{\theta} Z_Q \left(\frac{\mu}{\sqrt{\Phi^\dagger\Phi}}\right) Q^\dagger Q. \tag{1}$$

Taylor expanding Z around μ and projecting out the $FF^\dagger$ terms yields a supersymmetry breaking mass for the scalar field $\tilde{Q}$:

$$m_{\tilde{Q}}^2 = -\frac{1}{4}\frac{d^2 \ln Z_Q}{d(\ln\mu)^2} m_{3/2}^2 = -\frac{1}{4}\left(\frac{\partial\gamma_Q}{\partial g}\beta_g + \frac{\partial\gamma_Q}{\partial y}\beta_y\right) m_{3/2}^2. \tag{2}$$

Similar calculations can be done for the gauginos and the A terms:

$$M_i = -\frac{g_i^2}{2}\frac{dg_i^{-2}}{d\ln\mu} m_{3/2} = \frac{\beta_{g_i}}{g_i} m_{3/2}, \tag{3}$$

$$A_y = \frac{1}{2}\sum_a \frac{d\ln Z_{Q_a}}{d\ln\mu} m_{3/2} = -\frac{\beta_y}{y} m_{3/2} \tag{4}$$

where the sum over a includes all fields associated with the Yukawa coupling y in the superpotential.

There are several important characteristics of the AMSB spectrum to note. First, the equations for the supersymmetry breaking contributions are scale invariant. That is, the value of the soft masses at any scale is obtained by simply plugging in the gauge couplings and Yukawa couplings at that scale into the above formulas. Second, the masses are related to the gravitino mass by a one loop suppression. In AMSB $M_i \sim m_{3/2}\alpha_i/4\pi$, whereas in SUGRA $M_i \sim m_{3/2}$. While the AMSB contributions are always present in a theory independent of how supersymmetry breaking is accomplished, they may be highly suppressed compared to standard hidden sector models. Therefore, for AMSB to be the primary source of scalar masses, one needs to assume or arrange that supersymmetry breaking is not directly communicated from a hidden sector. This can be accomplished, for example, by assuming supersymmetry breaking on a distant brane [1]. Finally, the squared masses of the sleptons are negative (tachyonic) because $\beta_g > 0$ for $U(1)$ and $SU(2)$ gauge groups. This problem rules out the simplest AMSB model based solely on eqs. 2-4.

Given the tachyonic slepton problem, it might seem most rational to view AMSB as a good idea that did not quite work out. However, there are many reasons to reflect more carefully on AMSB. As already mentioned above, AMSB contributions to scalar masses are always present if supersymmetry is broken. Soft masses in the MSSM come for free, whereas in all other successful theories of supersymmetry breaking a communication mechanism must be detailed. In particle, hidden sector models require singlets to give the gauginos an acceptable mass. In AMSB, singlets are not necessary. Also, there may be small variations on the AMSB idea that can produce a realistic spectrum and can have important phenomenological consequences. This is our motivation for writing this note.

3 Two realistic minimal models of AMSB: mAMSB and DAMSB

As we discussed in the introduction, the pure AMSB model gives negative squared masses for the sleptons, thus breaking electromagnetic gauge invariance, so some additional contributions must be included. The simplest assumption that solves this problem is to add at the GUT scale a single universal scalar mass m_0^2 to all the sfermions' squared masses. We will call this model mAMSB. The description and many phenomenological implications of this model are given in Refs. [3, 4]. The parameters of the model after the usual radiative electroweak symmetry breaking are then

$$m_0, \quad m_{3/2}, \quad \tan\beta, \quad \mathrm{sgn}\,\mu = \pm.$$

This model has been implemented in ISAJET 7.48 [5]; a pre-release version of ISAJET has been used to generate the events for this analysis.

For this note the AMSB parameters were chosen to be

$$m_0 = 200\,\mathrm{GeV}, \quad m_{3/2} = 35\,\mathrm{TeV}, \quad \tan\beta = 3, \quad \mathrm{sgn}\,\mu = +$$

For this choice of parameters the slepton squared masses are positive at the weak scale, but they are still negative at the GUT scale. This means that charge and color might be broken (CCB) at high temperatures in the early universe. However, at these high energies there are also large finite temperature effects on the mass, which are positive (symmetry restoration occurs at higher T). In fact, a large class of SUSY models with CCB minima naturally fall into the correct SM minimum when you carefully follow the evolution of the theory from high T to today. If CCB minima are excluded at all scales, then the value of m_0 must be substantially larger, so the sleptons must be quite heavy.

The masses from ISAJET 7.48 for this point are listed in Table 1. The mass spectrum has some similarity to that for SUGRA Point 5 studied previously [6, 7]: the gluino and squark masses are similar, and the decays $\tilde{\chi}_2^0 \to \tilde{\ell}\ell$ and $\tilde{\chi}_2^0 \to \tilde{\chi}_1^0 h$ are allowed. Thus, many of the techniques developed for Point 5 are applicable here. But there are also important differences. In particular, the $\tilde{\chi}_1^\pm$ is nearly degenerate with the $\tilde{\chi}_1^0$, not with the $\tilde{\chi}_2^0$. The mass splitting between the lightest chargino and the lightest neutralino must be calculated as the difference between the lightest eigenvalues of the full one-loop neutralino and chargino mass matrices. The mass splitting is always above $m_{\pi^\pm}$, thereby allowing the two-body decays $\chi_1^\pm \to \chi_1^0 + \pi^\pm$ [3, 8]. Decay lifetimes of $\chi^\pm$ are always less than 10 cm over mAMSB parameter space, and are often less than 1 cm.

Another unique feature of the spectrum is the near degeneracy of the $\tilde{\ell}_L$ and $\tilde{\ell}_R$ sleptons. The mass splitting is [3]

$$m_{\tilde{\ell}_L}^2 - m_{\tilde{\ell}_R}^2 \simeq 0.037\left(-m_Z^2\cos 2\beta + M_2^2 \ln\frac{m_{\tilde{\ell}_R}}{m_Z}\right). \tag{5}$$

There is no symmetry requiring this degeneracy, but rather it is an astonishing accident and prediction of the mAMSB model.

It is instructive to compare the masses from ISAJET with those calculated in Ref. [3] to provide weak-scale input to ISAJET. These masses are listed in the right hand side of Table 1. Since the agreement is clearly adequate for the purposes of the present study, no attempt has been made to understand or resolve the differences. It is clear, however, that if SUSY is discovered at the LHC and if masses or combinations of masses are measured

Table 1: Masses of the SUSY particles, in GeV, for the mAMSB model with $m_0 = 200\,\mathrm{GeV}$, $m_{3/2} = 35\,\mathrm{TeV}$, $\tan\beta = 3$, and $\mathrm{sgn}\,\mu = +$ from ISAJET (left side) and from Ref. [3] (right side) using the ISAJET sign conventions.

Sparticle	mass	Sparticle	mass	Sparticle	mass	Sparticle	mass
$\widetilde{g}$	815			$\widetilde{g}$	852		
$\widetilde{\chi}_1^\pm$	101	$\widetilde{\chi}_2^\pm$	658	$\widetilde{\chi}_1^\pm$	98	$\widetilde{\chi}_2^\pm$	535
$\widetilde{\chi}_1^0$	101	$\widetilde{\chi}_2^0$	322	$\widetilde{\chi}_1^0$	98	$\widetilde{\chi}_2^0$	316
$\widetilde{\chi}_3^0$	652	$\widetilde{\chi}_4^0$	657	$\widetilde{\chi}_3^0$	529	$\widetilde{\chi}_4^0$	534
$\widetilde{u}_L$	754	$\widetilde{u}_R$	758	$\widetilde{u}_L$	760	$\widetilde{u}_R$	814
$\widetilde{d}_L$	757	$\widetilde{d}_R$	763	$\widetilde{d}_L$	764	$\widetilde{d}_R$	819
$\widetilde{t}_1$	516	$\widetilde{t}_2$	745	$\widetilde{t}_1$	647	$\widetilde{t}_2$	778
$\widetilde{b}_1$	670	$\widetilde{b}_2$	763	$\widetilde{b}_1$	740	$\widetilde{b}_2$	819
$\widetilde{e}_L$	155	$\widetilde{e}_R$	153	$\widetilde{e}_L$	161	$\widetilde{e}_R$	159
$\widetilde{\nu}_e$	137	$\widetilde{\nu}_\tau$	137	$\widetilde{\nu}_e$	144	$\widetilde{\nu}_\tau$	144
$\widetilde{\tau}_1$	140	$\widetilde{\tau}_2$	166	$\widetilde{\tau}_1$	152	$\widetilde{\tau}_2$	167
h^0	107	H^0	699	h^0	98	H^0	572
A^0	697	$H^\pm$	701	A^0	569	$H^\pm$	575

with the expected precision, then more work is needed to compare the LHC results with theoretical models in a sufficiently reliable way.

Another variation on AMSB is deflected AMSB (DAMSB). The idea is based on Ref. [9] who demonstrated that realistic sparticle spectrums with non-tachyonic sleptons can be induced if a light *modulus* field X (SM singlet) is coupled to heavy, non-singlet vector-like messenger fields Ψ_i and $\bar{\Psi}_i$:

$$W_{\mathrm{mess}} = \lambda_\Psi X \Psi_i \bar{\Psi}_i.$$

To ensure gauge coupling unification we identify Ψ_i and $\bar{\Psi}_i$ as $5+\bar{5}$ representations of $SU(5)$. When the messengers are integrated out at some scale M_0, the beta functions do not match the AMSB masses, and the masses are deflected from the AMSB renormalization group trajectory. The subsequent evolution of the masses below M_0 induces positive mass squared for the sleptons, and a reasonable spectrum can result. Although there may be additional significant parameters associated with the generation of the μ and B_μ term in the model, we assume for this discussion that they do not affect the spectra of the MSSM fields. The values of μ and B_μ are then obtained by requiring that the conditions for EWSB work out properly.

The parameters of DAMSB are

$$m_{3/2}, \quad n, \quad M_0, \quad \tan\beta, \quad \mathrm{sgn}\,\mu = \pm$$

where n is the number of $5+\bar{5}$ messenger multiplets, and M_0 is the scale at which the messengers are integrated out. Practically, the spectrum is obtained by imposing the boundary

Table 2: Masses of the SUSY particles, in GeV, for the DAMSB model with $n = 5$, $M_0 = 10^{15}$ GeV, and $\tan\beta = 4$ from Ref. [10].

Sparticle	mass	Sparticle	mass
$\widetilde{g}$	500		
$\widetilde{\chi}_1^{\pm}$	145	$\widetilde{\chi}_2^{\pm}$	481
$\widetilde{\chi}_1^0$	136	$\widetilde{\chi}_2^0$	152
$\widetilde{\chi}_3^0$	462	$\widetilde{\chi}_4^0$	483
$\widetilde{u}_L$	432	$\widetilde{u}_R$	384
$\widetilde{d}_L$	439	$\widetilde{d}_R$	371
$\widetilde{t}_1$	306	$\widetilde{t}_2$	454
$\widetilde{b}_1$	371	$\widetilde{b}_2$	406
$\widetilde{e}_L$	257	$\widetilde{e}_R$	190
$\widetilde{\nu}_e$	246	$\widetilde{\nu}_\tau$	246
$\widetilde{\tau}_1$	190	$\widetilde{\tau}_2$	257
h^0	98	H^0	297
A^0	293	$H^{\pm}$	303

conditions at M_0, and then using SUSY soft mass renormalization group equations to evolve these masses down to the weak scale. Expressions for the boundary conditions can be found in Refs. [9, 10], and details on how to generate the low-energy spectrum are given in [10]. The resulting spectrum of superpartners is substantially different from that of mAMSB. The most characteristic feature of the DAMSB spectrum is the near proximity of all superpartner masses. In Table 2 we show the spectrum of a model with $n = 5$, $M_0 = 10^{15}$ GeV, and $\tan\beta = 4$ as given in [10]. The LSP is the lightest neutralino, which is a Higgsino. (Actually, the LSP is the fermionic component of the modulus X, but the decay of χ_1^0 to it is much greater than collider time scales.) All the gauginos and squarks are between 300 GeV and 500 GeV, while the sleptons and higgsinos are a bit lighter (~ 150 GeV to ~ 250 GeV) in this case.

In summary, we have outlined two interesting directions to pursue in modifying AMSB to make a realistic spectrum. The first direction we call mAMSB, and is constructed by adding a common scalar mass to the sfermions at the GUT scale to solve the negative squared slepton mass problem of pure AMSB. The other direction that we outlined is deflected anomaly mediation that is based on throwing the scalar masses off the pure AMSB renormalization group trajectory by integrating out heavy messenger states coupled to a modulus. The spectra of the two approaches are significantly different, and we should expect the LHC signatures to be different as well. In this note, we study the mAMSB carefully in a few observables to demonstrate how it is distinctive from other, standard approaches to supersymmetry breaking, such as mSUGRA and GMSB.

4 LHC studies of the example mAMSB model point

We now turn to a study of the example mAMSB spectra presented in Table 1. A sample of 10^5 signal events was generated; since the total signal cross section is 16 nb, this corresponds to an integrated LHC luminosity of $6\,\mathrm{fb}^{-1}$. All distributions shown in this note are normalized to $10\,\mathrm{fb}^{-1}$, corresponding to one year at low luminosity at the LHC. Events were selected by requiring

- At least four jets with $p_T > 100, 50, 50, 50\,\mathrm{GeV}$;
- $\not{E}_T > \min(100\,\mathrm{GeV}, 0.2M_{\mathrm{eff}})$;
- Transverse sphericity $S_T > 0.2$;
- $M_{\mathrm{eff}} > 600\,\mathrm{GeV}$;

where the "effective mass" M_{eff} is given by the scalar sum of the missing E_T and the p_T's of the four hardest jets,

$$M_{\mathrm{eff}} = \not{E}_T + p_{T,1} + p_{T,2} + p_{T,3} + p_{T,4}.$$

Standard model backgrounds from gluon and light quark jets, $t\bar{t}$, $W+\mathrm{jets}$, $Z+\mathrm{jets}$, and WW have also been generated, generally with much less equivalent luminosity. The M_{eff} distributions for the signal and the sum of all backgrounds with all except the last cut are shown in Figure 1. The ISAJET IDENT codes for the SUSY events contributing to this plot are also shown. It is clear from this plot that the Standard Model backgrounds are small with these cuts, as would be expected from previous studies [6, 7].

The mass distribution for $\ell^+\ell^-$ pairs with the same and opposite flavor is shown in Figure 2. The opposite-flavor distribution is small, and there is a clear endpoint in the same-flavor distribution at

$$M_{\ell\ell}^{\max} = \sqrt{\frac{(M_{\tilde{\chi}_2^0}^2 - M_{\tilde{\ell}}^2)(M_{\tilde{\ell}}^2 - M_{\tilde{\chi}_1^0}^2)}{M_{\tilde{\ell}}^2}} = 213.6, 215.3\,\mathrm{GeV}$$

corresponding to the endpoints for the decays $\tilde{\chi}_2^0 \to \tilde{\ell}_{L,R}^{\pm}\ell^{\mp} \to \tilde{\chi}_1^0\ell^+\ell^-$. This is similar to what is seen in SUGRA Point 5, but in that case only one slepton contributes. It is clear from the $e^+e^- + \mu^+\mu^- - e^{\pm}\mu^{\mp}$ dilepton distribution with finer bins shown in the same figure that the endpoints for $\tilde{\ell}_R$ and $\tilde{\ell}_L$ cannot be resolved with the expected ATLAS dilepton mass resolution. More work is needed to see if the presence of two different endpoints could be inferred from the shape of the edge of the dilepton distribution.

Since the main source for $\tilde{\chi}_2^0$ is $\tilde{q}_R \to \tilde{\chi}_2^0 q$, information on the squark masses can be obtained by combining the leptons from $\tilde{\chi}_2^0 \to \tilde{\ell}\ell$ decays with one of the two hardest jets in the event, since the hardest jets are generally products of the squark decays. Figure 3 shows the distribution for the smaller of the two $\ell^+\ell^- j$ masses formed with the two leptons and each of the two hardest jets in the event. The dashed curve in this figure shows the same

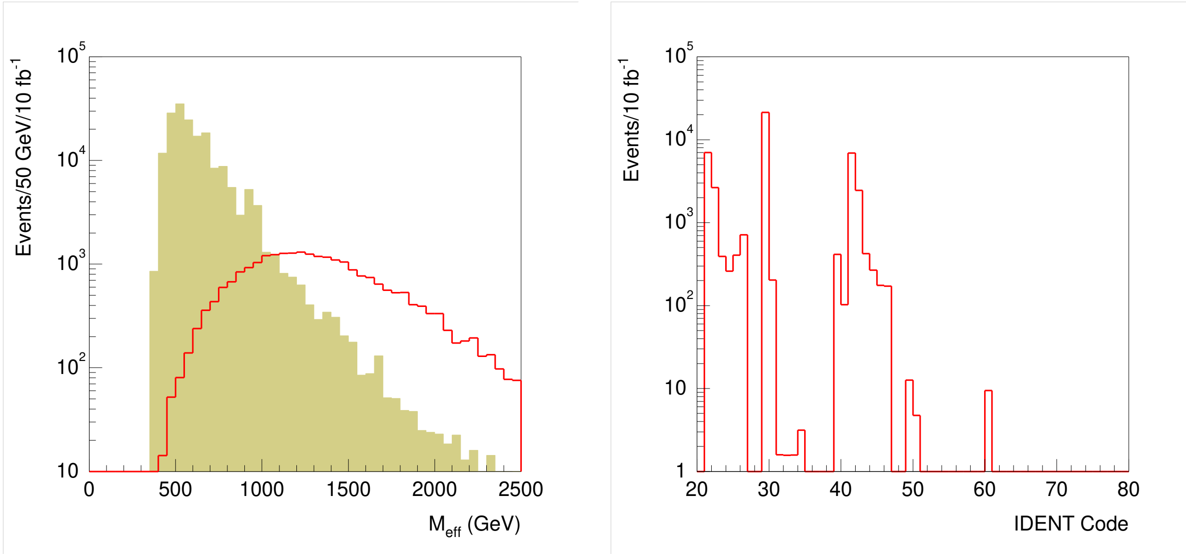

Figure 1: Left: Effective mass distribution for signal (curve) and Standard Model background (shaded). Right: ISAJET IDENT codes for all produced particles contributing to $M_{\rm eff}$ distribution after cuts. The dominant contributions are $\tilde q_L$ (21–26), $\tilde g$ (29), and $\tilde q_R$ (41–46).

distribution for $M_{\ell\ell} > 175\,\mathrm{GeV}$, for which the backgrounds are smaller. Both distributions should have endpoints at the kinematic limit for $\tilde q_R \to \tilde\chi_2^0 \to \tilde\ell\ell \to \tilde\chi_1^0\ell\ell$,

$$\left[\frac{(M_{\tilde q_R}^2 - M_{\tilde\chi_2^0}^2)(M_{\tilde\chi_2^0}^2 - M_{\tilde\chi_1^0}^2)}{M_{\tilde\chi_2^0}^2}\right]^{1/2} = 652.9\,\mathrm{GeV}.$$

Figure 3 also shows the $\ell^\pm j$ mass distribution formed with each of the two leptons combined with the jet that gives the smaller of the two $\ell\ell j$ masses. This should have a 3-body endpoint at

$$\left[\frac{(M_{\tilde q_R}^2 - M_{\tilde\chi_2^0}^2)(M_{\tilde\chi_2^0}^2 - M_{\tilde\ell}^2)}{M_{\tilde\chi_2^0}^2}\right]^{1/2} = 605.4\,\mathrm{GeV}.$$

The branching ratio for $\tilde b_1 \to \tilde\chi_2^0 b$ is very small, so the same distributions with b-tagged jets contain only a handful of events and cannot be used to determine the $\tilde b_1$ mass.

The decay chain $\tilde q_R \to \tilde\chi_2^0 q \to \tilde\ell_{L,R}^\pm \ell^\mp q \to \tilde\chi_1^0 \ell^+\ell^- q$ also implies a lower limit on the $\ell\ell q$ mass for a given limit on $z = \cos\theta^*$ or equivalently on the $\ell\ell$ mass. For $z > 0$ (or equivalently

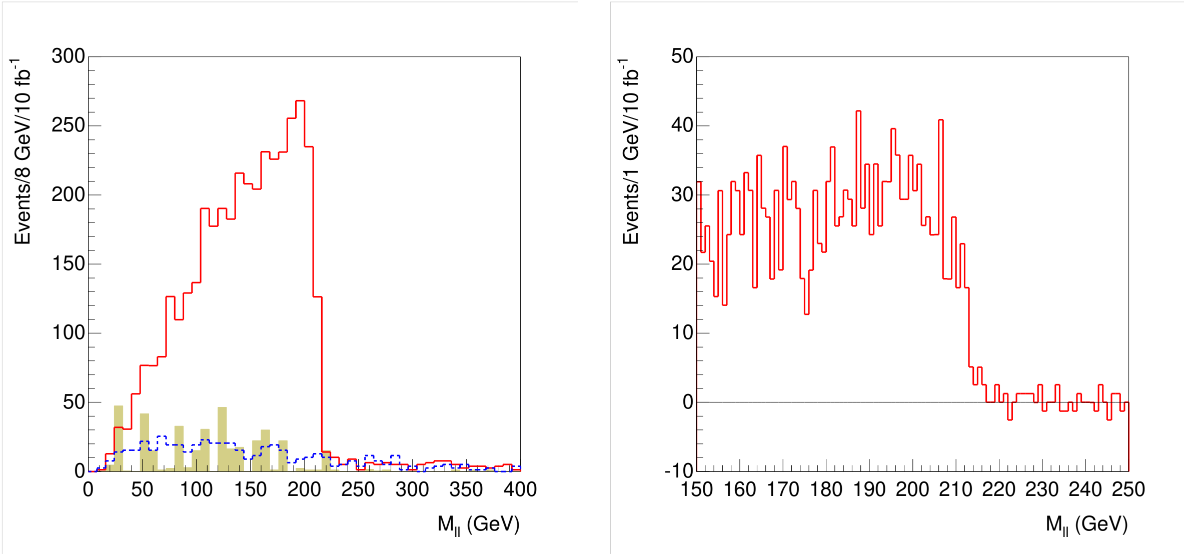

Figure 2: Mass distribution for opposite sign dileptons. Left: Distributions for same flavor signal (solid curve), opposite flavor signal (dashed curve), and Standard Model same flavor background (shaded). Right: $e^+e^- + \mu^+\mu^- - e^\pm\mu^\mp$ distribution for signal on a finer scale.

$M_{\ell\ell} > M_{\ell\ell}^{\max}/\sqrt{2})$ this lower limit is

$$
\begin{aligned}
(M_{\ell\ell q}^{\min})^2 &= \tfrac{1}{4M_2^2M_e^2}\times \\
&\Big[-M_1^2M_2^4 + 3M_1^2M_2^2M_e^2 - M_2^4M_e^2 - M_2^2M_e^4 - M_1^2M_2^2M_q^2 - \\
&\quad M_1^2M_e^2M_q^2 + 3M_2^2M_e^2M_q^2 - M_e^4M_q^2 + (M_2^2 - M_q^2)\times \\
&\quad \sqrt{(M_1^4 + M_e^4)(M_2^2 + M_e^2)^2 + 2M_1^2M_e^2(M_2^4 - 6M_2^2M_e^2 + M_e^4)}\Big] \\
M_{\ell\ell q}^{\min} &= 376.6\,\mathrm{GeV}
\end{aligned}
\tag{6}
$$

where M_q, M_2, M_e, and M_1 are the (average) squark, $\tilde\chi_2^0$, (average) slepton, and $\tilde\chi_1^0$ masses. To determine this lower edge, the larger of the two $\ell\ell j$ masses formed from two opposite-sign leptons and one of the two hardest jets is plotted in Figure 4. An endpoint at about the right value can clearly be seen.

The $\ell^+\ell^-$, $\ell^+\ell^-q$, $\ell^\pm q$, and lower $\ell^+\ell^-q$ edges provide four constraints on the four masses involved. Since the cross sections are similar to those for SUGRA Point 5, we take the errors at high luminosity to be negligible on the $\ell^+\ell^-$ edge, 1% on the $\ell^+\ell^-q$ and $\ell^\pm q$ upper edges, and 2% on the $\ell^+\ell^-q$ lower edge. Random masses were generated within ±50% of their nominal values, and the χ^2 for the four measurements with these errors were used to determine the probability for each set of masses. The resulting distribution for the $\tilde\chi_1^0$ mass, also shown in Figure 4, has a width of ±11.7%, about the same as for Point 5; the errors for

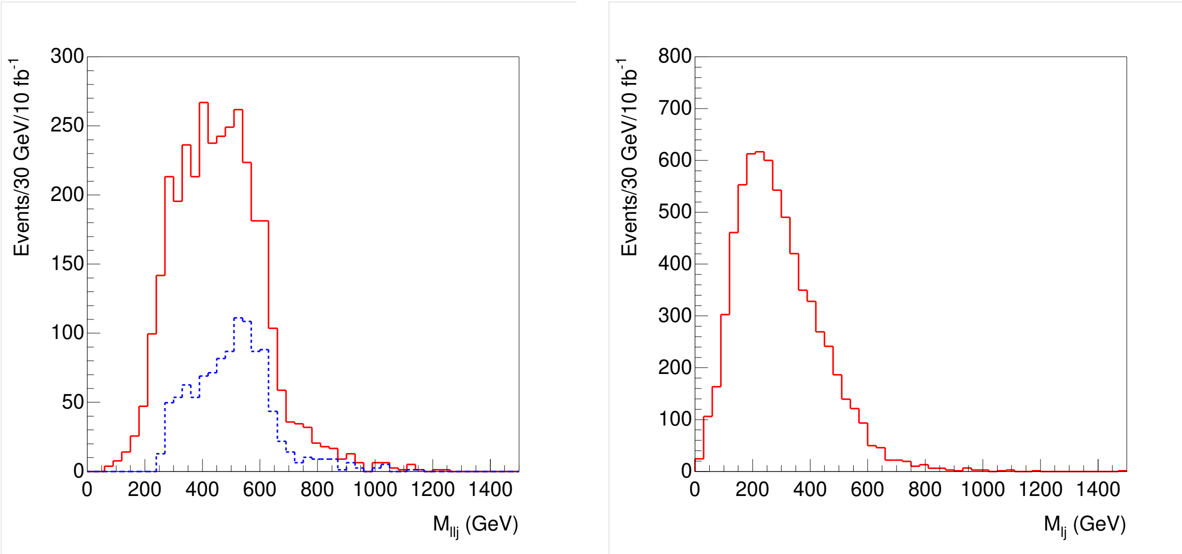

Figure 3: Mass distribution for $e^+e^- + \mu^+\mu^- - e^\pm\mu^\mp$ events combined with one of the two hardest jets. Left: $\ell^+\ell^- j$ mass distribution (solid) and same with $M_{\ell\ell} > 175\,\mathrm{GeV}$ (dashed). Right: $\ell^\pm j$ mass distribution for the one of the two hardest jets that gives the smaller $\ell\ell j$ mass.

the other masses are also comparable. Of course, the masses being measured in this case are different: for example the squark mass is the average of the $\tilde{q}_R$ rather than the $\tilde{q}_L$ masses.

The leptons from $\tilde{\chi}_1^\pm \to \tilde{\chi}_1^0 \ell^\pm \nu$ are very soft. This implies that the rate for events with one or three leptons or for two leptons with opposite flavor are all suppressed. Figure 5 shows as a solid histogram the multiplicity of leptons with $p_T > 10\,\mathrm{GeV}$ and $|\eta| < 2.5$ for the AMSB signal with a veto on hadronic τ decays. The same figure shows the distribution for a model with the same weak-scale mass parameters except that the gaugino masses M_1 and M_2 are interchanged. This model has a wino $\tilde{\chi}_1^\pm$ approximately degenerate with the $\tilde{\chi}_2^0$ rather than with the $\tilde{\chi}_1^0$. Clearly the AMSB model has a much smaller rate for single leptons and a somewhat smaller rate for three leptons; these rates can be used to distinguish AMSB and SUGRA-like models.

While the decay $\tilde{\chi}_2^0 \to \tilde{\chi}_1^0 h$ is kinematically allowed, the branching ratio is only about 0.03%. Other sources of h in SUSY events are also quite small, so in contrast to SUGRA Point 5 there is no strong $h \to b\bar{b}$ signal. However, there is a fairly large branching ratio for $\tilde{g} \to \tilde{b}\bar{b}, \tilde{t}\bar{t}$ with $\tilde{b} \to \tilde{\chi}_1^0 b$, $\tilde{t} \to \chi_1^+ b$, giving two hard b jets and hence structure in the M_{bb} distribution. For this analysis b jets were tagged by assuming that any B hadron with $p_{T,B} > 10\,\mathrm{GeV}$ and $|\eta_B| < 2$ is tagged with an efficiency $\epsilon_B = 60\%$; the jet with the smallest

$$R = \sqrt{(\Delta\eta)^2 + (\Delta\phi)^2}$$

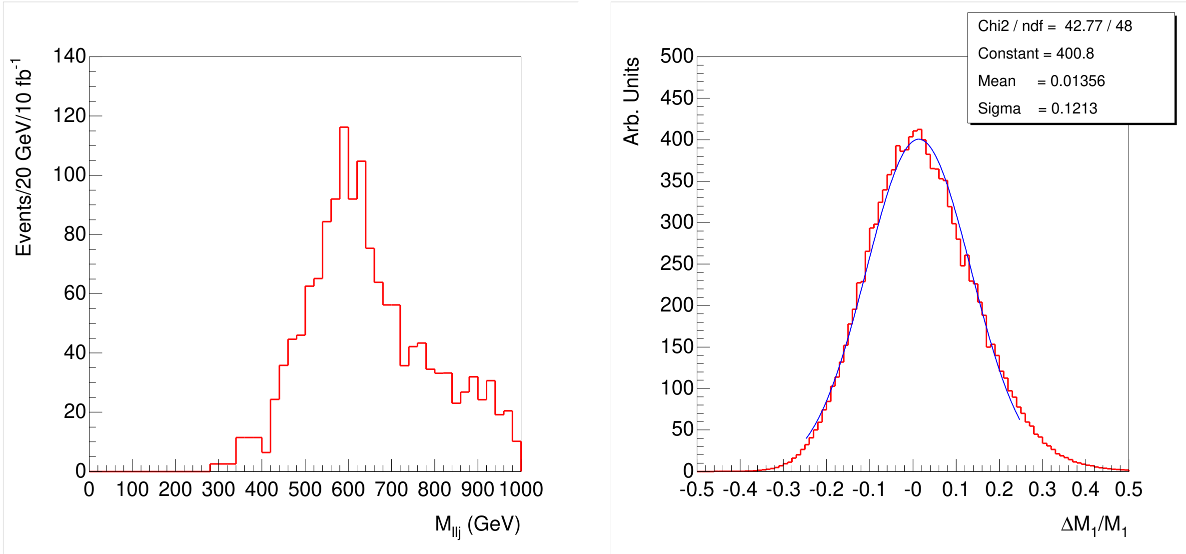

Figure 4: Left: Lower edge from larger $\ell\ell j$ mass combining $e^+e^- + \mu^+\mu^- - e^\pm\mu^\mp$ with one of the two hardest jets. Right: Model-independent fit for $\tilde\chi_1^0$ mass.

was then taken to be b jets. The two hardest jets generally come from the squarks. To reconstruct $\tilde g \to \tilde b \bar b$ one of the two hardest jets, tagged as a b, was combined with any remaining jet, also tagged as a b. In addition to the standard multijet and $\not\!\!E_T$ cuts, a cut $M_{\rm eff} > 1200\,{\rm GeV}$ was made to reduce the Standard Model background. The resulting distributions for the b jet multiplicity and for the smallest bb dijet mass are shown in Figure 6. The dijet mass should have an endpoint at the kinematic limit for $\tilde g \to \tilde b_1 \bar b \to \tilde\chi_1^0 b \bar b$,

$$M_{bb}^{\rm max} = \sqrt{\frac{(M_{\tilde g}^2 - M_{\tilde b}^2)(M_{\tilde b}^2 - M_{\tilde\chi_1^0}^2)}{M_{\tilde b}^2}} = 418.7\,{\rm GeV}.$$

While the figure is roughly consistent with this, the endpoint is not very sharp; more work is needed to assign an error and to understand the high mass tail. There should also be a $b\bar t$ endpoint resulting from $\tilde g \to \tilde t \bar t$, $\tilde t \to \tilde\chi_1^+ b$, with $M_{\tilde\chi_1^+} \approx M_{\tilde\chi_1^0}$ and essentially invisible. Of course m_t has to be kept in the formula. This would be an apparent strong flavor violation in gluino decays and so quite characteristic of these models. Reconstructing the top is more complicated, so this has not yet been studied.

The splitting between the $\tilde\chi_1^\pm$ and $\tilde\chi_1^0$ is very small in AMSB models. ISAJET gives a splitting of 0.189 GeV for this point and $c\tau = 2.8\,{\rm cm}$, with the dominant decay being the two-body mode $\tilde\chi_1^\pm \to \tilde\chi_1^0 \pi$ via a virtual W. Ref. [3] gives a somewhat smaller value of μ and so a smaller splitting. The lifetime is of course quite sensitive to the exact splitting. Since the pion or electron is soft and so difficult to reconstruct, it seems better to look for the tail of long-lived winos. The signature is an isolated stiff track in a fraction of the

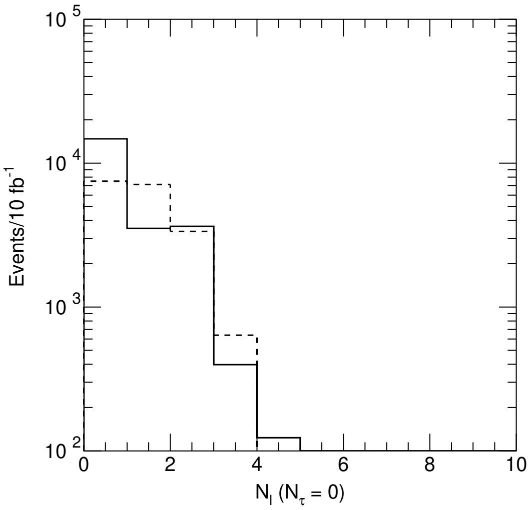

Figure 5: Lepton multiplicity with a hadronic τ veto. Solid: AMSB model. Dashed: Same but with $M_1 \leftrightarrow M_2$.

events that ends in the tracking volume and produces no signal in the calorimeter or muon system. Figure 7 shows the radial track length R_T distribution in units of $c\tau$ for winos with $|\eta| < 1$ and the (generated) momentum distribution for those with $R_T > 10c\tau$. Note that the ATLAS detector has three layers of pixels with very low occupancy at radii of 4, 11, and 14 cm and four double layers of silicon strips between 30 and 50 cm. It seems likely that the background for tracks that end after the pixel layers would be small.

It is instructive to compare this signature to that for GMSB models with an NLSP slepton. Both models predict long-lived charged particles with $\beta < 1$. In the GMSB models, two NLSP sleptons occur in every SUSY event, and they decay into a hard e's, μ's, or τ's plus nearly massless $\tilde{G}$'s. In the AMSB models, only a fraction of the SUSY events contain long-lived charged tracks, and these decay into a soft pion or electron plus an invisible particle. A detailed tracking simulation should be done for both cases.

Acknowledgements: This work was supported in part by the U.S. Department of Energy under Contract DE-AC02-98CH10886. We also acknowledge the support of the Les Houches Physics Center, where part of this work was done.

References

[1] L. Randall and R. Sundrum, hep-th/9810155.

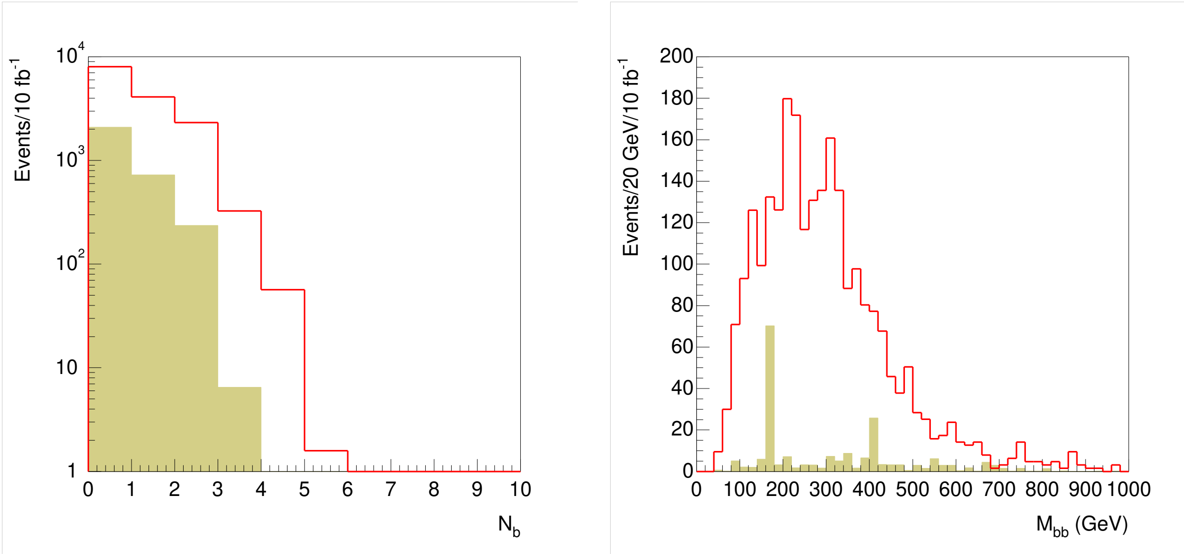

Figure 6: Left: Multiplicity of b jets for signal (curve) and Standard Model background (shaded). Right: Smallest mass for pairs of b jets for signal (curve) and Standard Model background (shaded). Both plots have $M_{\rm eff} > 1200\,$GeV in addition to the standard cuts and include a b tagging efficiency $\epsilon_b = 60\%$.

[2] G.F. Giudice, M.A. Luty, H. Murayama and R. Rattazzi, JHEP **12**, 027 (1998), hep–ph/9810442.

[3] T. Gherghetta, G.F. Giudice, and J.D. Wells, hep–ph/9904378.

[4] J. L. Feng and T. Moroi, hep–ph/9907319.

[5] H. Baer, F.E. Paige, S.D. Protopescu and X. Tata, hep–ph/9810440.

[6] I. Hinchliffe, F.E. Paige, M.D. Shapiro, J. Soderqvist, and W. Yao, Phys. Rev. **D55**, 5520 (1997).

[7] ATLAS Collaboration, *ATLAS Detector and Physics Performance Technical Design Report*, CERN/LHCC/99-15.

[8] J.L. Feng, T. Moroi, L. Randall, M. Strassler and S. Su, Phys. Rev. Lett. **83**, 1731 (1999), hep–ph/9904250.

[9] A. Pomarol and R. Rattazzi, JHEP **05**, 013 (1999), hep–ph/9903448.

[10] R. Rattazzi, A. Strumia and J.D. Wells, hep–ph/9912390.

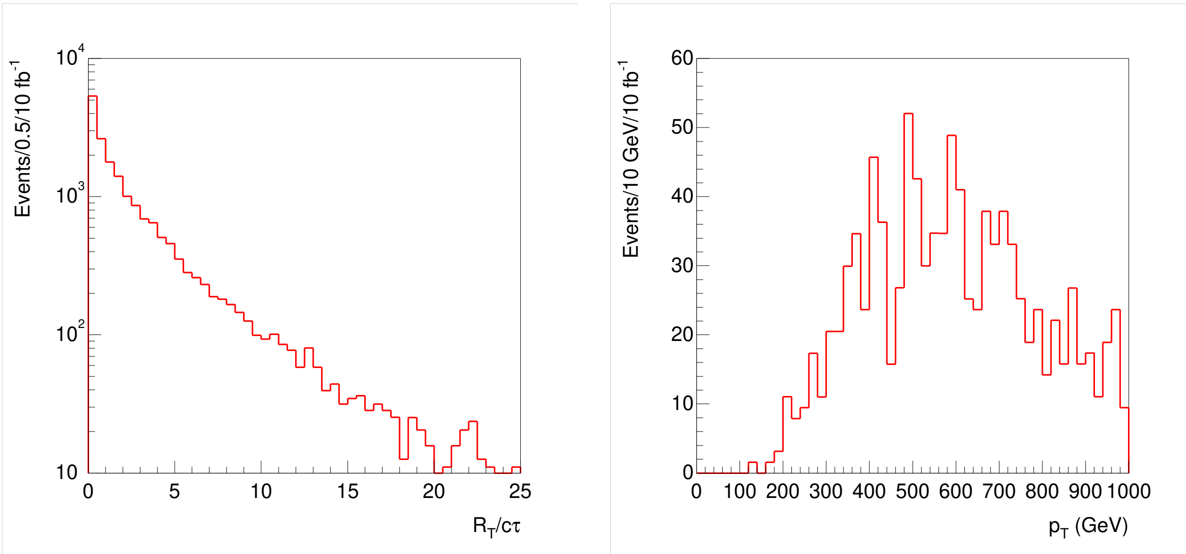

Figure 7: Left: Radial track length distributions for $\tilde{\chi}_1^{\pm}$ in the barrel region, $|\eta| < 1$. Right: p distribution for $\tilde{\chi}_1^{\pm}$ with $R_T > 10c\tau$.

Introduction to GMSB phenomenology at TeV colliders

S. AMBROSANIO*

Abstract

We give a brief account of models with gauge–mediated supersymmetry breaking, as a general introduction for the following two contributions.

1 Introduction to Gauge-Mediated SUSY Breaking

Since no superpartners have been detected at collider experiments so far, supersymmetry (SUSY) cannot be an exact symmetry of Nature. The requirement of "soft" supersymmetry breaking [1] alone is not sufficient to reduce the free parameters to a number suitable for predictive phenomenological studies. Hence, motivated theoretical hypotheses on the nature of SUSY breaking and the mechanism through which it is transmitted to the visible sector of the theory [here assumed to be the one predicted by the minimal SUSY extension of the standard model (MSSM)] are highly desirable. If SUSY is broken at energies of the order of the Planck mass and the SUSY breaking sector communicates with the MSSM sector through gravitational interactions only, one falls in the supergravity-inspired (SUGRA) scheme. The most recognized alternative to SUGRA is based instead on the hypothesis that SUSY breaking occurs at relatively low energy scales and is mediated mainly by gauge interactions (GMSB) [2–4]. A good theoretical reason to consider such a possibility is that it provides a natural, automatic suppression of the SUSY contributions to flavor-changing neutral currents and CP-violating processes. A pleasant consequence is that, at least in the simplest versions of GMSB, the MSSM spectrum and other observables depend on just a handful of parameters, typically

$$M_{\rm mess},\ N_{\rm mess},\ \Lambda,\ \tilde{b},\ {\rm sign}(\mu), \tag{1}$$

where $M_{\rm mess}$ is the overall messenger scale; $N_{\rm mess}$ is the so-called messenger index, parameterizing the structure of the messenger sector; Λ is the universal soft SUSY breaking scale felt by the low-energy sector; $\tilde{b}$ is the ratio of the vacuum expectation values of the two Higgs doublets; ${\rm sign}(\mu)$ is the ambiguity left for the SUSY higgsino mass after conditions for correct electroweak symmetry breaking (EWSB) are imposed (see e.g. Refs. [5–8]).

The phenomenology of GMSB (and, more generally, of any theory with low-energy SUSY breaking) is characterized by the presence of a very light gravitino $\tilde{G}$ [9],

$$m_{3/2} \equiv m_{\tilde{G}} = \frac{F}{\sqrt{3}M_P'} \simeq \left(\frac{\sqrt{F}}{100\ {\rm TeV}}\right)^2 2.37\ {\rm eV}, \tag{2}$$

*E-mail: `ambros@mail.cern.ch`

where $\sqrt{F}$ is the fundamental scale of SUSY breaking, 100 TeV is a typical value for it, and $M'_P = 2.44 \times 10^{18}$ GeV is the reduced Planck mass. Hence, the $\tilde{G}$ is always the lightest SUSY particle (LSP) in these theories. If R-parity is assumed to be conserved, any produced MSSM particle will finally decay into the gravitino. Depending on $\sqrt{F}$, the interactions of the gravitino, although much weaker than gauge and Yukawa interactions, can still be strong enough to be of relevance for collider physics. As a result, in most cases the last step of any SUSY decay chain is the decay of the next-to-lightest SUSY particle (NLSP), which can occur outside or inside a typical detector or even close to the interaction point. The pattern of the resulting spectacular signatures is determined by the identity of the NLSP and its lifetime before decaying into the $\tilde{G}$,

$$c\tau_{\rm NLSP} \simeq \frac{1}{100\mathcal{B}} \left(\frac{\sqrt{F}}{100 \text{ TeV}}\right)^4 \left(\frac{m_{\rm NLSP}}{100 \text{ GeV}}\right)^{-5}, \tag{3}$$

where $\mathcal{B}$ is a number of order unity depending on the nature of the NLSP.

The identity of the NLSP [or, to be more precise, the identity of the sparticle(s) having a large branching ratio (BR) for decaying into the gravitino and the relevant SM partner] determines four main scenarios giving rise to qualitatively different phenomenology:

Neutralino NLSP scenario: Occurs whenever $m_{\tilde{N}_1} < (m_{\tilde{\tau}_1} - m_\tau)$. Here typically a decay of the $\tilde{N}_1$ to $\tilde{G}\gamma$ is the final step of decay chains following any SUSY production process. As a consequence, the main inclusive signature at colliders is prompt or displaced photon pairs + X + missing energy. $\tilde{N}_1$ decays to $\tilde{G}Z^0$ and other minor channels may also be relevant at TeV colliders.

Stau NLSP scenario: Defined by $m_{\tilde{\tau}_1} < \text{Min}[m_{\tilde{N}_1}, m_{\tilde{\ell}_R}] - m_\tau$, features $\tilde{\tau}_1 \to \tilde{G}\tau$ decays, producing τ pairs or charged semi-stable $\tilde{\tau}_1$ tracks or decay kinks + X + missing energy. Here and in the following, ℓ stands for e or μ.

Slepton co-NLSP scenario: When $m_{\tilde{\ell}_R} < \text{Min}[m_{\tilde{N}_1}, m_{\tilde{\tau}_1} + m_\tau]$, $\tilde{\ell}_R \to \tilde{G}\ell$ decays are also open with large BR. In addition to the signatures of the stau NLSP scenario, one also gets $\ell^+\ell^-$ pairs or $\tilde{\ell}_R$ tracks or decay kinks.

Neutralino-stau co-NLSP scenario: If $|m_{\tilde{\tau}_1} - m_{\tilde{N}_1}| < m_\tau$ and $m_{\tilde{N}_1} < m_{\tilde{\ell}_R}$, both signatures of the neutralino NLSP and stau NLSP scenario are present at the same time, since $\tilde{N}_1 \leftrightarrow \tilde{\tau}_1$ 2–body decays are not allowed by phase space.

Note that in the GMSB parameter space the relation $m_{\tilde{\ell}_R} > m_{\tilde{\tau}_1}$ always holds. Also, one should keep in mind that the classification above is only valid as an indicative scheme in the limit m_e, $m_\mu \to 0$, neglecting also those cases where a fine-tuned choice of $\sqrt{F}$ and the sparticle masses may give rise to competition between phase-space suppressed decay channels from one ordinary sparticle to another and sparticle decays to the gravitino [10].

In this report, two important aspects of the GMSB phenomenology at TeV colliders will be treated:

(A) The consequences of the GMSB hypothesis on the light Higgs spectrum using the most accurate tools available today for model generation and m_h calculation;

(B) Studies and possible measurements at the LHC with the ATLAS detector in the stau NLSP or slepton co-NLSP scenarios, with focus on determining the fundamental SUSY breaking scale $\sqrt{F}$.

For this purpose, we generated about 30000 GMSB models under well defined hypotheses, using the program `SUSYFIRE` [11], as described in the following section.

2 GMSB Models

In the GMSB framework, the pattern of the MSSM spectrum is simple, as all sparticle masses are generated in the same way and scale approximately with a single parameter Λ, which sets the amount of soft SUSY breaking felt by the visible sector. As a consequence, scalar and gaugino masses are related to each other at a high energy scale, which is not the case in other SUSY frameworks, e.g. SUGRA. Also, it is possible to impose other conditions at a lower scale to achieve EWSB and further reduce the dimension of the parameter space.

To build our GMSB models, we adopt the usual phenomenological approach, in particular following Ref. [8], where problems relevant for GMSB physics at TeV colliders were also approached. We do not specify the origin of the SUSY higgsino mass μ, nor do we assume that the analogous soft SUSY breaking parameter $B\mu$ vanishes at the messenger scale. Instead, we impose correct EWSB to trade μ and $B\mu$ for M_Z and $\tilde{b}$, leaving the sign of μ undetermined. However, we are aware that to build a satisfactory GMSB model one should also solve the latter problem in a more fundamental way, perhaps by providing a dynamical mechanism to generate μ and $B\mu$, possibly with values of the same order of magnitude. This might be accomplished radiatively through some new interactions. However, in this case the other soft terms in the Higgs potential, namely $m^2_{H_{1,2}}$, will be also affected and this will in turn change the values of $|\mu|$ and $B\mu$ coming from EWSB conditions [4–6]. Within the study **(A)**, we are currently considering some "non-minimal" possibilities for GMSB models that to some extent take this problem into account, and we are trying to assess the impact on the light Higgs mass. We do not treat this topic here, but refer to [12] for further details.

To determine the MSSM spectrum and low-energy parameters, we solve the renormalization group (RG) evolution with the following boundary conditions at the $M_{\rm mess}$ scale,

$$\begin{aligned} M_a &= N_{\rm mess}\Lambda g\left(\frac{\Lambda}{M_{\rm mess}}\right)\frac{\alpha_a}{4\pi}, \quad (a=1,2,3) \\ \tilde{m}^2 &= 2N_{\rm mess}\Lambda^2 f\left(\frac{\Lambda}{M_{\rm mess}}\right)\sum_a\left(\frac{\alpha_a}{4\pi}\right)^2 C_a, \end{aligned} \tag{4}$$

respectively for the gaugino and the scalar masses. In Eq. (4), g and f are the one-loop and two-loop functions whose exact expressions can be found e.g. in Ref. [7], and C_a are the quadratic Casimir invariants for the scalar fields. As usual, the scalar trilinear couplings A_f are assumed to vanish at the messenger scale, as suggested by the fact that they (and not their squares) are generated via gauge interactions with the messenger fields at the two loop-level only.

To single out the interesting region of the GMSB parameter space, we proceed as follows. Barring the case where a neutralino is the NLSP and decays outside the detector (large $\sqrt{F}$), the GMSB signatures are very spectacular and are generally free from SM backgrounds. Keeping this in mind and being interested in GMSB phenomenology at future TeV colliders, we consider only models where the NLSP mass is larger than 100 GeV, assuming that searches at LEP and the Tevatron, if unsuccessful, will in the end exclude a softer spectrum in most cases. We require that $M_{\rm mess} > 1.01\Lambda$, to prevent an excess of fine-tuning of the messenger masses, and that the mass of the lightest messenger scalar be at least 10 TeV. We also impose $M_{\rm mess} > M_{\rm GUT}\,\exp(-125/N_{\rm mess})$, to ensure perturbativity of gauge interactions up to the GUT scale. Further, we do not consider models with $M_{\rm mess} \gtrsim 10^5\Lambda$. As a result of this and other constraints, the messenger index $N_{\rm mess}$, which we assume to be an integer independent of the gauge group, cannot be larger than 8. To prevent the top Yukawa coupling from blowing up below the GUT scale, we require $\tilde{b} > 1.2$ (and in some cases > 1.5). This is also motivated by the current bounds from SUSY Higgs searches at LEP II [13]. Models with $\tilde{b} \gtrsim 55$ (with a mild dependence on Λ) are forbidden by the EWSB requirement and typically fail to give $m_A^2 > 0$.

To calculate the NLSP lifetime relevant to our study **(B)**, one needs to specify the value of the fundamental SUSY breaking scale $\sqrt{F}$ on a model-by-model basis. Using perturbativity arguments, for each given set of GMSB parameters, it is possible to determine a lower bound according to Ref. [7],

$$\sqrt{F} \geq \sqrt{F_{\rm mess}} \equiv \sqrt{\Lambda M_{\rm mess}} > \Lambda. \tag{5}$$

On the contrary, no solid arguments can be used to set an upper limit on $\sqrt{F}$ of relevance for collider physics, although some semi-qualitative cosmological arguments are sometimes evoked.

In order to generate our model samples using `SUSYFIRE`, we used logarithmic steps for Λ (between about 45 TeV$/N_{\rm mess}$ and about 220 TeV$/\sqrt{N_{\rm mess}}$, which corresponds to excluding models with sparticle masses above ~ 4 TeV), $M_{\rm mess}/\Lambda$ (between 1.01 and 10^5) and $\tilde{b}$ (between 1.2 and about 60), subject to the constraints described above. `SUSYFIRE` starts from the values of SM particle masses and gauge couplings at the weak scale and then evolves up to the messenger scale through RGEs. At the messenger scale, it imposes the boundary conditions (4) for the soft sparticle masses and then evolves the full set of RGEs back to the weak scale. The decoupling of each sparticle at the proper threshold is taken into account. Two-loop RGEs are used for gauge couplings, third generation Yukawa couplings and gaugino soft masses. The other RGEs are taken at the one-loop level. At the scale $\sqrt{m_{\tilde{t}_1} m_{\tilde{t}_2}}$, EWSB conditions are imposed by means of the one-loop effective potential approach, including corrections from stops, sbottoms and staus. The program then evolves up again to $M_{\rm mess}$ and so on. Three or four iterations are usually enough to get a good approximation for the MSSM spectrum.

References

[1] For a recent pedagogical review of supersymmetry and supersymmetry breaking, see S.P. Martin, "A Supersymmetry Primer", in "Perspectives on Supersymmetry", G.L. Kane ed., World Scientific 1998, hep–ph/9709356 and references therein.

[2] M. Dine, W. Fischler and M. Srednicki, Nucl. Phys. **B189**, 575 (1981); S. Dimopoulos and S. Raby, Nucl. Phys. **B192**, 353 (1981); M. Dine and W. Fischler, Phys. Lett. **110B**, 227 (1982); M. Dine and M. Srednicki, Nucl. Phys. **B202**, 238 (1982); M. Dine and W. Fischler, Nucl. Phys. **B204**, 346 (1982); L. Alvarez–Gaumé, M. Claudson and M.B. Wise, Nucl. Phys. **B207**, 96 (1982); C.R. Nappi and B.A. Ovrut, Phys. Lett. **113B**, 175 (1982); S. Dimopoulos and S. Raby, Nucl. Phys. **B219**, 479 (1983).

[3] M. Dine and A.E. Nelson, Phys. Rev. **D48**, 1277 (1993); M. Dine and A.E. Nelson, Y. Shirman, Phys. Rev. **D51**, 1362 (1995); M. Dine and A.E. Nelson, Y. Nir, Y. Shirman, Phys. Rev. **D53**, 2658 (1996).

[4] For a recent review, see G.F. Giudice and R. Rattazzi, hep–ph/9801271.

[5] S. Dimopoulos, S. Thomas and J.D. Wells, Phys. Rev. **D54**, 3283 (1996); Nucl. Phys. **B488**, 39 (1997).

[6] J.A. Bagger, K. Matchev, D.M. Pierce and R. Zhang, Phys. Rev. **D55**, 3188 (1997).

[7] S. Ambrosanio, G.D. Kribs and S. P. Martin, Phys. Rev. **D56**, 1761 (1997).

[8] S. Ambrosanio and G.A. Blair, Eur. Phys. J. **C12**, 287 (2000).

[9] P. Fayet, Phys. Lett. **70B**, 461 (1977); Phys. Lett. **86B**, 272 (1979); Phys. Lett. **B175**, 471 (1986) and in "Unification of the fundamental particle interactions", eds. S. Ferrara, J. Ellis, P. van Nieuwenhuizen (Plenum, New York, 1980) p. 587.

[10] A relevant example is discussed in: S. Ambrosanio, G.D. Kribs and S.P. Martin, Nucl. Phys. **B516**, 55 (1998).

[11] An updated, generalized and `Fortran`-linked version of the program used in Ref. [7]. It generates minimal and non-minimal GMSB and SUGRA models. For inquiries about this software package, please send e-mail to `ambros@mail.cern.ch`.

[12] S. Ambrosanio, S. Heinemeyer and G. Weiglein, in preparation.

[13] A. Dedes, S. Heinemeyer, P. Teixeira-Dias and G. Weiglein, hep–ph/9912249, to appear in Jour. Phys. G.

The light Higgs boson spectrum in GMSB models

S. AMBROSANIO, S. HEINEMEYER AND G. WEIGLEIN

Abstract

This study deals with the characteristics of the light Higgs boson spectrum allowed by the (minimal and non-minimal) GMSB framework. Today's most accurate GMSB model generation and two-loop Feynman-diagrammatic calculation of m_h have been combined. The Higgs masses are shown in dependence of various model parameters at the messenger and electroweak scales. In the minimal model, an upper limit on m_h of about 124 GeV is found for $m_t = 175$ GeV.

1 Introduction

Within the MSSM, the masses of the $\mathcal{CP}$-even neutral Higgs bosons are calculable in terms of the other low-energy parameters. The mass of the lightest Higgs boson, m_h, has been of particular interest, as it is bounded to be smaller than the Z^0 boson mass at the tree level. The one-loop results [1–4] for m_h have been supplemented in the last years with the leading two-loop corrections, performed in the renormalization group (RG) approach [5, 6], in the effective potential approach [7] and most recently in the Feynman-diagrammatic (FD) approach [8–10]. The two-loop corrections have turned out to be sizeable. They can lower the one-loop results by up to 20%. These calculations predict an upper bound on m_h of about $m_h \leq 130$ GeV for an unconstrained MSSM with $m_t = 175$ GeV and a common SUSY mass scale $M_{\rm SUSY} \leq 1$ TeV.

As discussed in Sec. 1, the GMSB scenario provides a relatively simple set of constraints and thus constitutes a very predictive and readily testable realization of the MSSM. The main goal of the present analysis is to study the spectrum of the lightest neutral $\mathcal{CP}$-even Higgs boson, m_h, within the GMSB framework. Particular emphasis is given to the maximal value of m_h achievable in GMSB after an exhaustive scanning of the parameter space. Our results are discussed in terms of the GMSB constraints on the low-energy parameters and compared to the cases of a SUGRA-inspired or an unconstrained MSSM.

2 Calculation of m_h

We employ the currently most accurate calculation to evaluate m_h, based on the FD approach as given in Refs. [8–10]. The most important radiative corrections to m_h arise from the top and scalar top sector of the MSSM, with the input parameters m_t, the masses of the scalar top quarks, $m_{\tilde{t}_1}$, $m_{\tilde{t}_2}$, and the $\tilde{t}$-mixing angle, $\theta_{\tilde{t}}$. Here we adopt the conventions introduced in Ref. [9]. The complete diagrammatic one-loop result [3] has been combined with the dominant two-loop corrections of $\mathcal{O}(\alpha\alpha_s)$ [8, 9] and with the subdominant corrections of $\mathcal{O}(\tilde{G}_F^2 m_t^6)$ [5, 6]. GMSB models are generated with the program `SUSYFIRE`, according to the discussion of [11]. For this study, we consider only models with $\tilde{b} > 1.5$ [12] and $m_A > 80$ GeV [13]. In addition, we always use $m_t = 175$ GeV. A change of 1 GeV in m_t translates roughly into a shift of 1 GeV (with the same sign) in m_h as well. Thus, changing m_t affects our results on m_h in an easily predictable way.

The results of the m_h calculation have been implemented in the `Fortran` code `FeynHiggs` [14]. This program has been combined with `SUSYFIRE`, which has been used to calculate the low energy parameters $m_{\tilde{t}_1}$, $m_{\tilde{t}_2}$, $\theta_{\tilde{t}}$, μ, M_1, M_2, $m_{\tilde{g}}$, ... for each of the ∼30000 GMSB models generated. These have then been passed to `FeynHiggs` for the m_h evaluation in a coherent way. Indeed, we transfer the $\overline{\mathrm{MS}}$ parameters in the `SUSYFIRE` output to on-shell parameters before feeding them into `FeynHiggs`. Compact expressions for the relevant transition formulas can be found in Refs. [15,16].

Compared to an existing analysis in the GMSB framework [17], we use a more complete evaluation of m_h. This leads in particular to smaller values of m_h for a given set of input parameters in our analysis. Also, in Ref. [17] although some GMSB scenarios with generalized messenger sectors were considered, the parameter space for the "minimal" case with a unique, integer messenger index $N_{\rm mess} = N_1 = N_2 = N_3$ was not fully explored. Indeed, Λ was in most cases limited to values smaller than 100 TeV and $M_{\rm mess}$ was fixed to 10^5 TeV. Furthermore, partly as a consequence of the above assumptions, the authors did not consider models with $N_{\rm mess} > 4$, i.e. their requirements for perturbativity of the MSSM gauge couplings up to the GUT scale were stronger than ours. We will see in the following section that maximal m_h values in our analysis are instead obtained for larger values of the messenger scale and the messenger index.

3 The Light Higgs Spectrum in GMSB

In the following, we give some results in the form of scatter plots showing the pattern in GMSB for m_h, m_A as well as other low-energy parameters of relevance for the light Higgs spectrum.

In Fig. 1(a), we show the dependence of m_h on $\tilde{b}$, where only models with $\tilde{b} > 1.5$, $m_A > 80$ GeV and $m_{\rm NLSP} > 100$ GeV are considered, while m_t is fixed to 175 GeV. The dependence is strong for small $\tilde{b} \lesssim 10$, while for larger $\tilde{b}$ the increase of the lightest Higgs mass is rather mild. The maximum values for $m_h \simeq 124$ GeV are achieved for $\tilde{b} > 50$. It should be noted that for very large $\tilde{b} \gtrsim 52$, we also find a few models with relatively small $m_h \lesssim 100$ GeV. This is due to the fact that in this case EWSB conditions tend to drive m_A toward very small values [11]. This is made visible by the scatter plot in Fig. 1(b), where the pseudoscalar Higgs mass is shown as a function of $\tilde{b}$. For such small values of m_A and for large $\tilde{b}$, the relation $m_h \approx m_A$ holds. Thus small m_h values are quite natural in this region of the parameter space. On the other hand, one can see that extremely large values of $m_A \gtrsim 2$ TeV can only be obtained for small or moderate $\tilde{b} \lesssim 10$ GeV. A comparison between Fig 1(a) and (b) reveals that the largest m_h values $\gtrsim 123$ GeV correspond in GMSB to m_A values in the 300–800 GeV range. Indeed, it has been checked that such large m_h values are in general obtained in the FD calculation for $300 \lesssim m_A \lesssim 1000$ GeV, see Ref. [9].

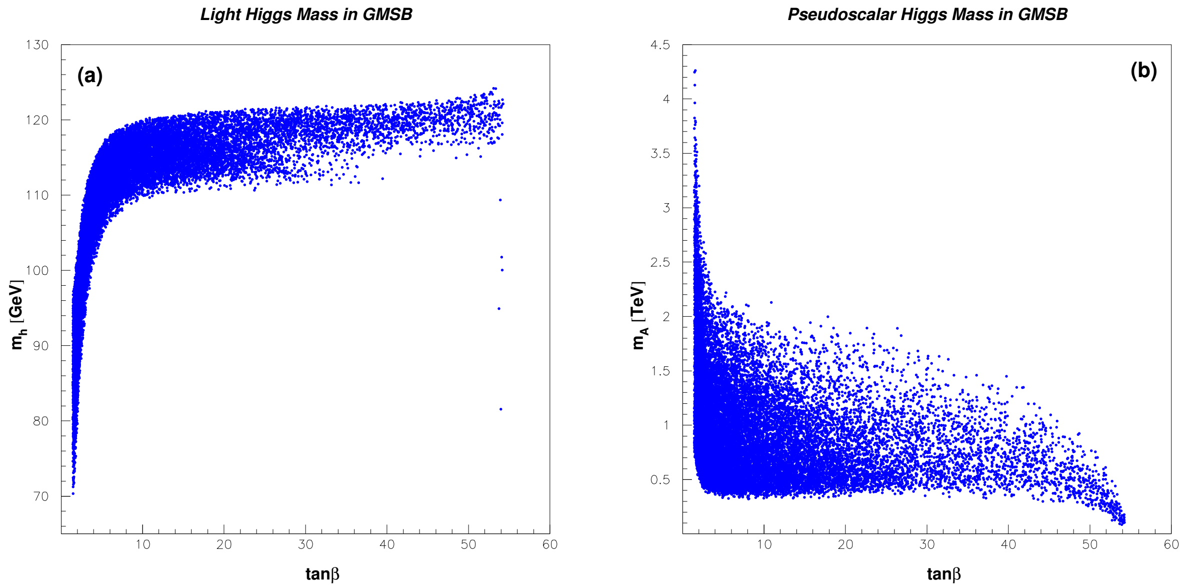

Figure 1: *Scatter plots for the light scalar (a) and pseudoscalar (b) Higgs masses as functions of* $\tilde{b}$*. Only GMSB models with* $\tilde{b} > 1.5$*,* $m_A > 80$ *GeV and* $m_{\rm NLSP} > 100$ *GeV are considered.*

In Fig. 2, we show the dependence of the lightest Higgs boson mass on the stop mixing parameter $x_{\rm top}$ defined by

$$x_{\rm top} \equiv \frac{A_{\rm top} - \mu/\tilde{b}}{m_S}, \quad \text{where} \quad m_S = \sqrt{(m^2_{\tilde{t}_1} + m^2_{\tilde{t}_2})/2}. \tag{1}$$

For equal soft SUSY breaking parameters in the stop sector with the D-terms neglected, $x_{\rm top}$ corresponds to the ratio X_t/M_S of the off-diagonal and diagonal entries in the stop mixing matrix, see e.g. Ref. [16].

Maximal m_h values are obtained for $x_{\rm top} \approx \pm 2$, a minimum is reached around $x_{\rm top} \approx 0$. Thus, for large m_h values a large numerator in Eq. (1) is required. From Fig. 3(a), one can see that in GMSB only negative values of $A_{\rm top}$ are allowed at the electroweak scale, as a consequence of the fact that the trilinear couplings are negligible at the messenger scale. Due to the logarithmic dependence of m_h on the stop masses, relatively large values of $|A_{\rm top}|$ are needed for large m_h. In addition, large $\tilde{b}$ is also required. From Fig. 3(b) one can check that this leads to values of $x_{\rm top} \approx -0.95$, which can only be achieved for positive μ. Fig. 4(a) shows the dependence of $A_{\rm top}$ on μ. Large values of $|A_{\rm top}|$ are only reached for large $|\mu|$ values. Therefore maximal h masses are obtained for relatively large and positive μ, as can be seen in Fig. 4(b).[†]

All these arguments about the combination of low energy parameters needed for large

[†]In general, for large values of $|\mu|$ and $\tilde{b}$ the effects of the corrections from the b–$\tilde{b}$ sector can become important, leading to a decrease in m_h. For the GMSB models under consideration, however, this is not the case as a consequence of the relatively large $\tilde{b}$ masses.

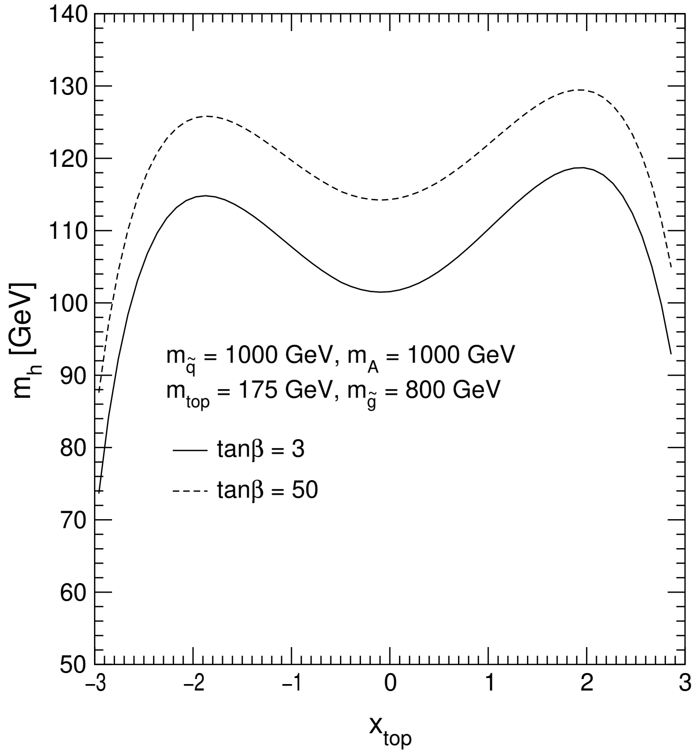

Figure 2: *The light CP-even Higgs boson mass is given as a function of* $x_{\rm top}$ *for* $\tilde{b} = 3, 50$, $m_A = 1000$ *GeV, a common soft SUSY breaking scale for the squarks,* $m_{\tilde{q}} = 1000$ *GeV, and a gluino mass* $m_{\tilde{g}} = 800$ *GeV.*

m_h in GMSB are summarized in Tab. 1. where we report the 10 models in our sample that give rise to the highest m_h values. Together with m_h, Tab. 1 shows the corresponding input GMSB parameters (Eq. (1) in [11]) as well as the values of the low energy parameters mentioned above.

It is interesting to note that all the models shown in Tab. 1 feature a large messenger index and values of the messenger scale not far from the maximum we allowed while generating GMSB models. We could not construct a single model with $m_h \gtrsim 122.5$ GeV having $N_{\rm mess} < 6$ or $M_{\rm mess} < 10^5$ TeV, for $m_t = 175$ GeV. It is hence worth mentioning here that our choice of imposing $M_{\rm mess}/\Lambda < 10^5 \Rightarrow M_{\rm mess} \lesssim 2 \times 10^{10}$ GeV does not correspond to any solid theoretical prejudice. On the other hand it is true that $M_{\rm mess} \gtrsim 3 \times 10^8$ GeV always corresponds to gravitino masses larger than ~ 1 keV, due to Eqs. (2) and (5) in [11]. The latter circumstance might be disfavored by cosmological arguments [18]. A curious consequence is that the GMSB models with the highest m_h belong always to the stau NLSP or slepton co-NLSP scenarios.

Note also that restricting ourselves to GMSB models with $\Lambda < 100$ TeV, $M_{\rm mess} < 10^5$ TeV and $N_{\rm mess} \leq 4$, we find a maximal m_h value of 122.2 GeV, for $m_t = 175$ GeV and $\tilde{b} \sim 52$. This is to be compared with the one-loop result of Ref. [17], $m_h(\max) = 131.7$, for $\tilde{b}$ around 30 (the assumed value of m_t is not quoted).

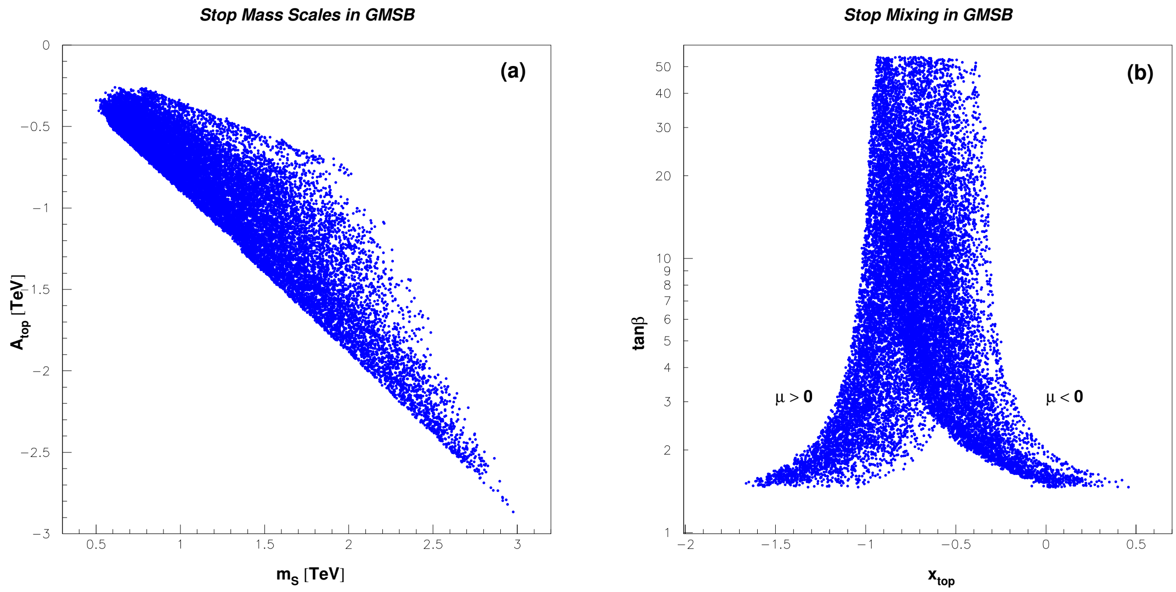

Figure 3: *Scatter plots of* A_{top} *vs.* m_S*, the mass scale appearing in the denominator of Eq. (1) (a)* and $\tilde{b}$ *vs.* x_{top} *(b).*

Values for m_h slightly larger than those we found here may also arise from non-minimal contributions to the Higgs potential, in connection with a dynamical generation of μ and $B\mu$ [11]. A treatment of this problem can be found in Ref. [19].

One should also keep in mind that our analysis still suffers from uncertainties due to unknown higher order corrections both in the RGEs for GMSB model generation and in the evaluation of m_h from low energy parameters. A rough estimate of these effects leads to shifts in m_h not larger than 3 to 5 GeV.

4 Conclusions

We conclude that in the minimal GMSB framework described above, values of $m_h \gtrsim 124.2$ GeV are not allowed for $m_t = 175$ GeV. This is almost 6 GeV smaller than the maximum value for m_h one can achieve in the MSSM without any constraints or assumptions about the structure of the theory at high energy scales [9, 20, 21]. On the other hand, the alternative mSUGRA framework allows values of m_h that are ~ 3 GeV larger than in GMSB [12]. This makes the GMSB scenario slightly easier to explore via Higgs boson search. This result was expected in the light of the rather strong GMSB requirements, such as the presence of a unique soft SUSY breaking scale, the relative heaviness of the squarks and the gluino compared to non-strongly interacting sparticles, and the fact that the soft SUSY breaking trilinear couplings A_f get nonzero values at the electroweak scale only by RGE evolution. Nevertheless, once the whole parameter space is explored, it is not true that mGMSB gives rise to m_h values that are considerably smaller than in mSUGRA. Even smaller differences in the maximal m_h might be present when considering non-minimal, complex messenger sectors [17] or additional contributions to the Higgs potential [19, 22]. In any case, as for mSUGRA, current LEP II or Tevatron data on Higgs boson searches are far from excluding mGMSB, and the upgraded Tevatron and the LHC will certainly be needed to deeply test any realistic SUSY model.

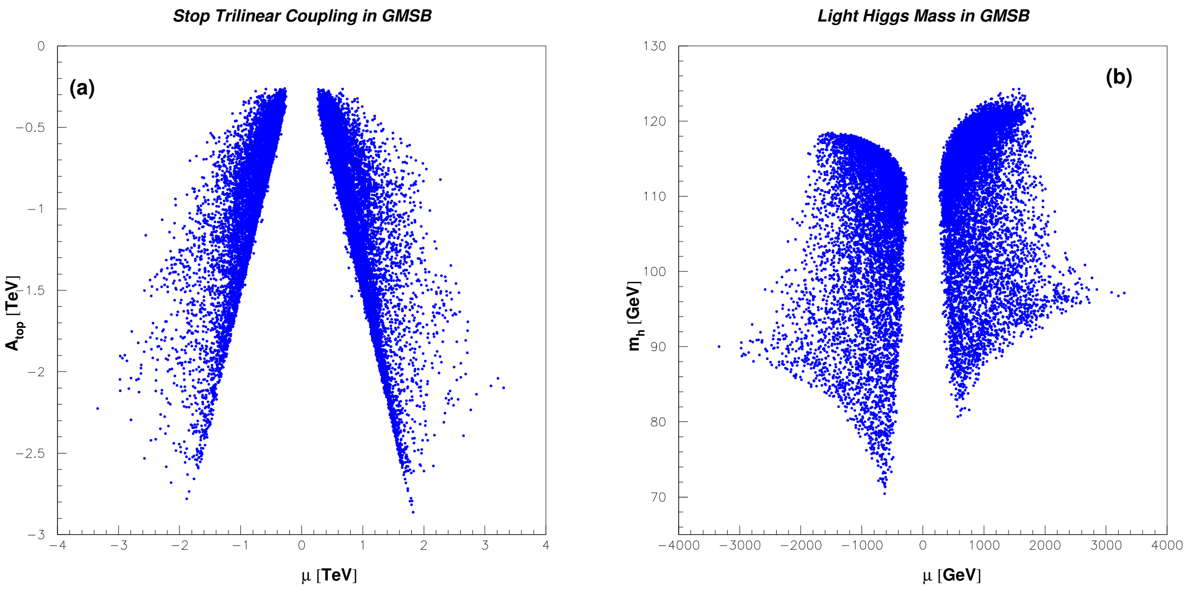

Figure 4: *Scatter plots for* $A_{\rm top}$ *(a) and the light scalar Higgs mass (b) vs. the SUSY higgsino mass* μ *evaluated at the electroweak scale.*

References

[1] H. Haber and R. Hempfling, Phys. Rev. Lett. **66**, 1815 (1991); J. Ellis, G. Ridolfi and F. Zwirner, Phys. Lett. **B257**, 83 (1991); Phys. Lett. **B262**, 477 (1991).

[2] P. Chankowski, S. Pokorski and J. Rosiek, Nucl. Phys. **B423**, 437 (1994).

[3] A. Dabelstein, Nucl. Phys. **B456**, 25 (1995); Z. Phys. **C67**, 495 (1995).

[4] J. Bagger, K. Matchev, D. Pierce and R. Zhang, Nucl. Phys. **B491**, 3 (1997).

[5] J. Casas, J. Espinosa, M. Quirós and A. Riotto, Nucl. Phys. **B436**, 3 (1995), E: ibid **B439** (1995) 466; M. Carena, J. Espinosa, M. Quirós and C. Wagner, Phys. Lett. **B355**, 209 (1995); M. Carena, M. Quirós and C. Wagner, Nucl. Phys. **B461**, 407 (1996).

ID	m_h GeV	$N_{\rm mess}$	$M_{\rm mess}$ 10^6 TeV	Λ TeV	μ GeV	$\tilde{b}$	m_A GeV	$m_{\tilde{t}_1}$ GeV	$m_{\tilde{t}_2}$ GeV	$A_{\rm top}$ GeV	$x_{\rm top}$
A1	124.2	7	1.00	72.7	1470	53.4	367	2320	2510	-2150	-0.90
A2	124.2	8	4.48	66.7	1570	53.1	436	2400	2600	-2310	-0.94
A3	123.7	6	2.07	87.0	1580	52.8	485	2420	2630	-2240	-0.90
A4	123.7	8	4.67	52.4	1270	52.9	373	1930	2100	-1850	-0.93
A5	123.5	8	4.89	51.1	1250	52.7	388	1880	2050	-1810	-0.93
A6	123.5	6	2.54	67.1	1260	53.0	349	1910	2080	-1760	-0.89
A7	123.4	8	4.62	61.6	1470	51.9	549	2230	2430	-2160	-0.94
A8	123.4	6	4.15	88.1	1630	51.9	609	2450	2670	-2300	-0.91
A9	123.3	7	3.77	70.3	1490	51.8	567	2260	2460	-2150	-0.92
A10	123.3	8	3.74	72.1	1677	50.7	756	2580	2800	-2500	-0.94

Table 1: *The 10 GMSB models giving rise to the highest m_h values in our sample. For each model, together with the light Higgs mass, we show the values of the GMSB input parameters and other low energy parameters of interest for calculating m_h.*

[6] H. Haber, R. Hempfling and A. Hoang, Z. Phys. **C75**, 539 (1997).

[7] R. Hempfling and A. Hoang, Phys. Lett. **B331**, 99 (1994); R.-J. Zhang, Phys. Lett. **B447**, 89 (1999).

[8] S. Heinemeyer, W. Hollik and G. Weiglein, Phys. Rev. **D58**, 091701 (1998); Phys. Lett. **B440**, 296 (1998).

[9] S. Heinemeyer, W. Hollik and G. Weiglein, Eur. Phys. J. **C9**, 343 (1999).

[10] S. Heinemeyer, W. Hollik and G. Weiglein, Phys. Lett. **B455**, 179 (1999).

[11] S. Ambrosanio, These Proceedings.

[12] A. Dedes, S. Heinemeyer, P. Teixeira-Dias and G. Weiglein, hep–ph/9912249, to appear in Jour. Phys. G.

[13] P. McNamara, "Combined LEP Higgs search results up to $\sqrt{s} = 196$ GeV", talk given at the LEPC meeting, September 7, 1999.

[14] S. Heinemeyer, W. Hollik and G. Weiglein, Comp. Phys. Comm. **124** (2000) 76.

[15] S. Heinemeyer, W. Hollik and G. Weiglein, hep–ph/9910283.

[16] M. Carena, H. Haber, S. Heinemeyer, W. Hollik, C. Wagner and G. Weiglein, DESY 197-99, hep–ph/0001002.

[17] T.A. Kaeding and S. Nandi, hep–ph/9906432.

[18] See e.g.: H. Pagels and J.R. Primack, Phys. Rev. Lett. **48**, 223 (1982).

[19] S. Ambrosanio, S. Heinemeyer and G. Weiglein, in preparation.

[20] S. Heinemeyer, W. Hollik and G. Weiglein, hep–ph/9909540.

[21] M. Carena, S. Heinemeyer, C. Wagner and G. Weiglein, hep–ph/9912223.

[22] S. Dimopoulos, S. Thomas and J.D. Wells, Phys. Rev. **D54**, 3283 (1996); Nucl. Phys. **B488**, 39 (1997).

Measuring the SUSY breaking scale at the LHC in the slepton NLSP scenario of GMSB models

S. AMBROSANIO, B. MELE, S. PETRARCA, G. POLESELLO AND A. RIMOLDI

Abstract

This study is focused on the measurement of the fundamental SUSY breaking scale $\sqrt{F}$ at the LHC in the GMSB scenario where a stau is the next-to-lightest SUSY particle (NLSP) and decays into a gravitino with $c\tau_{\rm NLSP}$ in the range 0.5 m to 1 km. This implies the measurement of mass and lifetime of long lived sleptons. The identification is performed by determining the time of flight in the ATLAS muon chambers. Accessible range and precision on $\sqrt{F}$ achievable with a counting method are assessed.

1 Introduction

The fundamental scale of SUSY breaking $\sqrt{F}$ is perhaps the most important quantity to determine from phenomenology in a SUSY theory. In the mSUGRA framework, the gravitino mass sets the scale of the soft SUSY breaking masses in the MSSM ($\sim 0.1 - 1$ TeV), so that $\sqrt{F}$ is typically large $\sim 10^{10-11}$ GeV (Eq. (2) in [1]). As a consequence, the interactions of the $\tilde{G}$ with the other MSSM particles $\sim F^{-1}$ are too weak for the gravitino to be of relevance in collider physics and there is no direct way to access $\sqrt{F}$ experimentally. In GMSB theories, the situation is completely different. The soft SUSY breaking scale of the MSSM and the sparticle masses are set by gauge interactions between the messenger and low energy sectors to be $\sim \alpha_{\rm SM}\Lambda$ (Eq. (4) in [1]), so that typical Λ values are $\sim 10 - 100$ TeV. On the other hand, $\sqrt{F}$ is subject to the lower bound (5) in [1] only, which tells us that values well below 10^{10} GeV and even as low as several tens of TeV are perfectly reasonable. The $\tilde{G}$ is in this case the LSP and its interactions are strong enough to allow NLSP decays to the $\tilde{G}$ inside a typical detector size. The latter circumstance gives us a chance for extracting $\sqrt{F}$ experimentally through a measurement of the NLSP mass and lifetime (Eq. (3) in [1]).

Furthermore, the possibility of determining $\sqrt{F}$ with good precision opens a window on the physics of the SUSY breaking ("secluded") sector and the way this SUSY breaking is transmitted to the messenger sector. Indeed, the characteristic scale of SUSY breaking felt by the messengers (and hence the MSSM sector) given by $\sqrt{F_{\rm mess}}$ in Eq. (5) can also be determined once the MSSM spectrum is known. By comparing the measured values of $\sqrt{F}$ and $\sqrt{F_{\rm mess}}$ it might well be possible to get information on the way the secluded and messenger sectors communicate with each other. For instance, if it turns out that $\sqrt{F_{\rm mess}} \ll \sqrt{F}$, then it is very likely that the communication occurs radiatively and the ratio $\sqrt{F_{\rm mess}/F}$ is given by some loop factor. On the contrary, if the communication occurs via a direct interaction, this ratio is just given by a Yukawa-type coupling constant, with values $\lesssim 1$, see Refs. [2, 3].

An experimental method to determine $\sqrt{F}$ at a TeV scale e^+e^- collider through the measurement of the NLSP mass and lifetime was presented in Ref. [4], in the neutralino NLSP scenario. Here, we are concerned with the same problem, but at a hadron collider, the LHC, and in the stau NLSP or slepton co-NLSP scenarios. These scenarios provide a great opportunity at the LHC, since the characteristic signatures with semi-stable charged tracks are muon-like, but come from massive sleptons with β significantly smaller than 1. In particular, we perform our simulations in the ATLAS muon detector, whose large size and excellent time resolution [5] allow a precision measurement of the slepton time of flight from the production vertex out to the muon chambers and hence of the slepton velocity. Moreover, in the stau NLSP or slepton co-NLSP scenarios, the knowledge of the NLSP mass and lifetime is sufficient to determine $\sqrt{F}$, since the factor $\mathcal{B}$ in Eq.(3) of [1] is exactly equal to 1. This is not the case in the neutralino NLSP scenario where $\mathcal{B}$ depends at least on the neutralino physical composition and more information and measurements are needed for extracting a precise value of $\sqrt{F}$.

2 Choice of the Sample Models and Event Simulation

The two main parameters affecting the experimental measurement at the LHC of the slepton NLSP properties are the slepton mass and momentum distribution. Indeed, at a hadron collider most of the NLSPs come from squark and gluino production followed by cascade decays. Thus, the momentum distribution is in general a function of the whole MSSM spectrum. However, one can approximately assume that most of the information on the NLSP momentum distribution is provided by the squark mass scale $m_{\tilde{q}}$ only (in the stau NLSP scenario or slepton co-NLSP scenarios of GMSB, one generally finds $m_{\tilde{g}} \gtrsim m_{\tilde{q}}$). To perform detailed simulations, we select a representative set of GMSB models generated by `SUSYFIRE`. We limit ourselves to models with $m_{\rm NLSP} > 100$ GeV, motivated by the discussion in [1], and $m_{\tilde{q}} < 2$ TeV, in order to yield an adequate event statistics after a three-year low-luminosity run (corresponding to 30 fb^{-1}) at the LHC. Within these ranges, we choose eight extreme points (four in the stau NLSP scenario and four in the slepton co-NLSP scenario) allowed by GMSB in the ($m_{\rm NLSP}$, $m_{\tilde{q}}$) plane, in order to cover the various possibilities.

In Tab. 1, we list the input GMSB parameters we used, while in Tab. 2 we report the corresponding values of the stau mass, the squark mass scale and the gluino mass. The "NLSP" column indicates whether the model belongs to the stau NLSP or slepton co-NLSP scenario. The last column gives the total cross section in pb for producing any pairs of SUSY particles at the LHC.

For each model, the events were generated with the `ISAJET` Monte Carlo [6] that incorporates the calculation of the SUSY mass spectrum and branching fraction using the GMSB parameters as input. We have checked that for the eight model points considered the sparticle masses calculated with `ISAJET` are in good agreement with the output of `SUSYFIRE`.

The generated events were then passed through `ATLFAST` [7], a fast particle-level simulation of the ATLAS detector. The `ATLFAST` package, however, was only used to evaluate the efficiency of the calorimetric trigger that selects the GMSB events. The detailed response of

ID	$M_{\rm mess}$ (TeV)	$N_{\rm mess}$	Λ (TeV)	$\tilde{b}$	sign(μ)
B1	1.79×10^4	3	26.6	7.22	−
B2	5.28×10^4	3	26.0	2.28	−
B3	4.36×10^2	5	41.9	53.7	+
B4	1.51×10^2	4	28.3	1.27	−
B5	3.88×10^4	6	58.6	41.9	+
B6	2.31×10^5	3	65.2	1.83	−
B7	7.57×10^5	3	104	8.54	−
B8	4.79×10^2	5	71.9	3.27	−

Table 1: *Input parameters of the sample GMSB models chosen for our study.*

ID	$m_{\tilde{\tau}_1}$ (GeV)	"NLSP"	$m_{\tilde{q}}$ (GeV)	$m_{\tilde{g}}$ (GeV)	σ (pb)
B1	100.1	$\tilde{\tau}$	577	631	42
B2	100.4	$\tilde{\ell}$	563	617	50
B3	101.0	$\tilde{\tau}$	1190	1480	0.59
B4	103.4	$\tilde{\ell}$	721	859	10
B5	251.2	$\tilde{\tau}$	1910	2370	0.023
B6	245.3	$\tilde{\ell}$	1290	1410	0.36
B7	399.2	$\tilde{\tau}$	2000	2170	0.017
B8	302.9	$\tilde{\ell}$	1960	2430	0.022

Table 2: *Features of the sample GMSB model points studied.*

the detector to the slepton NLSP has been parameterized for this work using the results of a full simulation study, as described in the next section.

3 Slepton detection

The experimental signatures of heavy long-lived charged particles at a hadron collider have already been studied both in the framework of GMSB and in more general scenarios [8–11]. The two main observables one can use to separate these particles from muons are the high specific ionization and the time of flight in the detector.

We concentrate here on the measurement of the time of flight, made possible by the timing precision ($\lesssim 1$ ns) and the size of the ATLAS muon spectrometer.

It was demonstrated with a full simulation of the ATLAS muon detector [12] that the β of a particle can be measured with a resolution that can be approximately parameterized as $\sigma(\beta)/\beta^2 = 0.028$. The resolution on the transverse momentum measurement for heavy particles is found to be comparable to the one expected for muons. We have therefore simulated the detector response to NLSP sleptons by smearing the slepton momentum and β according to the parameterizations in Ref. [12].

An important issue is the online selection of the SUSY events. We have not made any attempt to evaluate whether the heavy sleptons can be selected using the muon trigger. For the event selection, we rely on the calorimetric E_T^{miss} trigger, consisting in the requirement of at least one hadronic jet with $p_T > 50$ GeV, and a transverse momentum imbalance calculated only from the energy deposition in the calorimeter larger than 50 GeV. We checked that this trigger has an efficiency in excess of 80% for all the considered models.

A detailed discussion of the experimental assumptions underlying the results presented here is given in Ref. [13].

4 Event Selection and Slepton Mass Measurement

In order to select a clean sample of sleptons, we apply the following requirements:

- at least one hadronic jet with $P_T > 50$ GeV and a calorimetric $E_T^{\mathrm{miss}} > 50$ GeV (trigger requirement);
- at least one candidate slepton satisfying the following cuts:
  - $|\eta|$ <2.4 to ensure that the particle is in the acceptance of the muon trigger chamber, and therefore both coordinates can be measured;
  - $\beta_{\mathrm{meas}} < 0.91$, where β_{meas} is the β of the particle measured with the time of flight in the precision chambers;
  - The P_T of the slepton candidate, after the energy loss in the calorimeters has been taken into account, must be larger than 10 GeV, to ensure that the particle traverse all of the muon stations.

If we consider an integrated luminosity of 30 fb^{-1}, a number of events ranging from a few hundred for the models with 2 TeV squark mass scale to a few hundred thousand for a 500 GeV mass scale survive these cuts and can be used for measuring the NLSP properties.

From the measurements of the slepton momentum and of particle β, the mass can be determined using the standard relation $m = p\frac{\sqrt{1-\beta^2}}{\beta}$. For each value of β and momentum, the measurement error is known and it is given by the parameterizations in Ref. [12]. Therefore, the most straightforward way of measuring the mass is just to use the weighted average of all the masses calculated with the above formula.

In order to perform this calculation, the particle momentum is needed, which implies measuring the η coordinate. In fact, with the precision chambers only one can only measure the momentum components transverse to the beam axis.

The measurement of the second coordinate must be provided by the trigger chambers, for which only a limited time window around the beam crossing is read out, therefore restricting the β range where this measurement is available. Hence, we have evaluated the achieved measurement precision for two different β intervals: $0.6 < \beta < 0.91$ and $0.8 < \beta < 0.91$ for the eight sample points. We found a statistical error well below the 0.1% level for those model points having $m_{\tilde{q}} < 1300$ GeV. Even for the three models (B5, B7, B8) with lower statistics ($m_{\tilde{q}} \simeq 2$ TeV), the error stays below the 0.4% level.

Many more details, tables and figures about this part of our study can be found in Ref. [13].

5 Slepton Lifetime Measurement

The measurement of the NLSP lifetime at a high energy e^+e^- collider was studied in detail in Ref. [4] for the neutralino NLSP case. Similar to that study, the measurement of the slepton NLSP lifetime we are interested in here can be performed by exploiting the fact that two NLSPs are produced in each event. One can therefore select N_1 events where a slepton is detected through the time-of-flight measurement described above, count the number of times N_2 when a second slepton is observed and use this information to measure the lifetime. Although in principle very simple, in practice this method requires an excellent control on all possible sources of inefficiency for detecting the second slepton.

We give here the basis of the method, without mentioning the experimental details. We provide an estimate of the achievable statistical error for the models considered and a parameterization of the effect on the lifetime measurement of a generic systematic uncertainty on the slepton efficiency. In case the sparticle spectrum and BRs can be measured from the SUSY events, as e.g. shown in Ref. [14], an accurate simulation of all the SUSY production processes can be performed, and the results from this section are representative of the measurement precision achievable in a real experiment.

Another method based on the same principles, but assuming minimal knowledge of the SUSY spectrum, is described in Ref. [13], where a detailed estimate of the achievable systematic precision is given.

We define N_1 starting from the event sample defined by the cuts discussed in Sec. 4, with the additional requirement that, for a given value of the slepton lifetime, at least one of the produced sleptons decays at at a distance from the interaction vertex > 10 m, and is therefore reconstructed in the muon system. For the events thus selected, we define N_2 as the subsample where a second particle with a transverse momentum > 10 GeV is identified in the muon system. The search for the second particle should be as inclusive as possible, in order to minimize the corrections to the ratio. In particular, the cut $\beta_{\text{meas}} < 0.91$ is not applied, but particles with a mass measured from β and momentum incompatible with the measured slepton mass are rejected. This leaves a background of high momentum muons in the sample that can be statistically subtracted using the momentum distribution of electrons. The ratio

$$R = \frac{N_2}{N_1} \tag{1}$$

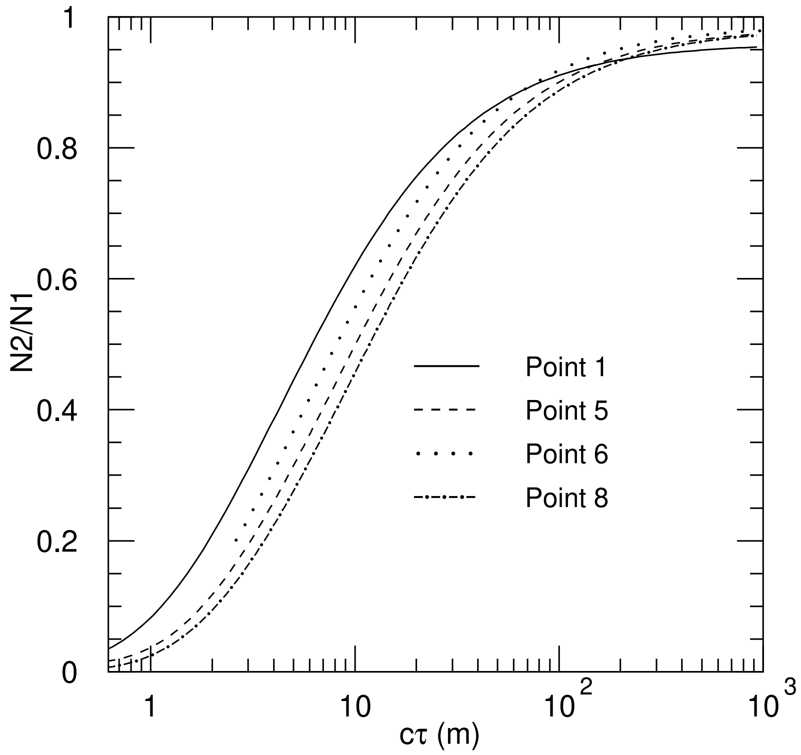

Figure 1: *The ratio $R = N_2/N_1$ defined in the text as a function of the slepton lifetime $c\tau$. Only the curves corresponding to the model points B1, B5, B6, B8 are shown.*

is a function of the slepton lifetime. Its dependence on the NLSP lifetime $c\tau$ in meters in shown in Fig. 1 for four among our eight sample models. The curves for the model points not shown are either very similar to one of the curves we show or are mostly included between the external curves corresponding to points B1 and B8, thus providing no essential additional information. Note that the curve for model 6 starts from $c\tau = 2.5$ m and not from $c\tau = 50$ cm, as for the other models. This is due to the large value of $M_{\rm mess}$ (cfr. Tab. 1), determining a minimum NLSP lifetime allowed by theory which is macroscopic in this case (Eqs. (3) and (5) in [1]).

The probability for a particle of mass m, momentum p and proper lifetime τ to travel a distance L before decaying is given by the expression

$$P(L) = e^{-mL/pc\tau}. \tag{2}$$

N_2 is therefore a function of the momentum distribution of the slepton, which is determined by the details of the SUSY spectrum. One therefore needs to be able to simulate the full SUSY cascade decays in order to construct the $c\tau$–R relationship.

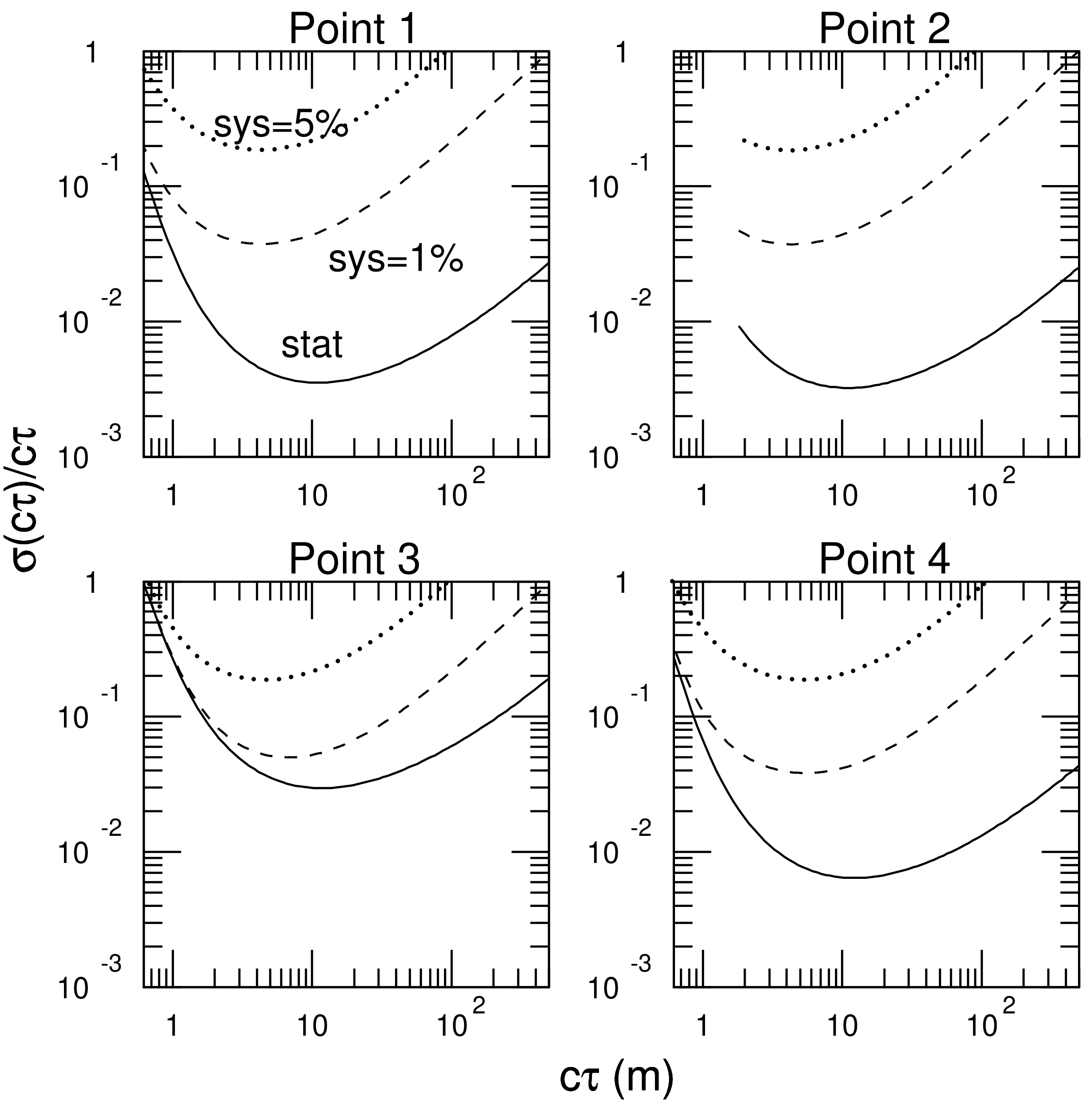

Figure 2: *Fractional error on the measurement of the slepton lifetime $c\tau$, for model sample points B1 to B4. We assume an integrated luminosity of 30 fb^{-1}. The curves are shown for three different assumptions on the fractional systematic error on the R measurement: statistical error only (full line), 1% systematic error (dashed line), 5% systematic error (dotted line).*

The statistical error on R can be evaluated as

$$\sigma(R) = \sqrt{\frac{R(1-R)}{N_1}}. \tag{3}$$

Relevant for the precision with which the SUSY breaking scale can be measured is instead

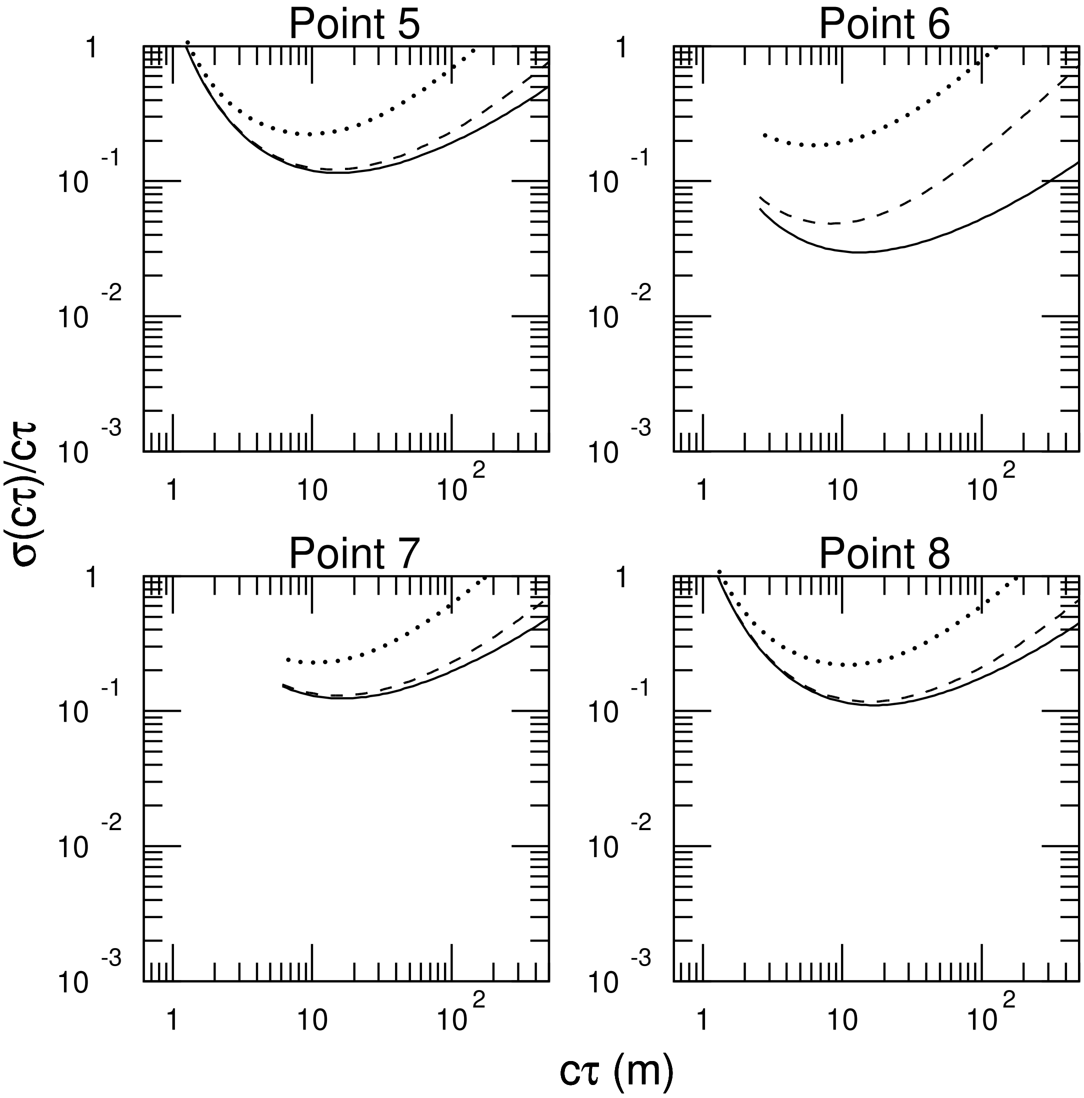

Figure 3: *The same as in Fig. 3, but for the model sample points B5 to B8.*

the error on the measured $c\tau$. This can be extracted from the curves shown in Fig. 1 and can be evaluated as

$$\sigma(\mathrm{c}\tau) = \sigma(R)/\left[\frac{\partial R(c\tau)}{\partial c\tau}\right]. \tag{4}$$

The measurement precision calculated according to this formula is shown in Figs. 2 and 3 for the eight sample points, for an integrated luminosity of 30 fb^{-1}. The full line in the plots is the error on $c\tau$ considering the statistical error on R only. The available statistics is a function of the strongly interacting sparticles' mass scale. Even if a precise R–$c\tau$ relation can be built from the knowledge of the model details, there will be a systematic uncertainty in the evaluation of the losses in N_2, because of sleptons produced outside the η acceptance, or absorbed in the calorimeters, or escaping the calorimeter with a transverse momentum below the cuts. The full study of these uncertainties is in progress.

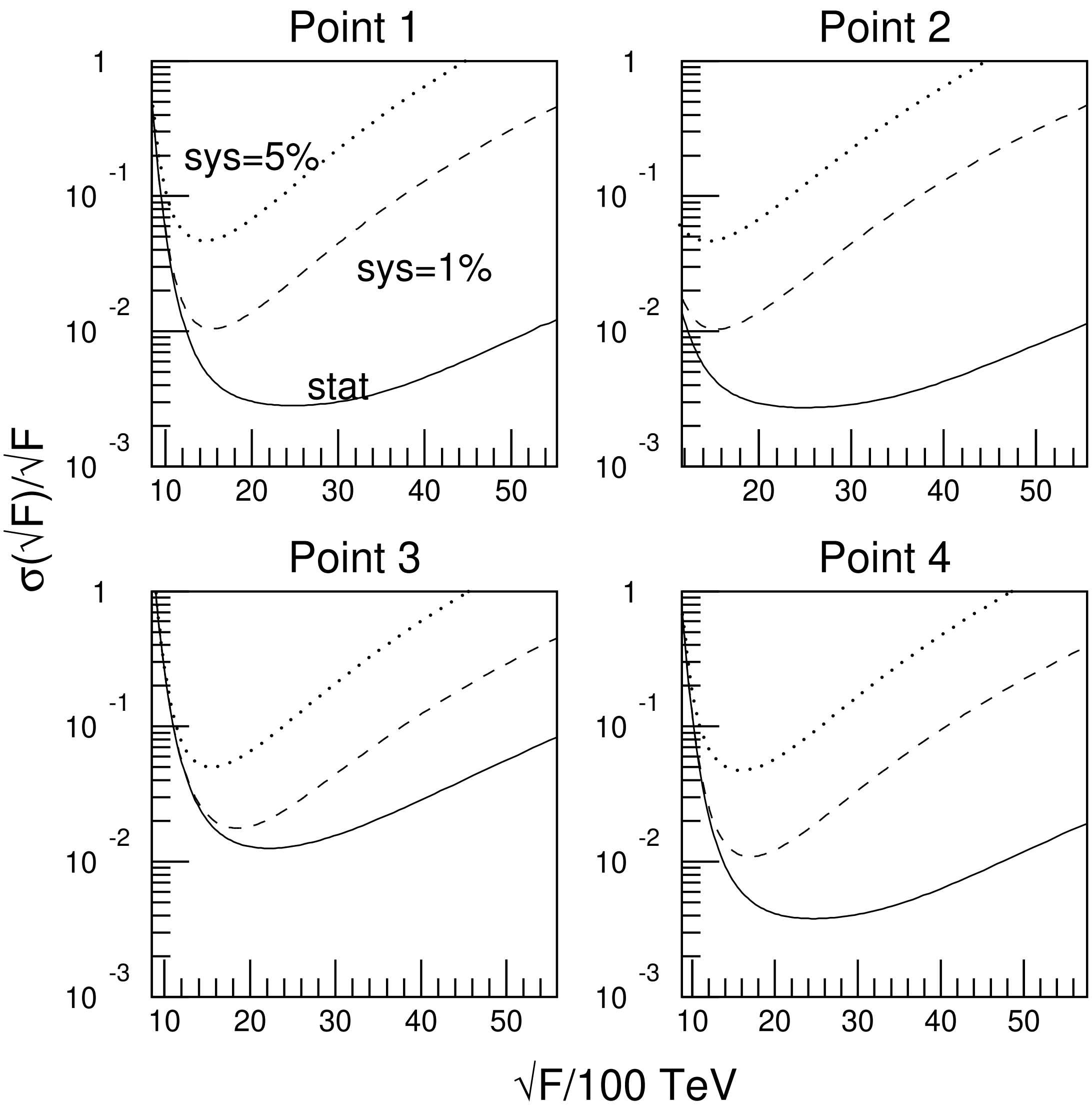

Figure 4: *Fractional error on the measurement of the SUSY breaking scale* $\sqrt{F}$ *for model sample points B1 to B4. We assume an integrated luminosity of 30 fb*$^{-1}$*. The curves are shown for the three different assumptions on the fractional systematic error used in Figs. 2 and 3.*

At this level, we just parameterize the systematic error as a term proportional to R, added in quadrature to the statistical error. We choose two values, $1\%R$ and $5\%R$, and propagate the error to the $c\tau$ measurement. The results are represented by the dashed and dotted lines in Figs. 2 and 3.

For the models with squark mass scales up to 1200 GeV, assuming a 1% systematic error on the measured ratio, a precision better than 10% on the $c\tau$ measurement can be obtained for lifetimes between 0.5–1 m and 50–80 m. If the systematic uncertainty grows to 5%, the 10% precision can only be achieved in the range 1–10 m. If the mass scale goes up to 2 TeV, even considering a pure statistical error only, a 10% precision is not achievable. However a 20% precision is possible over $c\tau$ ranges between 5 and 100 m, assuming a 1% systematic error.

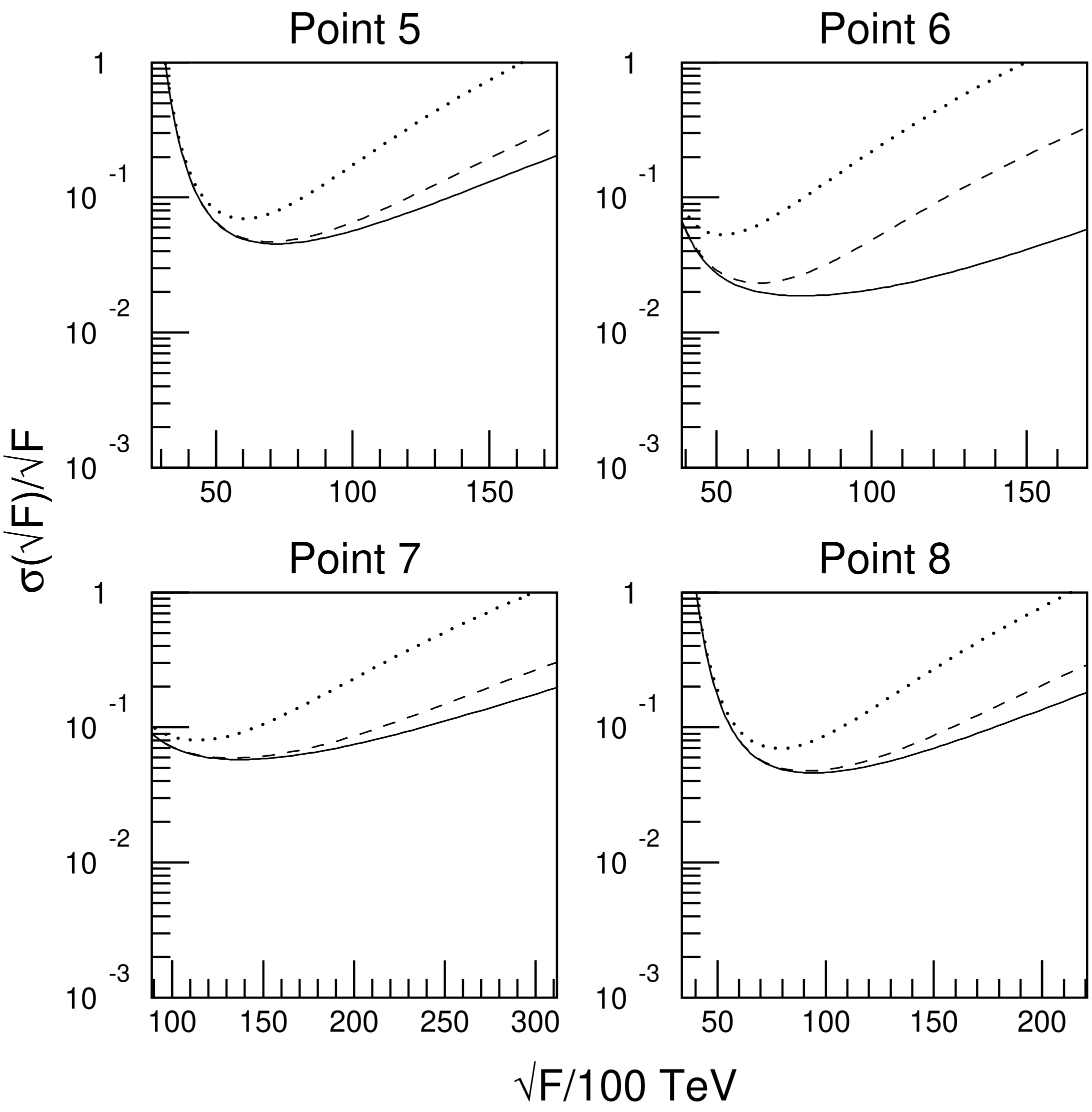

Figure 5: *The same as in Fig. 4, but for model sample points B5 to B8.*

Note that the curves corresponding to the model points B2, B6 and B7 do not start from $c\tau = 50$ cm, but from the theoretical lower limit on $c\tau$ of 1.8, 2.5 and 6.1 meters, respectively.

6 Determining the SUSY Breaking Scale $\sqrt{F}$

Using the measured values of $c\tau$ and the NLSP mass, the SUSY breaking scale $\sqrt{F}$ can be calculated from Eq.(3) in [1], where $\mathcal{B} = 1$ for the case where the NLSP is a slepton. From simple error propagation, the fractional uncertainty on the $\sqrt{F}$ measurement can be obtained adding in quadrature one fourth of the fractional error in $c\tau$ and five fourths of the fractional error on the slepton mass.

In Figs. 4 and 5, we show the fractional error on the $\sqrt{F}$ measurement as a function of $\sqrt{F}$ for our three different assumptions on the $c\tau$ error. The uncertainty is dominated by $c\tau$ for the higher part of the $\sqrt{F}$ range and grows quickly when approaching the lower limit on $\sqrt{F}$. This is because very few sleptons survive and the statistical error on both $m_{\tilde{\ell}}$ and $c\tau$ gets very large. If we assume a 1% systematic error on the ratio R from which $c\tau$ is measured (dashed lines in Figs. 4 and 5), the error on $\sqrt{F}$ is better than 10% for $1000 \lesssim \sqrt{F} \lesssim 4000$ TeV for model points B1–B4 with higher statistics. For points B5–B8, in general one can explore a range of higher $\sqrt{F}$ values with a small relative error, essentially due to the heaviness of the decaying NLSP in these models. Note also that the theoretical lower limit (5) in [1] on $\sqrt{F}$ is equal to about 1200, 1500, 3900, 8900 TeV respectively in model points B2, B5, B6, B7, while it stays well below 1000 TeV for the other models.

7 Conclusions

We have discussed a simple method to measure at the LHC with the ATLAS detector the fundamental SUSY breaking scale $\sqrt{F}$ in the GMSB scenarios where a slepton is the NLSP and decays to the gravitino with a lifetime in the range 0.5 m $\lesssim c\tau_{\rm NLSP} \lesssim 1$ km. This method requires the measurement of the time of flight of long lived sleptons and is based on counting events with one or two identified NLSPs. It relies on the assumptions that a good knowledge of the MSSM sparticle spectrum and BRs can be extracted from the observation of the SUSY events and that the systematic error in evaluating the slepton losses can be kept below the few percent level. We performed detailed, particle level simulations for eight representative GMSB models, some of them being particularly hard due to low statistics. We found that a level of precision of a few 10's % on the SUSY breaking scale measurement can be achieved in significant parts of the $1000 \lesssim \sqrt{F} \lesssim 30000$ TeV range, for all models considered. More details as well as a full study of the systematics associated with this procedure and another less "model-dependent" method to measure $\sqrt{F}$ is presented in detail in Ref. [13].

References

[1] S. Ambrosanio, These Proceedings.

[2] For a recent review, see G.F. Giudice and R. Rattazzi, hep–ph/9801271.

[3] S. Ambrosanio, G.D. Kribs and S. P. Martin, Phys. Rev. **D56**, 1761 (1997).

[4] S. Ambrosanio and G.A. Blair, Eur. Phys. J. **C12**, 287 (2000).

[5] The ATLAS Collaboration, "ATLAS Detector and Physics Performance Technical Design Report", ATLAS TDR 15, CERN/LHCC/99-15 (1999).

[6] H. Baer, F.E. Paige, S.D. Protopopescu and X. Tata, hep–ph/9305342; hep–ph/9804321.

[7] E. Richter-Was, D. Froidevaux and L. Poggioli, "`ATLFAST 2.0`: A fast simulation package for ATLAS", ATLAS Internal Note ATL-PHYS-98-131 (1998).

[8] A. Nisati, S. Petrarca and G. Salvini, Mod. Phys. Lett. **A12** (1997) 2213.

[9] M. Drees and X. Tata, Phys. Lett. **B252**, 695 (1990).

[10] J. L. Feng and T. Moroi, Phys. Rev. **D58**, 035001 (1998).

[11] S.P. Martin and J.D. Wells, Phys. Rev. **D59**, 035008 (1999).

[12] G. Polesello and A. Rimoldi, "Reconstruction of Quasi-stable Charged Sleptons in the ATLAS Muon Spectrometer", ATLAS Internal Note ATL-MUON-99-06.

[13] S. Ambrosanio, B. Mele, S. Petrarca, G. Polesello and A. Rimodi, in preparation.

[14] I. Hinchliffe and F.E. Paige, Phys. Rev. **D60**, 095002 (1999).